Gravitational Collapse and Black Holes

Diogo Luís Farinha Gomes da Silva

Thesis to obtain the Master of Science Degree in

Engineering Physics

Supervisor(s): Prof. José Pizarro de Sande e Lemos

Examination Committee

Chairperson: Prof. Ilídio Pereira Lopes
Supervisor: Prof. José Pizarro de Sande e Lemos
Members of the Committee: Prof. Filipe Artur Pacheco Neves Carteado Mena
Dr. Jorge Miguel Cruz Pereira Varelas da Rocha

July 2020

To Felícia

Acknowledgments

I thank my family and friends for their support and patience during these demanding times. I also acknowledge Professor José Sande Lemos for his availability and for the tenacity and intuition he always presented during our discussions.

Resumo

Uma estrela em colapso pode ser estudada, em primeira aproximação, usando uma distribuição de poeira restricta a condições iniciais semelhantes. Recentemente, desenvolvimentos em condições de junção permitiram os mesmos modelos a serem estudados com menor complexidade matemática. Também permitiram o uso de camadas finas para o mesmo propósito, embora estas permitam mais facilidade de uso. Embora estrelas e camadas finas de poeira aproximem a realidade, as propriedades gerais do colapso gravitacional são preservadas em ambos os modelos. Neste trabalho, aplicamos condições de junção no estudo de estrelas e camadas finas, marginalmente ligadas, ligadas e dispersas, sem rotação e esfericamente simétricas, compostas por poeira. Para todos os casos, calculamos a trajectória da superfície e descrevemos consequentemente a evolução do colapso. No seguimento, obtemos a estrutura causal dos espaços tempo do interior e exterior e revelamos como o colapso e eventual formação do buraco negro se desenrolam. Extendemos o estudo, no caso da camada fina marginalmente ligada, a vários sistemas de coordenadas representando o espaço tempo exterior de Schwarzschild por forma a dar ênfase a diferentes propriedades da sequência de eventos. Adicionalmente, também damos particular atenção às trajectórias das camadas finas dispersas e ligadas, em colapso, e à sua dependência com o parâmetro de energia M. Encontramos os casos limite com o rácio entre a massa da camada, m, e a energia, M. Assim, obtemos o conjunto de possíveis soluções para estrelas e camadas finas feitas de poeira, sem rotação e esfericamente simétricas, em colapso.

Palavras-chave: Camadas Finas, Condições de Junção, Colapso Gravitacional, Buracos Negros, Sistemas de Coordenadas, Gravitação

Abstract

A collapsing star can be studied, to first approximation, by using a distribution of dust with similar initial conditions. More recently, developments in junction conditions allowed the same models to be applied with lesser mathematical complexity. They also allowed thin shells to be used for the same purpose as well, albeit with gained simplicity. While dust stars and thin shells approximate reality, the general features of gravitational collapse are preserved in both models. In this work, we apply the junction conditions to study marginally bound, unbound and bound, non rotating and spherically symmetric, collapsing stars and thin shells of dust. For all cases we find the trajectory of the surface and thus describe the evolution of the collapse. Following that, we obtain the causal structure of the interior and exterior spacetimes and uncover how the collapse and eventual formation of the black hole unfolds. We extend the study, of the marginally bound thin shell, to various coordinate systems representing the exterior Schwarzschild spacetime to bring out different features of the sequence of events. Additionally, we also give particular attention to the trajectories of the unbound and bound collapsing thin shells and their dependency on the energy parameter M. We find the limiting cases with the ratio between the mass of the shell, m, and the energy, M. Thus we obtain the set of possible solutions for collapsing, spherically symmetric, non rotating, stars and thin shells made of dust.

Keywords: Thin Shell, Junction Conditions, Gravitational Collapse, Black Holes, Coordinate Systems, Gravitation

Contents

Acknowledgments . . . v

Resumo . . . vii

Abstract . . . ix

List of Figures . . . xv

Preface . . . xxiii

1 Introduction **1**

1.1 From General Relativity Onwards . . . 1

1.2 Gravitational Collapse and Black Holes . . . 1

1.3 Gravitational Collapse of Thin Shells . . . 3

1.4 Outline of the Thesis . . . 4

2 Collapsing Star: Oppenheimer-Snyder Marginally Bound Case **5**

2.1 Interior spacetime . . . 5

2.2 Exterior spacetime . . . 6

2.3 Application of Junction conditions . . . 7

2.3.1 First condition . . . 7

2.3.2 Second condition . . . 8

2.3.3 Solution . . . 8

2.3.4 Null Geodesics . . . 9

2.3.5 Event Horizon . . . 10

2.3.6 Apparent Horizon . . . 11

2.3.7 Causal Structure . . . 12

2.3.8 Causal Structure in Different Coordinate Systems . . . 12

2.3.9 Other Interior Spacetimes of Different Curvature . . . 13

3 Collapsing Star: Unbound Case **15**

3.1 Interior and Exterior Spacetimes . . . 15

3.2 Application of Junction Conditions . . . 15

3.2.1 Interior Solution . . . 16

3.2.2 Exterior Solution . . . 16

3.2.3 Null geodesics and Event Horizon . . . 17

3.2.4 Apparent Horizon . . . 17
3.2.5 Causal Structure . . . 17

4 Collapsing Star: Bound Case 19

4.1 Interior and Exterior Spacetimes . . . 19
4.2 Application of Junction Conditions . . . 19
4.2.1 Interior Solution . . . 20
4.2.2 Exterior Solution . . . 20
4.2.3 Null geodesics and Event Horizon . . . 21
4.2.4 Apparent Horizon . . . 21
4.2.5 Causal Structure . . . 21

5 Collapsing Thin Shell: Marginally Bound Case 23

5.1 Equation of Motion . . . 23
5.2 Proper Time Solution . . . 23
5.3 Interior Time Solution . . . 25
5.4 Exterior Time Solution . . . 26
5.4.1 Schwarzschild Coordinates . . . 26
5.4.2 Painlevé-Gullstrand Coordinates with $0 \leq E < 1$ . . . 29
5.4.3 Painlevé-Gullstrand Coordinates . . . 31
5.4.4 Painlevé-Gullstrand Coordinates with $E > 1$ . . . 33
5.4.5 Ingoing Eddington-Finkelstein Coordinates . . . 35
5.4.6 Novikov Coordinates . . . 37
5.4.7 Lemaître Coordinates . . . 39
5.4.8 Lemaître Coordinates with $E > 1$ . . . 41
5.4.9 Kruskal-Szekeres Coordinates . . . 44

6 Collapsing Thin Shell: Unbound Case 47

6.1 Equation of Motion . . . 47
6.2 Proper Time Solution . . . 47
6.3 Interior Time Solution . . . 48
6.4 Exterior Time Solution . . . 49
6.4.1 Schwarzschild Coordinates . . . 50
6.5 The limit of test particles, i.e., $m = 0$, and criticality . . . 51

7 Collapsing Thin Shell: Bound Case 53

7.1 Equation of Motion . . . 53
7.2 Proper Time Solution . . . 53
7.3 Interior Time Solution . . . 54
7.4 Exterior Time Solution . . . 56
7.4.1 Schwarzschild Coordinates . . . 56

8 Conclusions 59

A Junction Conditions 61

A.1 Theoretical development 61

A.1.1 First Condition 62

A.1.2 Second Condition 63

A.2 Thin Shells 64

A.2.1 Proper Time Description 64

A.2.2 Interior Time Description 66

A.2.3 Exterior Time Description 67

A.2.4 Newtonian Limit 67

B Oppenheimer-Snyder Collapse as done by Oppenheimer and Snyder 69

B.1 General Solution 69

B.2 Collapse of a Ball of Dust 71

B.3 Asymptotic Limits 75

B.4 The First-Order Partial Differential Equations 76

B.4.1 Solution for $\xi < R$ 77

B.4.2 Solution for $\xi > R$ 78

C Different Coordinate Systems 79

C.1 Schwarzschild Coordinates 80

C.2 Painlevé-Gullstrand Coordinates with $E < 1$ 80

C.3 Painlevé-Gullstrand Coordinates 81

C.4 Painlevé-Gullstrand Coordinates with $E > 1$ 82

C.5 Eddington-Finkelstein Coordinates 83

C.6 Novikov Coordinates 84

C.7 Lemaître Coordinates 86

C.8 Lemaître Coordinates with $E > 1$ 86

C.9 Kruskal-Szekeres Coordinates 90

Bibliography 93

Addendum 95

List of Figures

2.1 A falling particle as seen by a local observer, in proper time represented by a black line, and by an external observer, in its own external time coordinate represented by a blue line. The local observer can see the particle crossing the Schwarzschild radius while the external observer will see the same particle taking an infinite amount of time to reach that same distance. 7

2.2 Trajectory of the collapsing star coming from infinity with zero initial velocity, in blue, as described by (a) an interior comoving observer and (b) an external observer. They contract completely forming a singularity at the center of coordinates at the instants τ_C and T_C respectively. 9

2.3 The causal structure of the (2.3a) interior and (2.3b) exterior spacetimes. The outgoing light rays are shown in thin red lines, with the event horizon being the thick red line. The apparent horizon is shown with a thin black line, the singularity with a undulating black line and the trajectory of the surface of the collapsing star with a thick blue line. The light shaded region represents the region of trapped surfaces and the dark shaded region does not belong to the spacetime and is non physical. 12

2.4 The causal structure of the (2.4a) interior and (2.4b) exterior spacetimes in coordinate systems where null geodesics are diagonal straight lines. The outgoing light rays are shown in thin red lines, with the event horizon being the thick red line. The apparent horizon is shown with a thin black line, the singularity with a undulating black line and the trajectory of the surface of the collapsing star with a thick blue line. The light shaded region represents the region of trapped surfaces and the dark shaded region does not belong to the spacetime and is non physical. 14

3.1 The causal structure of the (3.1a) interior and (3.1b) exterior spacetimes. The outgoing light rays are shown in thin red lines, with the event horizon being the thick red line. The apparent horizon is shown with a thin black line, the singularity with a undulating black line and the trajectory of the surface of the collapsing star with a thick blue line. The light shaded region represents the region of trapped surfaces and the dark shaded region does not belong to the spacetime and is non physical. 18

4.1 The causal structure of the (4.1a) interior and (4.1b) exterior spacetimes. The outgoing light rays are shown in thin red lines, with the event horizon being the thick red line. The apparent horizon is shown with a thin black line, the singularity with a undulating black line and the trajectory of the surface of the collapsing star with a thick blue line. The light shaded region represents the region of trapped surfaces and the dark shaded region does not belong to the spacetime and is non physical. 22

5.1 Marginally bound thin shell collapse measured in proper time for different values of the energy and shell mass parameter, M. The values of the parameter are in natural units. . 24

5.2 Trajectories of thin shell collapsing from infinity for different values of M in the limit $M \to 0$ as seen by a local observer and starting from some initial distance taken to be very large. As the mass decreases, its velocity decreases. For very small masses the shell becomes approximately stationary at infinity. 25

5.3 Collapse of the thin shell reported with respect to the internal time, for different values of the energy and shell mass parameter, M. The values of the parameter are in natural units. 26

5.4 Trajectory of the collapsing thin shell as described by an eternal observer in Schwarzschild coordinates. The trajectory is normalized to the energy or mass parameter of the shell, M. Following Eq. (5.14), $T_c = 0$. 27

5.5 The causal structure of spacetime for $M = m$ in exterior Schwarzschild coordinates and interior Minkowski. The trajectory of the shell is the blue line. In red are drawn the outgoing null rays, with the last one reaching infinity, shown in a thicker line, corresponding to the event horizon. The light shaded region is the region of trapped surfaces and the timelike surface delimiting it, interior to the event horizon, corresponds to the apparent horizon. The dark shaded region is non physical and is used to separate the two different spacetimes. The singularity is the endpoint of the evolution and is shown in a curvilinear line. 29

5.6 Trajectory of the thin shell described in external Painlevé-Gullstrand coordinates with $E < 1$. In this coordinate system no singularity is observed at the Schwarzschild raidus $R = 2M$, but the description does not extend beyond the distance $r_{+0} = 2M/(1 - E^2)$. 30

5.7 The causal structure of spacetime for $M = m$ in exterior Painlevé-Gullstrand coordinates with $E < 1$ and interior Minkowski. The trajectory of the shell is the blue line. In red are drawn the outgoing null rays, with the last one reaching infinity, shown in a thicker line, corresponding to the event horizon. The light shaded region is the region of trapped surfaces and the timelike surface delimiting it, interior to the event horizon, corresponds to the apparent horizon. The dark shaded region is non physical and is used to separate the two different spacetimes. The singularity is the endpoint of the evolution and is shown in a curvilinear line. 31

5.8 Trajectory of the thin shell described in external Painlevé-Gullstrand coordinates. In this coordinate system no singularity is observed at the Schwarzschild radius, $R = 2M$. 32

5.9 The causal structure of spacetime for $M = m$ in exterior Painlevé-Gullstrand coordinates and interior Minkowski. The trajectory of the shell is the blue line. In red are drawn the outgoing null rays, with the last one reaching infinity, shown in a thicker line, corresponding to the event horizon. The light shaded region is the region of trapped surfaces and the timelike surface delimiting it, interior to the event horizon, corresponds to the apparent horizon. The dark shaded region is non physical and is used to separate the two different spacetimes. The singularity is the endpoint of the evolution and is shown in a curvilinear line. 33

5.10 Trajectory of the thin shell described in external Painlevé-Gullstrand coordinates with $E > 1$. In this coordinate system no singularity is observed at the Schwarzschild radius, $R = 2M$. 34

5.11 The causal structure of spacetime for $M = m$ in exterior Painlevé-Gullstrand coordinates with $E > 1$ and interior Minkowski. The trajectory of the shell is the blue line. In red are drawn the outgoing null rays, with the last one reaching infinity, shown in a thicker line, corresponding to the event horizon. The light shaded region is the region of trapped surfaces and the timelike surface delimiting it, interior to the event horizon, corresponds to the apparent horizon. The dark shaded region is non physical and is used to separate the two different spacetimes. The singularity is the endpoint of the evolution and is shown in a curvilinear line. 35

5.12 Trajectory of the thin shell described in external Eddington-Finkelstein coordinates. In this coordinate system the singularity seen in Schwarzschild coordinates at $R = 2M$ is absent. 36

5.13 The causal structure of spacetime for $M = m$ in exterior Eddington-Finkelstein coordinates and interior Minkowski. The trajectory of the shell is the blue line. In red are drawn the outgoing null rays, with the last one reaching infinity, shown in a thicker line, corresponding to the event horizon. The light shaded region is the region of trapped surfaces and the timelike surface delimiting it, interior to the event horizon, corresponds to the apparent horizon. The dark shaded region is non physical and is used to separate the two different spacetimes. The singularity is the endpoint of the evolution and is shown in a curvilinear line. 37

5.14 Trajectory of the thin shell described in external Novikov coordinates, in blue. In red are the outgoing null geodesics obtained in the same manner. In this coordinate system the singularity seen in Schwarzschild coordinates at $R = 2M$ is absent for the shell's trajectory. 38

5.15 The causal structure of spacetime for $M = m$ in exterior Novikov coordinates and interior Minkowski. The trajectory of the shell is the blue line. In red are drawn the outgoing null rays, with the last one reaching infinity, shown in a thicker line, corresponding to the event horizon. The light shaded region is the region of trapped surfaces and the timelike surface delimiting it, interior to the event horizon, corresponds to the apparent horizon. The dark shaded region is non physical and is used to separate the two different spacetimes. The singularity is the endpoint of the evolution and is shown in a curvilinear line. 39

5.16 Trajectory of the thin shell described in external Lemaître coordinates. In this coordinate system the singularity seen in Schwarzschild coordinates at $R = 2M$ is absent. 40

5.17 The causal structure of spacetime for $M = m$ in exterior Lemaître coordinates and interior Minkowski. The horizontal axis represents r_- for the interior region and ρ for the exterior, while the vertical axis represents t_- and τ respectively. The trajectory of the shell is the blue line. In red are drawn the outgoing null rays, with the last one reaching infinity, shown in a thicker line, corresponding to the event horizon. The light shaded region is the region of trapped surfaces and the timelike surface delimiting it, interior to the event horizon, corresponds to the apparent horizon. The dark shaded region is non physical and is used to separate the two different spacetimes. The singularity is the endpoint of the evolution and is shown in a curvilinear line. 41

5.18 Trajectory of the thin shell described in external Lemaître coordinates with energy parameter $E > 1$. In this coordinate system the singularity seen in Schwarzschild coordinates at $R = 2M$ is absent. 42

5.19 The causal structure of spacetime for $M = m$ in exterior Lemaître coordinates with energy parameter $E > 1$ and interior Minkowski. The horizontal axis represents r_- for the interior region and ρ for the exterior, while the vertical axis represents t_- and τ respectively. The trajectory of the shell is the blue line. In red are drawn the outgoing null rays, with the last one reaching infinity, shown in a thicker line, corresponding to the event horizon. The light shaded region is the region of trapped surfaces and the timelike surface delimiting it, interior to the event horizon, corresponds to the apparent horizon. The dark shaded region is non physical and is used to separate the two different spacetimes. The singularity is the endpoint of the evolution and is shown in a curvilinear line. 44

5.20 Trajectory of the thin shell described in external Kruskal-Szekeres coordinates. In this coordinate system the singularity seen in Schwarzschild coordinates at $R = 2M$ is absent. 45

5.21 The causal structure of spacetime for $M = m$ in exterior Kruskal-Szekeres coordinates and interior Minkowski. The trajectory of the shell is the blue line. In red are drawn the outgoing null rays, with the last one reaching infinity, shown in a thicker line, corresponding to the event horizon. The light shaded region is the region of trapped surfaces and the spacelike surface delimiting it, interior to the event horizon, corresponds to the apparent horizon. The dark shaded region is non physical and is used to separate the two different spacetimes. The singularity is the endpoint of the evolution and is shown in a curvilinear line. 46

6.1 With blue lines, the unbound thin shell collapse measured in proper time for different values of the rest mass of the shell, m, in relation to its energy parameter M. The dashed black line shows the trajectory of the marginally bound collapsing shell, studied in chapter 5. 48

6.2 With blue lines, the unbound shell collapse measured in internal time for different values of the rest mass of the shell, m, in relation to its energy parameter M. The dashed black line represents the trajectory of the marginally bound collapsing shell, studied in chapter 5. The dashed red line represents an ingoing null geodesic. 49

6.3 With blue lines, the unbound thin shell collapse in exterior Schwarzchild coordinates for different values of the shell's rest mass, m, relative to its energy parameter M. The dashed black line represents the trajectory of the marginally bound collapsing shell, studied in chapter 5. The dashed red line represents an ingoing null geodesic. 50

6.4 The causal structure of spacetime for $M > m$, i.e. the unbound case, in exterior Schwarzschild coordinates and interior Minkowski. The trajectory of the shell is the blue line. In red are drawn the outgoing null rays, with the last one reaching infinity, shown in a thicker line, corresponding to the event horizon. The light shaded region is the region of trapped surfaces and the spacelike surface delimiting it, interior to the event horizon, corresponds to the apparent horizon. The dark shaded region is non physical and is used to separate the two different spacetimes. The singularity is the endpoint of the evolution and is shown in a curvilinear line. 51

6.5 Trajectories of different shell in the limit of $m \to 0$, as seen by the local observer 52

6.6 (6.6a) Black hole formation and (6.6b) matter dispersion in the collapse of test particles obtained in the $m \to 0$ limit of the unbound shell collapse. The diagrams correspond to causal structures of the whole spacetime, with the interior Minkowski and exterior Schwarzschild regions represented. Red lines represent outgoing light rays and the non horizontal thick black line is the trajectory of the shell. On the black hole formation, the resulting singularity is found to be null, represented by an undulating black line parallel to the red line in (6.6a). 52

7.1 With blue lines, the bound shell collapse measured in proper time for different values of the rest mass of the shell, m, relative to its energy parameter M. These trajectories can be separated into two categories, those of $M < m < 2M$ in Figure 7.1a, and those of $m > 2M$ in Figure 7.1b. The dashed black line represents the trajectory of the marginally bound collapsing shell studied in chapter 5. 54

7.2 With blue lines, the bound shell collapse measured in internal time for different values of the rest mass of the shell, m, relative to its energy parameter M. These trajectories can be separated into two categories, those of $M < m < 2M$ in Figure 7.2a, and those of $m > 2M$ in Figure 7.2b. The dashed black line represents the trajectory of the marginally bound collapsing shell, studied in chapter 5. The dashed red line represents an ingoing null geodesic. 55

7.3 With blue lines, the bound shell collapse measured in external Schwarzschild time for different values of the rest mass of the shell, m, relative to its energy parameter M. These trajectories can be separated into two categories, those of $M < m < 2M$ in Figure 7.3a, and those of $m > 2M$ in Figure 7.3b. The dashed black line represents the trajectory of the marginally bound collapsing shell, studied in chapter 5. The dashed red line represents an ingoing null geodesic. 57

7.4 The causal structure of spacetime for $M < m$, bound case, in exterior Schwarzschild coordinates and interior Minkowski. The trajectory of the shell is the blue line. In red are drawn the outgoing null rays, with the last one reaching infinity, shown in a thicker line, corresponding to the event horizon. The light shaded region is the region of trapped surfaces and the spacelike surface delimiting it, interior to the event horizon, corresponds to the apparent horizon. The dark shaded region is non physical and is used to separate the two different spacetimes. The singularity is the endpoint of the evolution and is shown in a curvilinear line. 58

A.1 The two spacetimes separated by a timelike hypersurface. Each spacetime is described in its own coordinate system, x^α_- and x^α_+ for the interior and exterior respectively. The four vector n^α is the normal to the hypersurface. 62

C.1 The relations between the different coordinate systems, representing the Schwarzschild spacetime, reviewed for one and two coordinate transformations. The Novikov and Kruskal-Szekeres coordinate systems are maximal extensions of the Schwarzschild spacetime, while the Lemaître coordinate system and its generalization to $E > 1$ are not. The generalization of the Gullstrand-Painlevé coordinate system gives the Eddington-Finkelstein coordinate system as a limit case, of $E \to \infty$. The same does not occur between the generalization of the Lemaître coordinate system to $E > 1$ and the Kruskal-Szekeres coordinate system. 80

C.2 The null congruence for the black hole solution in Schwarzschild coordinates is displayed. For $r > 2M$ in red are the outgoing null geodesics and in blue are the ingoing null geodesics. For $r < 2M$ they are switched, red are ingoing and blue outgoing. The undulating line represents the singularity at the center of spatial coordinates. The dashed line represents the event horizon, at $r = 2M$. 81

C.3 The null congruence for the black hole solution in Painlevé-Gullstrand coordinates, with $E < 1$, is displayed. In red are the outgoing null geodesics and in blue are the ingoing null geodesics. The undulating line represents the singularity at the center of spatial coordinates. The dashed line represents the event horizon, $r = 2M$. Due to the coordinate transformation, Eq. (C.3), the ingoing null geodesics do not display any discontinuity at the event horizon. 82

C.4 The null congruence for the black hole solution in Painlevé-Gullstrand coordinates is displayed. In red are the outgoing null geodesics and in blue are the ingoing null geodesics. The undulating line represents the singularity at the center of spatial coordinates. The dashed line represents the event horizon, $r = 2M$. Due to the coordinate transformation, Eq. (C.6), the ingoing null geodesics do not display any discontinuity at the event horizon. 83

C.5 The null congruence for the black hole solution in Painlevé-Gullstrand coordinates, with $E > 1$, is displayed. In red are the outgoing null geodesics and in blue are the ingoing null geodesics. The undulating line represents the singularity at the center of spatial coordinates. The dashed line represents the event horizon, $r = 2M$. Due to the coordinate transformation, Eq. (C.9), the ingoing null geodesics do not display any discontinuity at the event horizon. 84

C.6 The null congruence for the black hole solution in Eddington-Finkelstein coordinates is displayed. In red are the outgoing null geodesics and in blue are the ingoing null geodesics. The undulating line represents the singularity at the center of spatial coordinates. The dashed line represents the event horizon, $r = 2M$. Due to the coordinate transformation, Eq. (C.12), the ingoing null geodesics do not display any discontinuity at the event horizon. 85

C.7 The null congruence in Novikov coordinates is displayed. In red are the outgoing null geodesics and in blue are the ingoing null geodesics. The undulating line at the top represents the black hole singularity, and the one at the bottom the white hole singularity. The dashed lines represent the event horizon, $r = 2M$, of each solution. With the coordinate transformations, Eqs. (C.3) and (C.20), outgoing and ingoing null geodesics become continuous through the event horizon. 86

C.8 The null congruence for the black hole solution in Lemaître coordinates is displayed. In red are the outgoing null geodesics and in blue are the ingoing null geodesics. The undulating line represents the singularity at the center of spatial coordinates. The dashed line represents the event horizon, $r = 2M$. 87

C.9 The null congruence for the black hole solution in generalized Lemaître coordinates, with energy $E > 1$, is displayed. In red are the outgoing null geodesics and in blue are the ingoing null geodesics. The undulating line represents the singularity at the center of spatial coordinates. The dashed line represents the event horizon, $r = 2M$. 88

C.10 The null congruence in Kruskal-Szekeres is displayed. In red are the outgoing geodesics and in blue are the ingoing null geodesics. The undulating line at the top represents the black hole singularity, and the one at the bottom the white hole singularity. The dashed lines represent the event horizon, $r = 2M$, of each solution. 92

Preface

I declare that this thesis is not substantially the same as any that I have submitted for a degree, diploma or other qualification at any other university and that no part of it has already been or is concurrently submitted for any such degree, diploma or other qualification.

The research presented in this thesis has been carried out at Centro de Astrofísica e Gravitação - CENTRA, in the Physics Department of Instituto Superior Técnico. This work was done in collaboration with my supervisor Prof. José Sande Lemos.

The works presented in this thesis are:

Chapters 2, 3, and 4, on Oppenheimer-Snyder collapse, are the outcome of my research through the important papers on the subject, with the presentation of the collapse in several coordinate systems being new.

Chapters 5, 6, and 7, on thin-shell collapse, are also the outcome of my research through the original papers, with the presentation of the collapse in several coordinate systems being new. The possibility of a bouncing solution in the zero mass unbound case, that can either yield a naked singularity or a black hole, is new and makes a connection to the Choptuik's critical case of scalar field collapse.

Appendix A describes the junction condition and thin shell formalism in general relativity that are necessary for chapters 2 to 7.

Appendix B presents the Oppenheimer-Snyder collapse as done in the original paper with all the passages spelt out, so is useful as these, with some of them being difficult to work out, cannot be found in the literature.

Appendix C presents the Schwarzschild spacetime in several coordinate systems, which in turn are used in the gravitational collapse chapters 2 to 7. In particular we find that the infinite energy limit, $E \to \infty$, of the Lemaître extension of the Schwarzschild metric ends in Minkowski spacetime, a totally unexpected development and a new result.

The addendum, written as an aftermath of the thesis, presents a new way of maximally extending the Schwarzschild metric, unifying the known extensions from Painlevé-Gullstrand to Kruskal-Szekeres. It is a paper submitted to publication that has already appeared in the arXiv. The reference is: J. P. S. Lemos and D. L. F. G. Silva, Maximal extension of the Schwarzschild metric: From Painlevé-Gullstrand to Kruskal-Szekeres, arXiv:2005.14211 [gr-qc].

Chapter 1

Introduction

1.1 From General Relativity Onwards

The phenomena of gravitational collapse was a remarkable and non trivial consequence of Einstein's theory of general relativity [1]. Despite the complexity in solving the field equations, a set of ten coupled partial differential equations, the first solution came just one year after, by the hand of Schwarzschild [2]. Assuming a non rotating, non charged, spherically symmetric source surrounded by vacuum, Schwarzschild found the resulting line element

$$\mathrm{d}s^2 = -\left(1 - \frac{2M}{r}\right)\mathrm{d}t^2 + \left(1 - \frac{2M}{r}\right)^{-1}\mathrm{d}r^2 + r^2(\mathrm{d}\theta^2 + \sin^2\theta\,\mathrm{d}\phi^2)\,, \tag{1.1}$$

with M a constant of integration identified with the mass of the point source. This solution displayed some non trivial properties. Among them were the two singularities, at the center of spatial coordinates $r = 0$ and at the Schwarzschild radius $r = r_S = 2M$. The $r = 2M$ singularity is seen to be a coordinate singularity, characteristic of the coordinates (t, r, θ, ϕ) and removable with appropriate coordinate transformations. The $r = 0$ singularity, however, is a true singularity. Additionally, the coordinates t and r switch characters as one goes inside the null surface with radius equal to the Schwarzschild radius, thus distinguishing this region.

1.2 Gravitational Collapse and Black Holes

By 1939, it was known a star with sufficient mass would not end as a neutron star [3]. Interested in understanding the fate of such object, Oppenheimer and Snyder studied the evolution of a massive star left to collapse [4]. Using a static, spherically symmetric star made of dust, i.e. frictionless material, no radiation or ejecta would be emitted, making the exterior a Schwarzschild spacetime. For the interior a cosmological model worked on by Tolman [5] was used. With these considerations, they found such an object would contract without stop, converging on the singularity at $r = 0$. Additionally, any observer on the star's surface would fall below the null surface of radius $r = 2M$ and be cut off the exterior universe.

Without any form of communicating, the event would trap any object, including light, that fell inside the $r = 2M$ surface. Indeed, while the absence of pressure would present itself a significant simplification, the resulting forces resulting from pressure would not be critical should the star be massive enough. As such, the description found by Oppenheimer and Snyder would describe a possible event. Such an object, one contracted beyond the null surface of radius $r = 2M$, would later be known as black hole [6], and their existence would be confirmed by the Event Horizon Telescope (EHT) in 2019 [7].

Other models would be used afterwards to study gravitational collapse under different conditions. In the book by Novikov and Frolov [8], building on Tolman's model, the black and white hole solutions are studied using Lemaître and Eddington-Finkelstein coordinate systems.

While the gravitational collapse saw great use in the study of stellar evolution and development of cosmological models, solving the field equations with the appropriate conditions was a significant hurdle. Naturally, the development of mathematical tools suited to solve the particular problems of collapsing distributions of matter and energy was sought after. In this front, a set of conditions relating the interior and exterior spacetimes were developed independently by Darmois [9], Misner and Sharp [10], and by Israel [11]. These junction conditions offset the need to construct a spacetime valid in the whole domain, allowing the solving on each region independently.

An example of the versatility of the junction conditions can be seen in the thesis of Beckedorff [12], followed by Misner, Thorne and Wheeler [13], where for the interior space a Friedmann-Lemaître-Robertson-Walker (FLRW) metric with positive curvature is used. The solution by Oppenheimer and Snyder can be seen to be equivalent to using a FLRW metric with zero curvature for the interior. The same solution was obtained by Hartle [14]. In other words, this solution corresponds to a star collapsing from infinity with zero initial velocity, i.e. the marginally bound case. For collapsing interior solutions, see also [15].

One particular area that has garnered much attention corresponds to the gravitational collapse of a minimally coupled scalar field. A scalar field presents the simplest choice to evaluate the non linear response of the field equations to a quantized description of matter. Christodoulou, in an exhaustive work [16], proved the existence of general solutions of gravitational collapse in these conditions, with the asymptotic formation of a black hole. Choptuik [17] found self similar solutions displaying phase transitions around a critical value for strength of the gravitational interactions, p. Should the value of this parameter be below a critical value, the scalar field would contract but then disperse. On the other hand, if the value of the parameter stands above the critical value p_c, a black hole forms with a mass given by $M_{BH} = |p - p_c|^{\gamma}$, with γ an exponent found to be universal between different families of scalar field solutions. This peculiar phenomena has seen extensive work with generalization to different types of matter and distributions. For an example in alternative theories of gravitation, see the work by Rocha and Tomašević [18] on critical collapse in Einstein-Maxwell-dilaton theories. For a comprehensive overview of this field, see the review by Gundlach and Martín-García [19].

Aside from black hole formation, gravitational collapse has also been used to gauge the cases where naked singularities could form. For example, Joshi, Dadhich and Maartens [20] showed, should the shear of a inhomogeneous, marginally bound, collapsing sphere of dust be strong enough, then the formation of the apparent horizon will be delayed indefinitely. This effectively means a naked singularity is formed. Later Mena, Nolan and Tavakol [21] showed the generalized case, of bound and unbound collapse, further required complete knowledge of both the initial shear and density inhomogeneity profiles in order to uniquely determine the formation of naked singularities.

1.3 Gravitational Collapse of Thin Shells

The junction conditions were well suited for the study of collapsing massive stars. Remarkably, they had an additional feature, in that junction conditions naturally allowed for thin shell distributions of matter and energy. Thin shells revealed themselves able to preserve the general features of gravitational collapse, by very much the same reasons one could ignore pressure, but were mathematically simpler to work with. Additionally thin shells have their own particular uses, such as acting as layers separating distinct spacetimes, e.g. composed of distinct types of matter, or in cosmological models as a separation between two phases of resulting from a phase transition [22].

It follows naturally that thin shells saw great interest as tools to complement the study of gravitational collapse. See for example the work by Adler, Bjorken, Chen and Liu [23] where stars of pressureless matter and thin light shells are used to study the formation of black and white holes, using Eddington-Finkelstein and Painlevé-Gullstrand coordinate systems. One sees immediately the power of the junction conditions, allowing for general results, while retaining simplicity. Indeed, its usefulness motivated the continued development of the junction conditions, as one may see in the work by Barrabès and Israel on the collapse of lightlike thin shells [24]. For a modern approach using a distributional formalism, see the book by Poisson [25]. As a result, thin shells have been used extensively. For example, thin shells have been used by Lynden-Bell and Lemos [26] to obtain the marginally bound Newtonian self-similar solutions of Penston [27] in general relativity, later extended to include the bound and unbound solutions [28]. Similarly, collapsing thin shells allowed to rebound have been used by Israel [29] as a model to understand asymmetric collapse. In this, the possibility of particle-antiparticle annihilation was hypothesized as a consequence of the time reversal inside the event horizon coupled with the degree of asymmetry in the collapsing star.

The study of collapsing bodies has also been used to make new predictions in several extensions to general relativity with higher dimensions. For example, Gao and Lemos [30] have applied an extension of the junction conditions to higher dimensions in order to study the dynamics of charged thin shells of dust and the strength of the cosmic censorship conjecture. For another example, see the work by Dias and Lemos [31] on the formation and stability of wormholes from thin shells in higher dimensional spaces. Indeed, as gravity should extend to any extra dimensions, gravitational collapse may be used to probe the features of higher dimensional topologies. Davis [32] studied the applicability of the junction condition formalism on the five dimensional Gauss-Bonnet brane theory. The inherent difficulties of this method led Crisóstomo and Olea [33] to generalize the Hamiltonian formalism developed by Hájíček and Kijowski [34] to d dimensional spacetimes. For an example of its application see the work by Dias, Gao and Lemos [35] on the formation of singularities from charged thin shells in Lovelock gravity. As such, the phenomena of gravitational collapse has seen wide adoption as a means to understand the features present in diverse extensions to gravitation.

1.4 Outline of the Thesis

In this thesis we study the gravitational collapse of dust stars and thin shells, looking for the generalized solutions in each range of energies, i.e. the bound, marginally bound and unbound cases. In chapter 2 we evaluate the case studied by Oppenheimer and Snyder, i.e. that of a collapsing star made of dust, using the modern approach with junction conditions. In chapter 3 we repeat the study for a star that starts its collapse coming from infinity with initial non zero velocity, i.e. an unbound star. In chapter 4 we repeat the formalism for a star that starts its collapse at rest from finite distance, i.e. a bound star. In chapter 5 we study the thin shell that initiates its collapse at rest from infinity, i.e. the marginally bound thin shell, mirroring the case studied by Oppenheimer and Snyder. In chapter 6 we study the collapsing unbound thin shell. In chapter 7 we study the collapsing bound thin shell. In chapter 8 we present the conclusions of this work. Additionally, a review of the junction conditions formalism is given in appendix A, a review of the original article by Oppenheimer and Snyder is given in appendix B and a review on the different coordinate systems representing the Schwarzschild spacetime is given in appendix C.

Chapter 2

Collapsing Star: Oppenheimer-Snyder Marginally Bound Case

The inability to find a static line element for a star of mass over $0.7M_{\odot}$ [3] suggests such a massive star, one that has used all its thermonuclear sources of energy, cannot form a stable neutron core. In this case, the neutron degeneracy pressure of the core would prove insufficient and the star would further collapse under its own gravitational field. In these circumstances, the question remains whether the star would evolve towards a new state of equilibrium or if it would contract continuously. To answer this, J.R. Oppenheimer and H. Snyder studied the qualitative features of spherically symmetric gravitational collapse using as a simple model a body made of dust [4]. The method employed by Oppenheimer and Snyder is studied in Appendix B. Here we will solve the same problem using junction conditions, reviewed in Appendix A. The conditions we will be using are

$$[h_{ab}] = 0\,, \tag{2.1}$$

$$[K_{ab}] = 0\,, \tag{2.2}$$

with h_{ab} the induced metric and K_{ab} the extrinsic curvature. For simplicity, we will ignore the influence of any escaping matter or radiation which could be ejected during the process of contraction. Furthermore, we will take the system to be non rotating. Accordingly, the line element will be spherically symmetric, and outside of the boundary of the star, it will also be static.

2.1 Interior spacetime

The interior spacetime will be that corresponding to a massive body. For simplicity we will be taking the mass distribution to be homogeneous and the pressure to be zero, that is, the body is considered to be composed of dust. Accordingly, the associated stress-energy tensor is then given by

$$T^{\alpha\beta} = \rho_0\, u^{\alpha}\, u^{\beta}\,, \tag{2.3}$$

with ρ_0 the energy density of the body, taken independent of the distance from the center, and u^α its velocity field.

Under these considerations there is a natural choice for the system of coordinates for the interior in those that accompany the collapse of the body, i.e. a comoving system of coordinates. In particular we take these in the form of a Friedmann-Lemaître-Robertson-Walker (FLRW) metric,

$$\mathrm{d}s^2 = -\mathrm{d}\tau^2 + \xi^2(\tau)\left[\frac{\mathrm{d}a^2}{1-k\,a^2} + a^2\left(\mathrm{d}\theta^2 + \sin^2\theta\,\mathrm{d}\phi^2\right)\right]\,, \tag{2.4}$$

where $\xi(\tau)$ is the scale factor of the spacetime, τ is the proper time, $a \in [0, A]$ is the radial coordinate, k is the curvature of space. Here we consider the particular case where the body collapses starting from infinity at rest. This case is equivalent to an open universe of zero curvature, i.e. the case where $k = 0$, giving thus

$$\mathrm{d}s^2 = -\mathrm{d}\tau^2 + \xi^2(\tau)\left[\mathrm{d}a^2 + a^2\left(\mathrm{d}\theta^2 + \sin^2\theta\,\mathrm{d}\phi^2\right)\right]\,, \tag{2.5}$$

2.2 Exterior spacetime

Taking a static, non rotating and spherically symmetric spacetime in vacuum then, by Birkhoff's theorem, it must be a Schwarzschild spacetime. This can be written in Schwarzschild coordinates,

$$\mathrm{d}s^2 = -\left(1-\frac{2M}{r}\right)\mathrm{d}t^2 + \left(1-\frac{2M}{r}\right)^{-1}\mathrm{d}r^2 + r^2(\mathrm{d}\theta^2 + \sin^2\theta\,\mathrm{d}\phi^2)\,, \tag{2.6}$$

with M the gravitational mass of the star. This coordinate system has a known coordinate singularity at $r = 2M$ the gravitational radius, also called the Schwarzschild radius. In this system of coordinates, the analogous case of a local observer falling from infinity starting at rest [36] follows

$$\frac{\mathrm{d}r}{\mathrm{d}\tau} = -\left(\frac{2M}{r}\right)^{\frac{1}{2}}\,. \tag{2.7}$$

Thus the local observer will report approaching the Schwarzschild radius with a velocity that tends to that of light. The solution is

$$\tau(r) = \mathrm{C} - \frac{2}{3(2M)^{1/2}}r^{3/2}\,, \tag{2.8}$$

with C a constant of integration. On the other hand, the external observer will report a decrease in speed by a factor $(1-2M/r)$,

$$\frac{\mathrm{d}r}{\mathrm{d}t} = -\left(1-\frac{2M}{r}\right)\left(\frac{2M}{r}\right)^{1/2}\,, \tag{2.9}$$

and thus the external observer will report that the falling particle slows down as it approaches the Schwarzschild radius and never crosses it. The solution is

$$t(r) = \mathrm{C} - \frac{2}{3(2M)^{1/2}}\left(r^{3/2} + 6M\,r^{1/2}\right) + 2M\ln\left|\frac{r^{1/2}+(2M)^{1/2}}{r^{1/2}-(2M)^{1/2}}\right|\,, \tag{2.10}$$

with C a constant of integration. Thus different observers will report different outcomes, Figure 2.1.

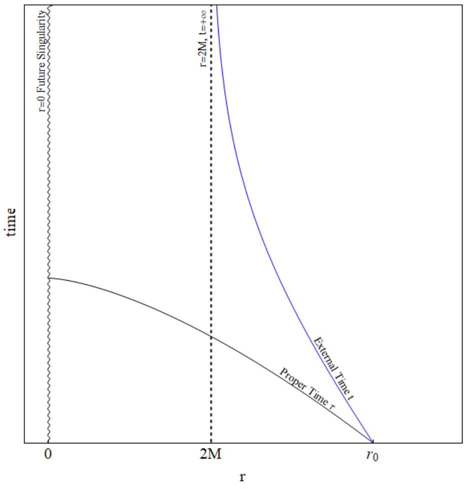

Figure 2.1: A falling particle as seen by a local observer, in proper time represented by a black line, and by an external observer, in its own external time coordinate represented by a blue line. The local observer can see the particle crossing the Schwarzschild radius while the external observer will see the same particle taking an infinite amount of time to reach that same distance.

While an external observer reports a singularity in the trajectory of the falling particle, this can be identified as a coordinate singularity. No scalar invariant can be found for which $r = 2M$ is a singularity. There is another singularity at the center of coordinates, $r = 0$, and the Kretschmann scalar shows this to be a proper singularity

$$K_S = R_{\alpha\beta\gamma\delta}\, R^{\alpha\beta\gamma\delta} = \frac{48M^2}{r^6}\,, \tag{2.11}$$

which is singular at $r = 0$.

2.3 Application of Junction conditions

Following from the previous, the two chosen metrics will be compatible if they verify the two junction conditions, Eqs. (2.1) and (2.2). Now we apply those.

2.3.1 First condition

From the condition that the metric must be continuous when evaluated over the surface of separation, Eq. (2.1), one finds for the previous two metrics, Eqs. (2.5) and (2.6),

$$1 = \left(1 - \frac{2M}{R}\right)\dot{T}^2 - \left(1 - \frac{2M}{R}\right)^{-1}\dot{R}^2\,, \tag{2.12}$$

$$R = \xi\, A\,, \tag{2.13}$$

where R and A are the Schwarzschild and FRLW radial coordinates of the surface of the star, respectively, and T is the Schwarzschild time coordinate of the surface of the star.

2.3.2 Second condition

Since there is no surface stress-energy tensor present, the second junction condition, Eq. (2.2), implies continuity of the extrinsic curvature. Thus we begin by obtaining the extrinsic curvature tensorial elements $K_{ab} = n_{\alpha;\beta} e^{\alpha}_{\ a} e^{\beta}_{\ b}$, Eq. (A.7), finding for the interior spacetime

$$
\begin{aligned}
{K_-}^{\tau}{}_{\tau} &= 0\,, && (2.14)\\
{K_-}^{\theta}{}_{\theta} &= -\frac{1}{\xi\, A}\,, && (2.15)\\
{K_-}^{\phi}{}_{\phi} &= {K_-}^{\theta}{}_{\theta}\,. && (2.16)
\end{aligned}
$$

For the exterior spacetime the same procedure gives

$$
\begin{aligned}
{K_+}^{\tau}{}_{\tau} &= -\frac{\ddot{R} + M/R^2}{\dot{T}\,(1-2M/R)}\,, && (2.17)\\
{K_+}^{\theta}{}_{\theta} &= -\dot{T}\frac{1}{R}\left(1-\frac{2M}{R}\right)\,, && (2.18)\\
{K_+}^{\phi}{}_{\phi} &= {K_+}^{\theta}{}_{\theta}\,. && (2.19)
\end{aligned}
$$

The second junction condition, reduced to continuity of the extrinsic curvature over the surface, Eq. (2.2), then gives

$$
\begin{aligned}
\ddot{R} &= -\frac{M}{R^2}\,, && (2.20)\\
\dot{R}^2 &= \frac{2M}{R}\,. && (2.21)
\end{aligned}
$$

where Eq. (2.21) is seen to imply Eq. (2.20) directly by differentiation.

2.3.3 Solution

Both differential equations, Eqs. (2.20) and (2.21), represent the same system. In particular, Eq. (2.21) is seen to be equal to that describing the falling particle in Schwarzschild coordinates, Eq. (2.7) and the exterior spacetime is Schwarzschild for both cases considered. Thus, the solutions for the trajectory of the surface of the collapsing body in the interior and exterior coordinate systems take the forms of Eqs. (2.8) and (2.10) respectively,

$$
\tau(R) = \frac{2}{3}\frac{R_0^{3/2}}{(2M)^{1/2}}\left[1-\left(\frac{R}{R_0}\right)^{3/2}\right] \implies R(\tau) = \left(1-\frac{3}{2}\frac{(2M)^{1/2}}{R_0^{3/2}}\tau\right)^{2/3} R_0\,, \qquad (2.22)
$$

$$
T(R) = T_0 - \frac{2}{3(2M)^{1/2}}\left(R^{3/2} + 6M\,R^{1/2}\right) + 2M\,\ln\left|\frac{R^{1/2}+(2M)^{1/2}}{R^{1/2}-(2M)^{1/2}}\right|\,, \qquad (2.23)
$$

with $T_0 = T(0)$ a constant denoting the time at which total contraction occurs, the constant C of Eq. (2.8) chosen so that $R(0) = R_0$ and $R \in [0, +\infty[$. The trajectories described by Eqs. (2.22) and (2.23) are shown in Figures 2.2a and 2.2b respectively.

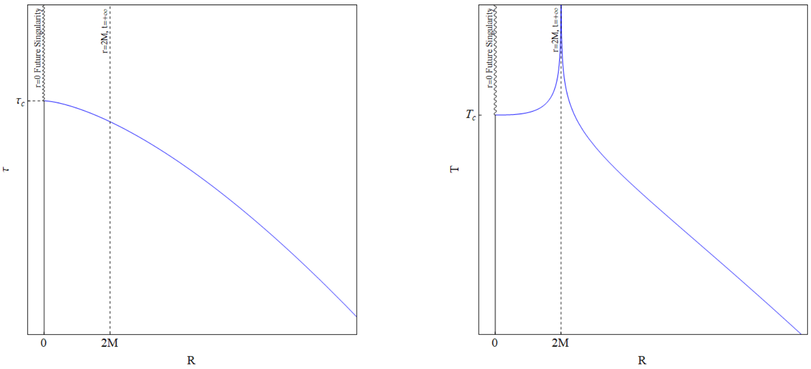

(a) Proper time trajectory.

(b) Exterior time trajectory.

Figure 2.2: Trajectory of the collapsing star coming from infinity with zero initial velocity, in blue, as described by (a) an interior comoving observer and (b) an external observer. They contract completely forming a singularity at the center of coordinates at the instants τ_C and T_C respectively.

From Eqs. (2.22) and (2.13) one can identify the scale factor of the spacetime, $\xi(\tau)$, with

$$\xi(\tau) = \left(1 - \frac{3}{2}\frac{(2M)^{1/2}}{R_0^{3/2}}\tau\right)^{2/3} , \tag{2.24}$$

and $A = R_0$.

Analysis of the differential equation defining the velocity of the system, Eq. (2.21), shows the star starts collapsing from infinity beginning at rest. Such is a consequence of the interior spacetime being taken with zero curvature. Furthermore, this implies the proper time in the interior solution, Eq. (2.22), is defined as $\tau \in]-\infty, \tau_c]$, with the the collapse proper time, τ_c, being

$$\tau_c = \frac{2}{3}\frac{R_0^{3/2}}{(2M)^{1/2}} . \tag{2.25}$$

The Schwarzschild time coordinate of the exterior solution is defined as $t \in]-\infty, \infty]$.

2.3.4 Null Geodesics

From the identification of the scale factor of the interior spacetime, Eq. (2.24), one can then deduce the null geodesics there. This, coupled with the usual solution for null geodesics in the exterior spacetime, i.e. Schwarzschild spacetime, allows one to build the causal structure of whole spacetime for the collapsing star. Accordingly, we start by applying the scale factor, Eq. (2.24), to the interior metric, Eq. (2.5), and set $\mathrm{d}s = \mathrm{d}\theta = \mathrm{d}\phi = 0$, obtaining the differential equation

$$\frac{\mathrm{d}a}{\mathrm{d}\tau} = \pm\left(1 - \frac{3}{2}\frac{(2M)^{1/2}}{R_0^{3/2}}\tau\right)^{-2/3} , \tag{2.26}$$

with the plus sign for the geodesics of outgoing light rays and the minus sign for the geodesics of ingoing light rays. The solution to Eq. (2.26) is

$$a = a_0 \pm \frac{2R_0^{3/2}}{(2M)^{1/2}} \left[\left(1 - \frac{3}{2} \frac{(2M)^{1/2}}{R_0^{3/2}} \tau_0 \right)^{1/3} - \left(1 - \frac{3}{2} \frac{(2M)^{1/2}}{R_0^{3/2}} \tau \right)^{1/3} \right] , \tag{2.27}$$

with the plus and minus signs representing the geodesics of outgoing and ingoing light rays, respectively, emitted from a_0 at the instant τ_0. The null geodesics extend through spacetime, from the point of emission, until the instant τ_f wherein ingoing null geodesics converge on the singularity and outgoing null geodesics either reach the surface or converge on the singularity as well. For ingoing light rays we set $a = R_0$ and $a_0 = 0$, while for outgoing light rays we set $a = 0$ and $a_0 = R_0$. Both cases give

$$\tau_f = \frac{2}{3} \frac{R_0^{3/2}}{(2M)^{1/2}} - \frac{2}{3} \frac{R_0^{3/2}}{(2M)^{1/2}} \left[\left(1 - \frac{3}{2} \frac{(2M)^{1/2}}{R_0^{3/2}} \tau_0 \right)^{1/3} - \frac{1}{2} \left(\frac{2M}{R_0} \right)^{1/2} \right]^3 , \tag{2.28}$$

which is seen to be smaller than the instant of total contraction, i.e. $\tau_f \leq \tau_c$, as expected.

For the exterior spacetime, the differential equation for null geodesics is

$$\frac{\mathrm{d}t}{\mathrm{d}r} = \pm \left(1 - \frac{2M}{r} \right)^{-1} , \tag{2.29}$$

with the plus and minus signs for the geodesics of outgoing and ingoing light rays, respectively. The solutions of Eq. (2.29) are

$$t = t_0 \pm \left(r - r_0 + 2M \ln \left| \frac{r - 2M}{r_0 - 2M} \right| \right) , \tag{2.30}$$

with the plus and minus signs for outgoing and ingoing light rays, emitted from r_0 at t_0, respectively.

2.3.5 Event Horizon

The event horizon is defined by the last light ray reaching infinity. From the null geodesics in Schwarzschild spacetime, described by Eq. (2.30), one finds

$$\lim_{r \to 2M} t = \infty \, , \tag{2.31}$$

so that the event horizon is a null surface with radius equal to the Schwarzschild radius, $r = 2M$. For the interior spacetime, one thus takes the event horizon as being defined by the light ray that reaches the surface as this crosses $r = 2M$ during contraction. Taking the result from the first junction condition relating the two coordinate systems, Eq. (2.13), one gets

$$2M = \xi(\tau_f) \, R_0 \, , \tag{2.32}$$

where we identify the appropriate limits, $r \to 2M$, $a \to R_0$ and use the proper time where the light ray reaches the surface, τ_f, given by Eq. (2.28). From this, and applying the scale factor, Eq. (2.24), we find the event horizon reaches the surface, $a = R_0$, at the instant

$$\tau^{(EH)} = \frac{2}{3}\frac{R_0^{3/2}}{(2M)^{1/2}} - \frac{2}{3}(2M)\,, \tag{2.33}$$

and applying the equation describing outgoing light rays in the interior spacetime, Eq. (2.27), we find the event horizon is emitted from the center, $a = 0$, at the instant

$$\tau_0^{(EH)} = \frac{2}{3}\frac{R_0^{3/2}}{(2M)^{1/2}} - \frac{9}{4}(2M)\,. \tag{2.34}$$

2.3.6 Apparent Horizon

The apparent horizon is defined by the boundary of the region of trapped surfaces [37]. J. B. Hartle derives the equation describing the boundary by considering the convergence of light rays for a different interior spacetime [14]. Similarly, we begin by considering the area of spherical flash of light

$$A = 4\pi r^2 = 4\pi\xi^2(\tau)a^2\,, \tag{2.35}$$

and check when an infinitesimal increase in the parameter parametrizing the equation, here the proper time τ, leads to a halt in the growth rate of the area. Thus we get

$$\left.\frac{\mathrm{d}A(\tau_0+\lambda)}{\mathrm{d}\lambda}\right|_{\lambda\to 0} = 0 \iff \left.\frac{\mathrm{d}}{\mathrm{d}\lambda}\left[\xi(\tau_0+\lambda)\,a(\tau_0+\lambda)\right]\right|_{\lambda\to 0} = 0\,, \tag{2.36}$$

where the function $a(\tau)$ is the one describing the trajectory of outgoing light rays in the interior spacetime, Eq. (2.27). Using the spacetime scale factor, Eq. (2.24), we get

$$\begin{aligned}&\frac{\mathrm{d}}{\mathrm{d}\lambda}\Bigg\{\left(1+\frac{3}{2}\frac{(2M)^{1/2}}{R_0^{3/2}}(\tau_0+\lambda)\right)^{2/3}\times\\ &\times\left(a_0+\frac{2R_0^{3/2}}{(2M)^{1/2}}\left[\left(1-\frac{3}{2}\frac{(2M)^{1/2}}{R_0^{3/2}}\tau_0\right)^{1/3}-\left(1-\frac{3}{2}\frac{(2M)^{1/2}}{R_0^{3/2}}(\tau_0+\lambda)\right)^{1/3}\right]\right)\Bigg\}\Bigg|_{\lambda\to 0}=0\,.\end{aligned} \tag{2.37}$$

Proceeding, and replacing in the end $\tau_0 \to \tau^{(AH)}$, we find the apparent horizon is described by

$$a = \frac{R_0^{3/2}}{(2M)^{1/2}}\left(1-\frac{3}{2}\frac{(2M)^{1/2}}{R_0^{3/2}}\tau^{(AH)}\right)^{1/3} \iff \tau^{(AH)} = \frac{2}{3}\frac{R_0^{3/2}}{(2M)^{1/2}}\left(1-\frac{(2M)^{3/2}}{R_0^{9/2}}\,a^3\right)\,. \tag{2.38}$$

One finds that the apparent horizon, described by Eq. (2.38), verifies

$$\tau^{(AH)}(a=0) = \frac{2}{3}\frac{R_0^{3/2}}{(2M)^{1/2}} = \tau_c \quad , \qquad \tau^{(AH)}(a=R_0) = \frac{2}{3}\frac{R_0^{3/2}}{(2M)^{1/2}} - \frac{2}{3}(2M) = \tau^{(EH)}\,, \tag{2.39}$$

as expected.

2.3.7 Causal Structure

With the trajectory of the collapsing star, Eq. (2.23), the equations for the null geodesics, Eqs. (2.27) and (2.30), and those describing the apparent horizon, Eq. (2.38), we can build the causal structure of both interior and exterior spacetimes for the collapsing star. This can be seen in Figures 2.3a and 2.3b.

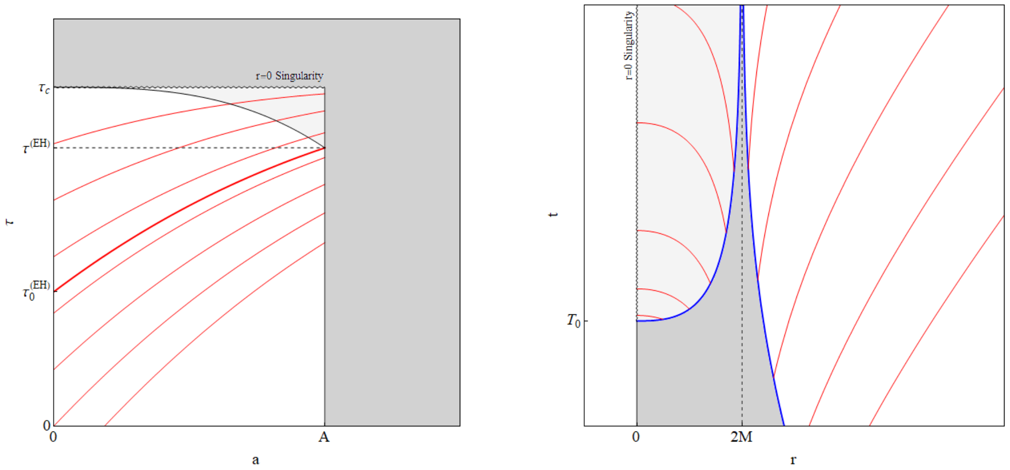

(a) Interior Causal Structure.

(b) Exterior Causal Structure.

Figure 2.3: The causal structure of the (2.3a) interior and (2.3b) exterior spacetimes. The outgoing light rays are shown in thin red lines, with the event horizon being the thick red line. The apparent horizon is shown with a thin black line, the singularity with a undulating black line and the trajectory of the surface of the collapsing star with a thick blue line. The light shaded region represents the region of trapped surfaces and the dark shaded region does not belong to the spacetime and is non physical.

2.3.8 Causal Structure in Different Coordinate Systems

For added clarity we now build the causal structure of both spacetimes in coordinate systems where the null geodesics are straight diagonal lines.

Interior Spacetime

We start with the equation of motion of the collapsing star's surface, Eq. (2.21), and introduce a new parameter η, such that we now have a pair of differential equations equivalent to the one we started from,

$$\frac{\partial R}{\partial \eta} = -\frac{1}{A}\sqrt{2MR} \quad , \qquad \frac{\partial \tau}{\partial \eta} = \frac{R}{A} \, , \tag{2.40}$$

which admit the solutions

$$R(\eta) = \frac{1}{4} 2M \left(\frac{\eta}{A}\right)^2 \quad , \qquad \tau(\eta) = \frac{1}{12} 2M \left(\frac{\eta}{A}\right)^3 \, . \tag{2.41}$$

The differential equations introduced, Eqs. (2.40), give the coordinate transformation $\mathrm{d}\tau = \xi \, \mathrm{d}\eta$. Applying this to the metric describing the interior spacetime, Eq. (2.5), gives us the new metric

$$\mathrm{d}s^2 = \xi^2(\eta)\left[-\mathrm{d}\eta^2 + \mathrm{d}a^2 + a^2(\mathrm{d}\theta^2 + \sin^2\theta \, \mathrm{d}\phi^2)\right] \, . \tag{2.42}$$

The null geodesics in the new metric of Eq. (2.42) are seen to be straight diagonal lines. Taking the event horizon as the light ray that crosses the surface as it passes $r = 2M$, we get $\xi(\eta')A = 2M$, i.e.$\eta' = -2A$. Thus the event horizon is described by

$$\eta^{(EH)} = -3A + a\,. \tag{2.43}$$

For the apparent horizon, we apply the simple formalism by D. M. Eardley and L. Smarr [38]. The apparent horizon is then defined by the equation

$$(\nabla\sqrt{g_{22}}) \cdot (\nabla\sqrt{g_{22}}) = 0\,. \tag{2.44}$$

From the metric, Eq. (2.42), we identify $\sqrt{g_{22}} = \xi(\eta)\,a$ and thus obtain

$$\eta^{(AH)} = -2a\,. \tag{2.45}$$

Exterior Spacetime

For the exterior spacetime we consider Kruskal coordinates. An overview of different coordinate systems are given in Appendix C. In Kruskal-Szekeres coordinates, null geodesics are also represented by diagonal straight lines, with the event horizon being that which crosses the origin of coordinates.

Causal Structure

With the equations describing the trajectory of the collapsing star, Eq. (2.23), the apparent horizon, Eq. (2.45), and the null geodeics being diagonal in both coordinate systems, we can build the causal structures for both spacetimes. These are shown in Figures 2.4a and 2.4b for the interior and exterior spacetimes respectively.

This representation shows clearly the star collapses beyond the Schwarzschild radius forming a singularity. Any observer falling with the surface becomes trapped once they pass the event horizon, unable to escape and forced to eventually fall into the singularity. The same occurs for light rays. From this one concludes the star has collapsed forming a black hole.

2.3.9 Other Interior Spacetimes of Different Curvature

Besides the case presented by Oppenheimer and Snyder in 1939, there are two additional cases in the form of the unbound and bound collapsing stars. The first one corresponds to a star that initiates contraction from infinity with non zero initial velocity. The second one corresponds to a star that initiates collapse at rest from some finite radial distance. These will be the focus for the next two sections.

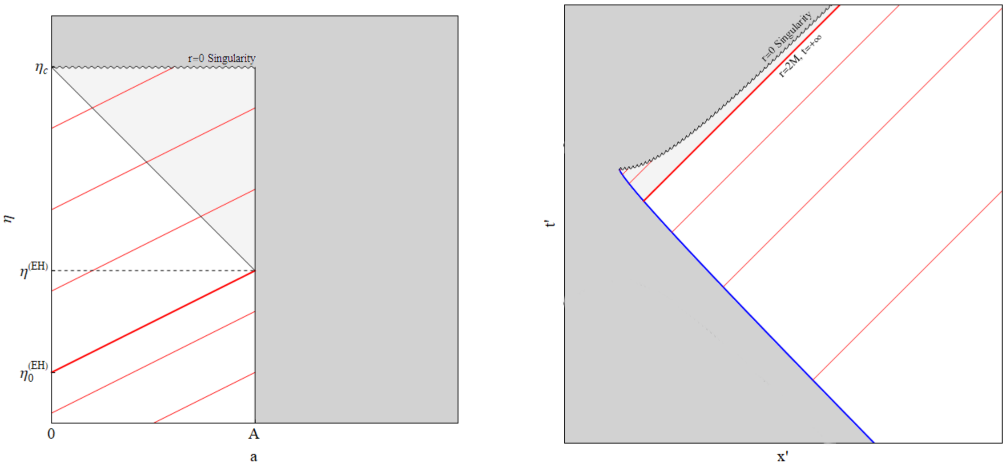

(a) Interior Causal Structure.

(b) Exterior Causal Structure.

Figure 2.4: The causal structure of the (2.4a) interior and (2.4b) exterior spacetimes in coordinate systems where null geodesics are diagonal straight lines. The outgoing light rays are shown in thin red lines, with the event horizon being the thick red line. The apparent horizon is shown with a thin black line, the singularity with a undulating black line and the trajectory of the surface of the collapsing star with a thick blue line. The light shaded region represents the region of trapped surfaces and the dark shaded region does not belong to the spacetime and is non physical.

Chapter 3

Collapsing Star: Unbound Case

3.1 Interior and Exterior Spacetimes

Having analyzed the marginally bound collapsing star, first studied by Oppenheimer and Snyder, we now proceed with the unbound case. Again we define two spacetimes, one for the interior and another for the exterior of some timelike surface. The particular choice made is then validated through the junction conditions, Eqs. (2.1) and (2.2). We start by considering a non rotating, spherically symmetric star. Additionally, we take for the interior a general Friedmann-Lemaître-Robertson-Walker (FLRW) metric

$$\mathrm{d}s^2 = -\mathrm{d}\tau^2 + \xi^2(\tau)\left[\frac{\mathrm{d}a^2}{1-k\,a^2} + a^2\left(\mathrm{d}\theta^2 + \sin^2\theta\,\mathrm{d}\phi^2\right)\right] , \tag{3.1}$$

where k will take the value -1, for negative curvature, thus obtaining

$$\mathrm{d}s^2 = -\mathrm{d}\tau^2 + \xi^2(\tau)\left[\frac{\mathrm{d}a^2}{1+a^2} + a^2\left(\mathrm{d}\theta^2 + \sin^2\theta\,\mathrm{d}\phi^2\right)\right] . \tag{3.2}$$

For the exterior, Birkhoff's theorem requires a Schwarzschild spacetime, which we will describe initially with a metric in Schwarzschild coordinates,

$$\mathrm{d}s^2 = -\left(1-\frac{2M}{r}\right)\mathrm{d}t^2 + \left(1-\frac{2M}{r}\right)^{-1}\mathrm{d}r^2 + r^2\left(\mathrm{d}\theta^2 + \sin^2\theta\,\mathrm{d}\phi^2\right) , \tag{3.3}$$

3.2 Application of Junction Conditions

The junction conditions, reviewed in Appendix A, are Eqs. (2.1) and (2.2), respectively

$$[h_{ab}] = 0\,, \tag{3.4}$$

$$[K_{ab}] = 0\,, \tag{3.5}$$

with h_{ab} the metric induced over the surface and $K_{ab} = n_{\alpha;\beta}e^{\alpha}_{\ a}e^{\beta}_{\ b}$ the extrinsic curvature.

Applying now the junction conditions, Eq. (3.4) and (3.5), to the metric, Eqs. (3.2), we find $\xi(\tau)A = R$

as well as the differential equations

$$1 = \left(1 - \frac{2M}{R}\right) \dot{T}^2 - \left(1 - \frac{2M}{R}\right)^{-1} \dot{R}^2 \, , \tag{3.6}$$

$$\dot{R}^2 = A^2 + \frac{2M}{R} \, , \tag{3.7}$$

and taking the latter, Eq. (3.7), to the asymptotic limit, $R \to \infty$, we find A to be the velocity of the surface at infinity. Thus we write $A = -v_{R\to\infty}$. For simplicity, let us write $v_0 = -v_{R\to\infty} = A$. Furthermore, Eq. (3.7), is seen to be the same as that describing a falling particle with initial energy $E^2 = 1 + v_0^2 > 1$.

3.2.1 Interior Solution

We now introduce a parameter η such that Eq. (3.7) becomes equivalent to the pair of differential equations

$$\frac{\partial R}{\partial \eta} = -\frac{R}{v_0}\sqrt{v_0^2 + \frac{2M}{R}} \quad , \qquad \frac{\partial \tau}{\partial \eta} = \frac{R}{v_0} \, . \tag{3.8}$$

The solutions for Eqs. (3.8) is

$$R(\eta) = \frac{M}{v_0^2}\left(\cosh\eta - 1\right) \quad , \qquad \tau(\eta) = \frac{M}{v_0^3}\left(\sinh\eta - \eta\right) \, , \tag{3.9}$$

with the parameter η thus being defined as $\eta \in]-\infty, 0]$. From the relation between the scale factor, ξ, and the radial coordinate of the surface, R, given by the first of Eqs. (3.9), we obtain

$$\xi(\eta) = \frac{M}{v_0^3}\left(\cosh\eta - 1\right) \, . \tag{3.10}$$

The differential equations, Eqs. (3.8), define a coordinate transformation $\mathrm{d}\tau = \xi(\eta)\mathrm{d}\eta$, which may be applied to the interior metric, Eq. (3.2), to give

$$\mathrm{d}s^2 = \xi^2(\eta)\left[-\mathrm{d}\eta^2 + \frac{\mathrm{d}a^2}{1+a^2} + a^2(\mathrm{d}\theta^2 + \sin^2\theta\,\mathrm{d}\phi^2)\right] \, , \tag{3.11}$$

which we will use for the remainder of this section.

3.2.2 Exterior Solution

By the previous remarks, the exterior solution will be the same as that found for the particle falling from infinity with non zero initial velocity. This can be seen explicitly also by applying the result of the first junction condition, Eq. (3.6), to that of the second junction condition, Eq. (3.7), giving

$$\frac{\mathrm{d}T}{\mathrm{d}R} = -\left(1 - \frac{2M}{R}\right)^{-1}\left(v_0^2 + \frac{2M}{R}\right)^{-1/2}(1+v_0^2)^{1/2} \, . \tag{3.12}$$

The solution to Eq. (3.12) is

$$\begin{aligned}T(R) = T_0 - \frac{1}{v_0^2}\left[R(1+v_0^2)(2M+v_0^2R)\right]^{1/2} + 2M\ln\left|\frac{[(1+v_0^2)R]^{1/2}+[2M+v_0^2R]^{1/2}}{[(1+v_0^2)R]^{1/2}-[2M+v_0^2R]^{1/2}}\right| +\\ + \frac{2M}{v_0^3}(1-2v_0^2)(1+v_0^2)^{1/2}\ln\left(\frac{v_0R^{1/2}+(2M+v_0^2R)^{1/2}}{(2M)^{1/2}}\right).\end{aligned} \tag{3.13}$$

The exterior spacetime can be expressed in Kruskal-Szekeres coordinates, of which there is an overview in Appendix C.9. This coordinate system will be used for the remainder of the section.

3.2.3 Null geodesics and Event Horizon

For the interior metric, Eq. (3.11), the null geodesics obey the differential equation

$$\frac{\partial \eta}{\partial a} = \pm \frac{1}{(1+a^2)^{1/2}}\,, \tag{3.14}$$

with the plus and minus signs representing outgoing and ingoing light rays respectively. The solutions are

$$\eta = \eta_0 \pm \operatorname{arcsinh} a\,, \tag{3.15}$$

with the plus and minus signs as before. With the event horizon being given by the light ray that crosses the surface as it passes the Schwarzschild radius $R = 2M$, and the scale factor, Eq. (3.10), one finds

$$\xi(\eta')v_0 = 2M \implies \eta^{(EH)} = -\operatorname{arccosh}(2v_0^2+1) - \operatorname{arcsinh} v_0 + \operatorname{arcsinh} a\,, \tag{3.16}$$

3.2.4 Apparent Horizon

The apparent horizon may be obtained using the formalism due to D. M. Eardley and L. Smarr [38], whereby it is defined through

$$(\nabla\sqrt{g_{22}})\cdot(\nabla\sqrt{g_{22}}) = 0\,, \tag{3.17}$$

which, with the identification $\sqrt{g_{22}} = \xi(\eta)\,a$, yields

$$\eta^{(AH)} = -\operatorname{arccosh}(2a^2+1)\,. \tag{3.18}$$

3.2.5 Causal Structure

With the null geodesics following Eq. (3.15) in the interior and diagonal lines in the exterior coordinate system, the trajectory of the collapsing star of the form of Eq. (3.13) and the event and apparent horizons described by Eqs. (3.16) and (3.18), respectively, we can build the causal structures of both spacetimes. This is represented in Figures 3.1a and 3.1b.

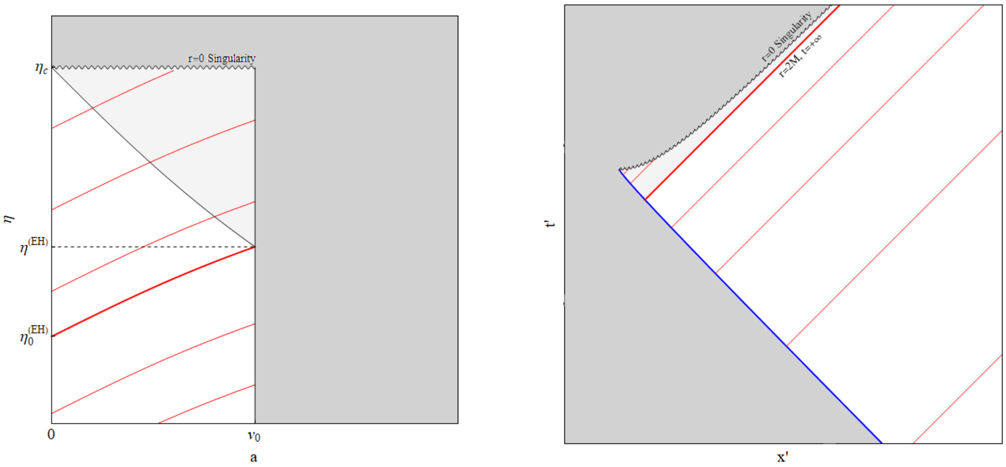
r=0 Singularity
η_c
η
$\eta^{(EH)}$
$\eta_0^{(EH)}$
0
v_0
a
r=0 Singularity
r=2M, t=+∞
t'
x'

(a) Interior Causal Structure.

(b) Exterior Causal Structure.

Figure 3.1: The causal structure of the (3.1a) interior and (3.1b) exterior spacetimes. The outgoing light rays are shown in thin red lines, with the event horizon being the thick red line. The apparent horizon is shown with a thin black line, the singularity with a undulating black line and the trajectory of the surface of the collapsing star with a thick blue line. The light shaded region represents the region of trapped surfaces and the dark shaded region does not belong to the spacetime and is non physical.

Chapter 4

Collapsing Star: Bound Case

4.1 Interior and Exterior Spacetimes

We now finish the analysis with the case of the bound collapsing star, first explored by J. B. Hartle, [14]. Again we define two spacetimes, one for the interior and another for the exterior of some timelike surface. The particular choice made is then validated through the junction conditions, Eqs. (2.1) and (2.2). We start by considering a non rotating, spherically symmetric star. Additionally, we take for the interior a general Friedmann-Lemaître-Robertson-Walker (FLRW) metric

$$\mathrm{d}s^2 = -\mathrm{d}\tau^2 + \xi^2(\tau)\left[\frac{\mathrm{d}a^2}{1-k\,a^2} + a^2\left(\mathrm{d}\theta^2 + \sin^2\theta\,\mathrm{d}\phi^2\right)\right]\,, \tag{4.1}$$

where k will take the value 1, for positive curvature, thus obtaining

$$\mathrm{d}s^2 = -\mathrm{d}\tau^2 + \xi^2(\tau)\left[\frac{\mathrm{d}a^2}{1-a^2} + a^2\left(\mathrm{d}\theta^2 + \sin^2\theta\,\mathrm{d}\phi^2\right)\right]\,. \tag{4.2}$$

For the exterior, Birkhoff's theorem requires a Schwarschild spacetime, which we will describe initially with a metric in Schwarzschild coordinates,

$$\mathrm{d}s^2 = -\left(1-\frac{2M}{r}\right)\mathrm{d}t^2 + \left(1-\frac{2M}{r}\right)^{-1}\mathrm{d}r^2 + r^2\left(\mathrm{d}\theta^2 + \sin^2\theta\,\mathrm{d}\phi^2\right)\,, \tag{4.3}$$

4.2 Application of Junction Conditions

The junction conditions, reviewed in Appendix A, are Eqs. (2.1) and (2.2), respectively

$$[h_{ab}] = 0\,, \tag{4.4}$$

$$[K_{ab}] = 0\,, \tag{4.5}$$

with h_{ab} the metric induced over the surface and $K_{ab} = n_{\alpha;\beta}e^{\alpha}_{\ a}e^{\beta}_{\ b}$ the extrinsic curvature.

Applying now the junction conditions, Eq. (4.4) and (4.5), to the metric, Eq. (4.2), we find $\xi(\tau)A = R$

as well as the differential equations

$$1 = \left(1 - \frac{2M}{R}\right)\dot{T}^2 - \left(1 - \frac{2M}{R}\right)^{-1}\dot{R}^2\,, \tag{4.6}$$

$$\dot{R}^2 = -A^2 + \frac{2M}{R}\,, \tag{4.7}$$

and from the latter, Eq. (4.7), we see the velocity is zero at a distance R_0 defined by

$$A^2 = \frac{2M}{R_0}\,, \tag{4.8}$$

so that this case represents a star collapsing from an initial radius R_0. Furthermore, Eq. (4.7) is seen to be the same as that describing a bound falling particle with energy $E^2 = 1 - A^2 = 1 - 2M/R_0^2 < 1$.

4.2.1 Interior Solution

We now introduce a parameter η such that Eq. (4.7) becomes equivalent to the pair of differential equations

$$\frac{\partial R}{\partial \eta} = -R\sqrt{\frac{R_0}{2M}}\sqrt{\frac{2M}{R} - \frac{2M}{R_0}} \quad , \qquad \frac{\partial \tau}{\partial \eta} = R\sqrt{\frac{R_0}{2M}}\,. \tag{4.9}$$

The solution for Eqs. (4.9) is

$$R(\eta) = \frac{R_0}{2}\left(1 + \cos\eta\right) \quad , \qquad \tau(\eta) = \frac{R_0}{2}\left(\eta + \sin\eta\right)\,, \tag{4.10}$$

with the parameter η thus being defined as $\eta \in [0, \pi]$. From the relation between the scale factor, ξ, and the radial coordinate of the surface, R, given by the first of Eqs. (4.10), we obtain

$$\xi(\eta) = \frac{R_0}{2}\sqrt{\frac{R_0}{2M}}\left(1 + \cos\eta\right)\,. \tag{4.11}$$

The differential equations, Eqs. (4.9), define a coordinate transformation $\mathrm{d}\tau = \xi(\eta)\mathrm{d}\eta$, which may be applied to the interior metric, Eq. (4.2), to give

$$\mathrm{d}s^2 = \xi^2(\eta)\left[-\mathrm{d}\eta^2 + \frac{\mathrm{d}a^2}{1 - a^2} + a^2(\mathrm{d}\theta^2 + \sin^2\theta\,\mathrm{d}\phi^2)\right]\,, \tag{4.12}$$

which we will use for the remainder of this section.

4.2.2 Exterior Solution

By the previous remarks, the exterior solution will be the same as that found for the bound particle falling from a distance R_0. This can be seen explicitly also by applying the result of the first junction condition, Eq. (4.6), to that of the second junction condition, Eq. (4.7), giving

$$\frac{\mathrm{d}T}{\mathrm{d}R} = -\left(1 - \frac{2M}{R}\right)^{-1}\left(\frac{2M}{R} - \frac{2M}{R_0}\right)^{-1/2}\left(1 - \frac{2M}{R_0}\right)^{1/2}\,. \tag{4.13}$$

The solution to Eq. (4.13) is

$$T(R) = T_0 + \left[\frac{R(R_0-2M)(R_0-R)}{2M}\right]^{1/2} - \frac{1}{4M}\left(\frac{2M}{R_0-2M}\right)^{1/2}\left(R_0^2+2MR_0-8M^2\right)\arccos\left(\frac{R_0-2R}{R_0}\right) - \\ - 2M\ln\left|\frac{2^{1/2}R_0(R-2M)}{4\left[MR(R_0-2M)(R_0-R)\right]^{1/2} - 2^{1/2}(4MR-2MR_0-RR_0)}\right| . \tag{4.14}$$

The exterior spacetime can be expressed in Kruskal-Szekeres coordinates, of which there is an overview in Appendix C.9. This coordinate system will be used for the remainder of the section.

4.2.3 Null geodesics and Event Horizon

For the interior metric, Eq. (4.12), the null geodesics obey the differential equation

$$\frac{\partial \eta}{\partial a} = \pm \frac{1}{(1-a^2)^{1/2}} , \tag{4.15}$$

with the plus and minus signs representing outgoing and ingoing light rays respectively. The solutions are

$$\eta = \eta_0 \pm \arcsin a , \tag{4.16}$$

with the plus and minus signs as before. With the event horizon being given by the light ray that crosses the surface as it passes the Schwarzschild radius $R = 2M$, and the scale factor, Eq. (4.11), one finds

$$\xi(\eta')A = 2M \implies \eta^{(EH)} = \arccos\left(2\frac{2M}{R_0} - 1\right) - \arcsin A + \arcsin a , \tag{4.17}$$

4.2.4 Apparent Horizon

The apparent horizon may be obtained using the formalism due to D. M. Eardley and L. Smarr [38], whereby it is defined through

$$(\nabla\sqrt{g_{22}}) \cdot (\nabla\sqrt{g_{22}}) = 0 , \tag{4.18}$$

which, with the identification $\sqrt{g_{22}} = \xi(\eta)\, a$ yields

$$\eta^{(AH)} = \arccos\left(2a^2 - 1\right) . \tag{4.19}$$

4.2.5 Causal Structure

With the null geodesics following Eq. (4.16) in the interior and diagonal lines in the exterior coordinate system, the trajectory of the collapsing star of the form of Eq. (4.14) and the event and apparent horizons described by Eqs. (4.17) and (4.19), respectively, we can build the causal structures of both spacetimes. This is represented in Figures 4.1a and 4.1b.

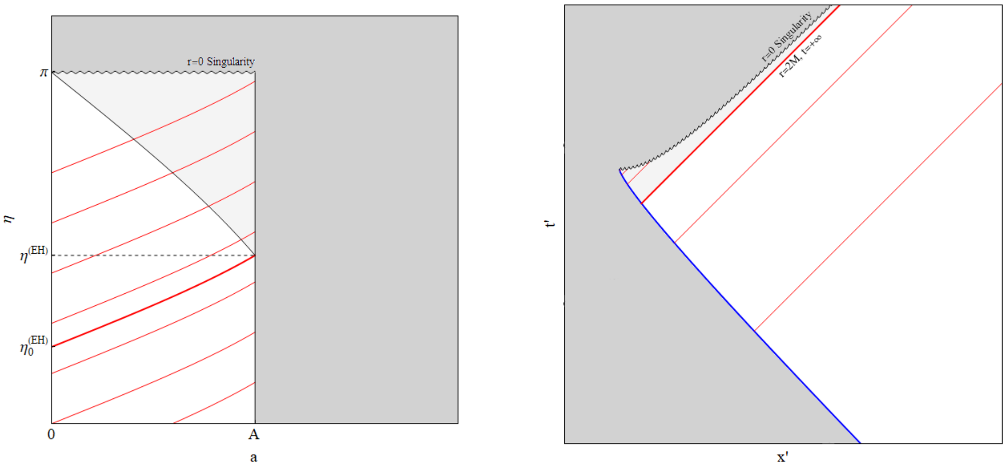

(a) Interior Causal Structure.

(b) Exterior Causal Structure.

Figure 4.1: The causal structure of the (4.1a) interior and (4.1b) exterior spacetimes. The outgoing light rays are shown in thin red lines, with the event horizon being the thick red line. The apparent horizon is shown with a thin black line, the singularity with a undulating black line and the trajectory of the surface of the collapsing star with a thick blue line. The light shaded region represents the region of trapped surfaces and the dark shaded region does not belong to the spacetime and is non physical.

Chapter 5

Collapsing Thin Shell: Marginally Bound Case

5.1 Equation of Motion

We now turn our attention to the case of the collapsing thin shell. Its motion is described by Eq. (A.31),

$$M = m\left(\dot{R}^2 + 1\right)^{1/2} - \frac{m^2}{2R}\,. \tag{5.1}$$

Its derivation is given in detail in Appendix A.

From Eq. (5.1), we find the case $M = m$ corresponds to the marginally bound case, i.e. a shell that falls from infinity with zero initial velocity, seen also in Appendix A.2. Indeed, starting with Eq. (A.32) with the minus sign, and setting $m = M$, we get

$$\dot{R} = -\left(\frac{M}{R} + \frac{M^2}{4R^2}\right)^{1/2}\,, \tag{5.2}$$

from which we find $\dot{R} = 0 \implies R \to \infty$. This case is then the one analogous to the star studied by Oppenheimer and Snyder, seen before in chapter 2.

5.2 Proper Time Solution

Trajectory of the Shell as seen by a Local Observer

The trajectory described by Eq. (5.2) is that of the shell in proper time, i.e. the one seen by an observer standing on the shell as it contracts. Rewriting it in the form of the proper time as a function of distance, $\tau(R)$, yields the solution

$$\tau(R) = -\frac{M}{6} + \frac{1}{6}\left(1 - \frac{2R}{M}\right)\left[M(M+4R)\right]^{1/2}\,, \tag{5.3}$$

where the shell comes from infinity at $\tau \to -\infty$ and collapses in the center of coordinates, $R = 0$, at $\tau = 0$. At the instant of collapse, a singularity is formed at $R = 0$, as per the Kretchsmann scalar of the associated Schwarzschild spacetime,

$$K_S = \frac{48M^2}{R^6}\,, \tag{5.4}$$

and the shell is reported to cross the Schwarzschild radius, $R = 2M$, an instant preceding that of total contraction by

$$\tau(2M) = -\frac{5}{3}M\,. \tag{5.5}$$

Various trajectories, for different values of M, are shown in Figure 5.1. We see that, as the shell's mass lowers, its contraction slows down. This behaviour can also be inferred directly from the equation of motion, Eq. (5.2).

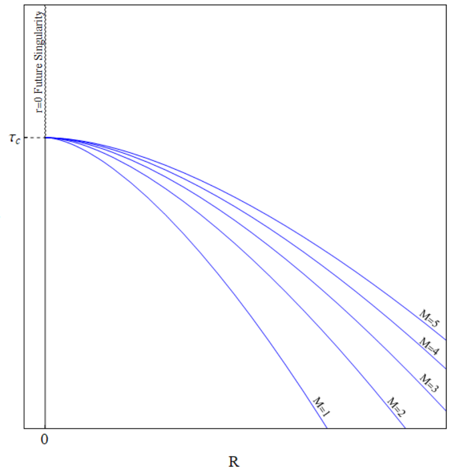

Figure 5.1: Marginally bound thin shell collapse measured in proper time for different values of the energy and shell mass parameter, M. The values of the parameter are in natural units.

The Limit of Zero Mass Shell

From the previous remarks, from the equation of motion, Eq. (5.2), we find the limit $M \to 0$ to give $\dot{R} \to 0$ everywhere except at $R = 0$ where it is indeterminate. This limit is also the one of zero energy and zero gravitational pull, the first from the identification of M with the energy of the system and the second from its identification with the Schwarzschild mass. The result follows by taking the solution, Eq. (5.3), in the mentioned limit. Doing so, the solution, Eq. (5.3), takes the form

$$\tau(R) \approx -\frac{2}{3}\frac{R^{3/2}}{M^{1/2}}\,, \tag{5.6}$$

so that for small M the system corresponds to a shell that stays at infinity. This result is represented in Figure 5.2.

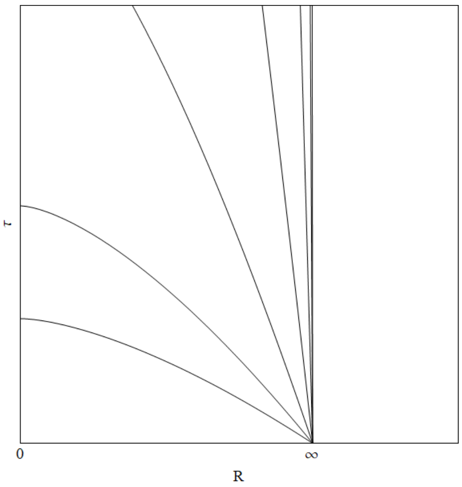

Figure 5.2: Trajectories of thin shell collapsing from infinity for different values of M in the limit $M \to 0$ as seen by a local observer and starting from some initial distance taken to be very large. As the mass decreases, its velocity decreases. For very small masses the shell becomes approximately stationary at infinity.

5.3 Interior Time Solution

Trajectory of the Shell as seen by an Internal Observer

The description of the shell's trajectory as seen by an observer in the interior, Minkowski, spacetime, can be obtained by applying the interior condition

$$1 = \dot{T}_-^2 - \dot{R}^2 \, , \tag{5.7}$$

to Eq. (5.2), or alternatively from Eq. (A.35) by setting $M = m$. Doing so yields the differential equation

$$\frac{\mathrm{d}T_-}{\mathrm{d}R} = - \left[MR + \frac{M^2}{4} \right]^{-1/2} \left(R^2 + MR + \frac{M^2}{4} \right)^{1/2} . \tag{5.8}$$

The analytical solution to this equation follows directly in the form

$$T_-(R) = \frac{M}{3} - \frac{1}{3} \left(1 + \frac{R}{M} \right) \left[M(M + 4R) \right]^{1/2} \, , \tag{5.9}$$

with the shell coming from infinity at $T_- \to -\infty$ and collapsing at the center of coordinates, $R = 0$, at $T_- = 0$. The internal observer is seen to report the shell as crossing the event horizon an instant preceding that of total contraction by

$$T_-(2M) = -\frac{8}{3} M \, , \tag{5.10}$$

which is greater than the interval of time reported by the local observer, Eq. (5.5), by M. Various trajectories, each for a different value of M, are drawn in Figure 5.3.

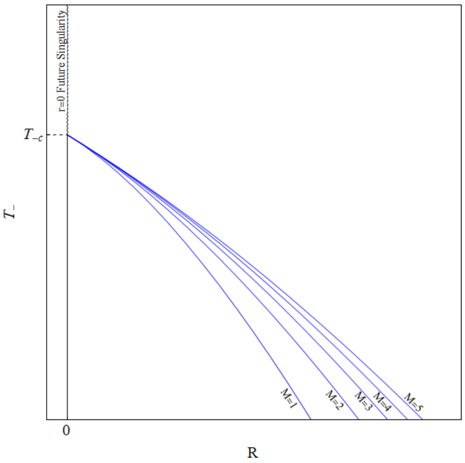

Figure 5.3: Collapse of the thin shell reported with respect to the internal time, for different values of the energy and shell mass parameter, M. The values of the parameter are in natural units.

Light Rays in the Interior Spacetime

Light rays travelling in the interior spacetime do so along diagonal lines. This follows from the Minkowski metric, Eq. (A.17), from which radial null geodesic are taken to obey $\mathrm{d}t_- = \pm \mathrm{d}r_-$. As such, light rays crossing the surface are described by

$$t_- = T_-(R) \pm (r_- - R)\,, \tag{5.11}$$

with R and $T_-(R)$ being the radial and interior time coordinates of the shell respectively. Accordingly, $r_- < R$ and the plus sign corresponds to ingoing light rays and the minus to outgoing light rays.

5.4 Exterior Time Solution

As noted in previous chapters and section A.2, the exterior is a Schwarzschild spacetime. Now we proceed to analyze the system in this region using different coordinate systems, starting with Schwarzschild coordinates. We will look not only for the trajectory of the system, but also for its general features. These are the trajectories of light rays emitted from the surface and the apparent and event horizons. Afterwards we will build the causal structure of the whole spacetime by complementing the interior Minkowski coordinate system with the exterior coordinate system under study. For a review of different coordinate systems representing the Schwarzschild spacetime, see appendix C.

5.4.1 Schwarzschild Coordinates

Trajectory of the Shell as seen by an External Observer

The equation of motion in the exterior spacetime, expressed in Schwarzschild coordinates, is obtained by applying the exterior condition

$$1 = \left(1 - \frac{2M}{R}\right)\dot{T}_+^2 - \left(1 - \frac{2M}{R}\right)^{-1}\dot{R}^2\,, \tag{5.12}$$

to Eq. (5.2), or alternatively from Eq. (A.38) by setting $M = m$. Doing so yields the differential equation

$$\frac{\mathrm{d}T_+}{\mathrm{d}R} = -\left(1 - \frac{2M}{R}\right)^{-1} \left[MR + \frac{M^2}{4}\right]^{-1/2} \left(R^2 - MR + \frac{M^2}{4}\right)^{1/2} . \tag{5.13}$$

The analytical solution to this equation can be obtained immediately in closed form,

$$T_+(R) = \frac{4M}{3} - \frac{1}{3}(R + 4M)\left(1 + \frac{4R}{M}\right)^{1/2} + 2M \ln\left|\frac{1}{2}\frac{3\,M^{1/2} + (M + 4R)^{1/2}}{3\,M^{1/2} - (M + 4R)^{1/2}}\right| , \tag{5.14}$$

where the shell comes from infinity at $T_+ \to \infty$. At $R = 2M$ the trajectory manifests a singularity, coinciding with the usual coordinate singularity at the Schwarzschild radius. The trajectory given by Eq. (5.14), normalized to M, is shown in Figure 5.4.

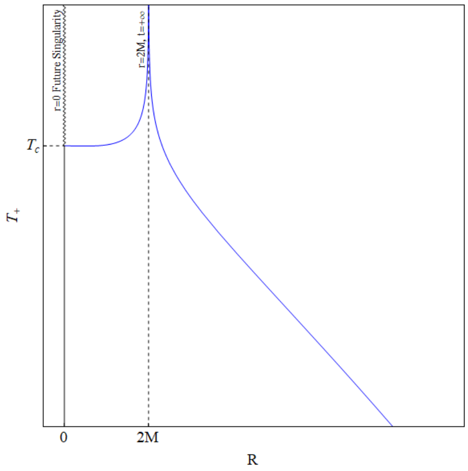

Figure 5.4: Trajectory of the collapsing thin shell as described by an eternal observer in Schwarzschild coordinates. The trajectory is normalized to the energy or mass parameter of the shell, M. Following Eq. (5.14), $T_c = 0$.

Light Rays in the Exterior Spacetime in Schwarzchild Coordinates

Light rays travel along null geodesics. In Schwarzschild coordinates, the light rays emitted from the shell have trajectories described by

$$t_+ = T_+(R) \pm \left(r_+ - R + 2M \ln\left|\frac{r_+ - 2M}{R - 2M}\right|\right) , \tag{5.15}$$

with R and $T_+(R)$ being the radial and exterior time coordinates of the shell, respectively. In this region $r_+ > R$ and the plus sign is associated with outgoing light rays, while the minus sign is associated with ingoing light rays. Like the shell's trajectory, the light ray trajectories display a singularity at the Schwarzschild radius $r_+ = 2M$.

We now take a light ray emitted from the center of coordinates at an instant t_0. Using the equations describing the trajectory of the shell and the trajectory of light rays described in the interior region, Eqs. (5.9) and (5.11) respectively, we can determine the distance of the shell from the center at the instant they both meet. Doing so, we find

$$t_0 = T_-(R) + R \implies R(t_0) = \frac{-4M^2 + 6Mt_0 + (-6M^2t_0 + 9Mt_0^2 + M|8M^2 - 18Mt_0 + 9t_0^2|)^{2/3}}{2(-6M^2t_0 + 9Mt_0^2 + M|8M^2 - 18Mt_0 + 9t_0^2|)^{1/3}} . \tag{5.16}$$

Such light rays are then emitted from the shell at the spacelike surface of coordinates $\big(R(t_0), T_+(R(t_0))\big)$, following afterwards

$$t_+ = T_+(R(t_0)) + r_+ - R(t_0) + 2M \ln \left| \frac{r_+ - 2M}{R(t_0) - 2M} \right| . \tag{5.17}$$

Thus the problem of a light ray emitted from the center of coordinates is completely determined, i.e. we can follow it along its whole trajectory from the interior to the exterior.

Event Horizon

The event horizon is defined by the first outgoing light ray that never reaches infinity [36]. We had verified both the trajectory of the thin shell and of the light rays display a singularity at the Schwarzschild radius, $R = r_+ = 2M$. Plugging the latter into the former, Eq. (5.15) into Eq. (5.14), and taking the limit of light rays emerging close to the Schwarzschild radius, we find

$$\lim_{r_+ \to 2M} t_+ = \lim_{r_+ \to 2M} \left(T_+ + r_+ - R + 2M \ln \left| \frac{r_+ + 2M}{R - 2M} \right| \right) \propto \lim_{\delta \to 0} 2M \ln |\delta| , \tag{5.18}$$

where $\delta = r_+ - 2M$. Thus light ray trajectories diverge in a logarithmic fashion. Thus we find the null spherical surface of Schwarzschild radius is the event horizon. By continuity we can determine the instant the interior observer sees the event horizon leave the spatial center of coordinates. With the corresponding trajectories of the shell and light rays, Eqs. (5.9) and (5.11), as well as Eq. (5.10), we find

$$t_0(2M) = T_-(2M) - 2M = -\frac{14}{3} M , \tag{5.19}$$

so that the time at which the event horizon leaves $r_- = 0$ increases linearly with the mass parameter M.

Apparent Horizon

The apparent horizon is defined as the boundary of the region of trapped surfaces [37]. Smarr and Eardley [38] define a normal vector and find the timelike surface on which this vector becomes null. This gives way to the relation

$$(\nabla \sqrt{g_{22}}) \cdot (\nabla \sqrt{g_{22}}) = 0 . \tag{5.20}$$

However, the discontinuity induced by the shell motivates a new definition of apparent horizon based on the immediate convergence of light rays

$$(\nabla \sqrt{g_{22}}) \cdot (\nabla \sqrt{g_{22}}) \Big|_{r \to R^+} \leq 0 , \tag{5.21}$$

where the evaluation is taken from the exterior region. It follows that the apparent horizon is defined by the shell's trajectory after passing the event horizon, $r_+ = 2M$.

Causal Structure

With all elements of the preceding discussion we can build the causal structure of the whole space-time, Figure 5.5. The trajectory of different light rays are shown, with the event horizon readily identifiable as well as the singularity. The region of trapped surfaces is shown shaded and the apparent horizon is made evident.

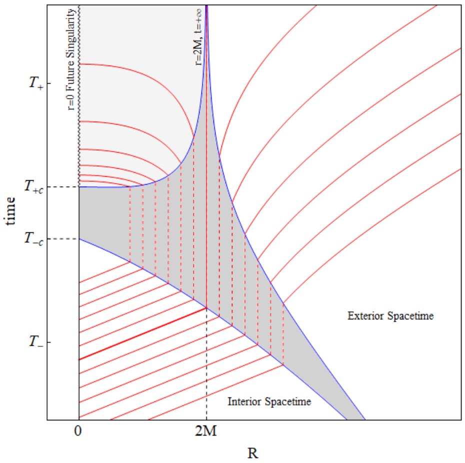

Figure 5.5: The causal structure of spacetime for $M = m$ in exterior Schwarzschild coordinates and interior Minkowski. The trajectory of the shell is the blue line. In red are drawn the outgoing null rays, with the last one reaching infinity, shown in a thicker line, corresponding to the event horizon. The light shaded region is the region of trapped surfaces and the timelike surface delimiting it, interior to the event horizon, corresponds to the apparent horizon. The dark shaded region is non physical and is used to separate the two different spacetimes. The singularity is the endpoint of the evolution and is shown in a curvilinear line.

5.4.2 Painlevé-Gullstrand Coordinates with $0 \leq E < 1$

Trajectory of the Shell as seen by an External Observer

We now analyze the system in Painlevé-Gullstrand coordinates with energy parameter $E < 1$. These are reviewed in the Appendix C.2. We now have a new system of coordinates $(\tau, r_+, \theta, \phi)$ related to the old one by the closed transformation relation

$$\begin{aligned}\tau =& E t_+ + r_+ \left(E^2 - 1 + \frac{2M}{r_+}\right)^{1/2} - 2ME \ln \left| \frac{2M - r_+ + 2E^2 r_+ + 2E r_+ (E^2 - 1 + 2M/r_+)^{1/2}}{r_+ - 2M} \right| - \\ & - M \frac{1 - 2E^2}{(1 - E^2)^{1/2}} \left(\frac{\pi}{2} - \arcsin \left[\frac{M - (1 - E^2) r_+}{M} \right] \right) .\end{aligned} \tag{5.22}$$

Applying Eq. (5.22) to the trajectory of the shell, Eq. (5.14), we now have

$$\begin{aligned}\tau_S(R) =& \frac{4ME}{3} - \frac{1}{3}(R+4M)E\left(1+\frac{4R}{M}\right)^{1/2} + 2ME\,\ln\left|\frac{1}{2}\frac{3\,M^{1/2}+(M+4R)^{1/2}}{3\,M^{1/2}-(M+4R)^{1/2}}\right| + \\ &+ R\left(E^2-1+\frac{2M}{R}\right)^{1/2} - M\frac{1-2E^2}{(1-E^2)^{1/2}}\left(\frac{\pi}{2}-\arcsin\left[\frac{M-(1-E^2)R}{M}\right]\right) - \\ &- 2ME\,\ln\left|\frac{2M-R+2RE^2+2RE(E^2-1+2M/R)^{1/2}}{R-2M}\right|.\end{aligned} \tag{5.23}$$

The trajectory described in this system displays no singularity at the Schwarzschild radius, $R = 2M$, as can be seen in Figure 5.6.

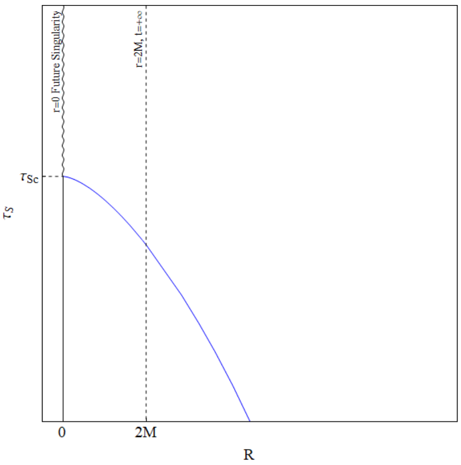

Figure 5.6: Trajectory of the thin shell described in external Painlevé-Gullstrand coordinates with $E < 1$. In this coordinate system no singularity is observed at the Schwarzschild raidus $R = 2M$, but the description does not extend beyond the distance $r_{+0} = 2M/(1-E^2)$.

Light Rays in the Exterior Spacetime in Painlevé-Gullstrand Coordinates with $E < 1$

Like as in for the case of the trajectory of the thin shell, the description of light ray trajectories can be obtained by the applying the coordinate transformation, Eq. (5.22), to the trajectories in Schwarzschild coordinates, Eq. (5.15). Doing so, we obtain

$$\begin{aligned}\tau =& \tau_S(R) + E\,(r_+ - R) + r_+\left(E^2-1+\frac{2M}{r_+}\right)^{1/2} - R\left(E^2-1+\frac{2M}{R}\right)^{1/2} - \\ &- 2ME\,\ln\left|\left(\frac{R-2M}{r_+-2M}\right)^2\frac{2M-r_++2E^2r_++2Er_+(E^2-1+2M/r_+)^{1/2}}{2M-R+2E^2R+2ER(E^2-1+2M/R)^{1/2}}\right| + \\ &+ M\frac{1-2E^2}{(1-E^2)^{1/2}}\left(\arcsin\left[\frac{M-(1-E^2)r_+}{M}\right]-\arcsin\left[\frac{M-(1-E^2)R}{M}\right]\right).\end{aligned} \tag{5.24}$$

Event Horizon

The trajectory of the thin shell in Painlevé-Gullstrand coordinates with $E < 1$, Eq. (5.23), was seen to have no singularity at the Schwarzschild radius. The same is not true for the null geodesics. Indeed, in the limit where the light ray is emitted from the surface at a radial distance close to the Shcwarzschild radius, we find

$$\lim_{r_+ \to 2M} \tau \propto \lim_{\delta \to 0} 4ME \ln |\delta| \, , \tag{5.25}$$

so that the light ray divergence occurs in a logarithmic fashion, irrespective of the behaviour observed of the shell. Thus, the spherical null surface of radius $r_+ = 2M$, seen by the external observer, corresponds to the event horizon.

Causal Structure

With the apparent horizon being the surface of the star after crossing the Schwarzschild radius, and gathering the remaining elements discussed, we can build the causal structure of the whole spacetime. This is shown in Figure 5.7. The trajectory of the shell and of outgoing light rays are shown. The event and apparent horizons are made evident.

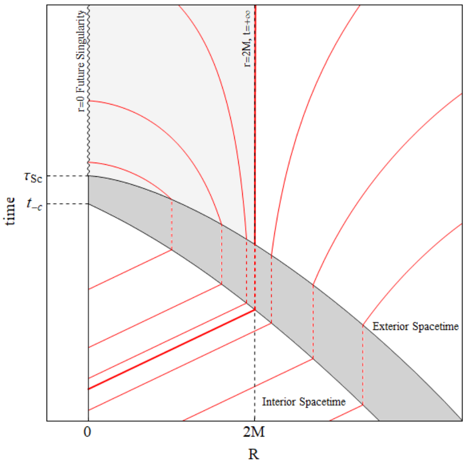

Figure 5.7: The causal structure of spacetime for $M = m$ in exterior Painlevé-Gullstrand coordinates with $E < 1$ and interior Minkowski. The trajectory of the shell is the blue line. In red are drawn the outgoing null rays, with the last one reaching infinity, shown in a thicker line, corresponding to the event horizon. The light shaded region is the region of trapped surfaces and the timelike surface delimiting it, interior to the event horizon, corresponds to the apparent horizon. The dark shaded region is non physical and is used to separate the two different spacetimes. The singularity is the endpoint of the evolution and is shown in a curvilinear line.

5.4.3 Painlevé-Gullstrand Coordinates

Trajectory of the Shell as seen by an External Observer

We now study the system in Painlevé-Gullstrand coordinates with $E = 1$, which are the usual Painlevé-Gullstrand coordinates. These are reviewed in Appendix C.3. The new system of coordinates, with $(\tau, r_+, \theta, \phi)$ is related to the old one by the closed transformation relation

$$\tau = t_+ + 4M \left(\frac{r_+}{2M}\right)^{1/2} - 2M \, \ln \left| \frac{r_+^{1/2} + (2M)^{1/2}}{r_+^{1/2} - (2M)^{1/2}} \right| . \tag{5.26}$$

Applying this relation to the trajectory of the thin shell in Schwarzschild coordinates, Eq. (5.14), we get

$$\tau_S(R) = \frac{4M}{3} - \frac{1}{3}(R+4M)\left(1+\frac{4R}{M}\right)^{1/2} + 2M\,\ln\left|\frac{1}{2}\left(\frac{3\,M^{1/2}+(M+4R)^{1/2}}{3\,M^{1/2}-(M+4R)^{1/2}}\right)\left(\frac{R^{1/2}-(2M)^{1/2}}{R^{1/2}+(2M)^{1/2}}\right)\right|. \tag{5.27}$$

In this coordinate system the trajectory of the shell does not diverge over the Schwarzschild radius, $R = 2M$, as can be seen in Figure 5.8.

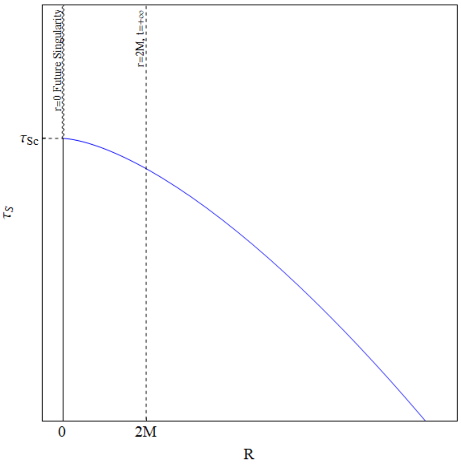

Figure 5.8: Trajectory of the thin shell described in external Painlevé-Gullstrand coordinates. In this coordinate system no singularity is observed at the Schwarzschild radius, $R = 2M$.

Light Rays in the Exterior Spacetime in Painlevé-Gullstrand Coordinates

We now apply the coordinate transformation, Eq. (5.26), to the Schwarzschild description of outgoing light ray trajectories, Eq. (5.15), to obtain

$$\tau = \tau_S(R) + r_+ - R + 2(2M)^{1/2}(r_+^{1/2} - R^{1/2}) + 2M\,\ln\left|\frac{(r_+ - 2M)(r_+^{1/2} - (2M)^{1/2})(R^{1/2} + (2M)^{1/2})}{(R-2M)(r_+^{1/2} + (2M)^{1/2})(R^{1/2} - (2M)^{1/2})}\right|. \tag{5.28}$$

Event Horizon

Unlike the trajectory of the shell, the outgoing light rays also display a singularity at the Schwarzschild radius, $r_+ = 2M$. Taking again the limit of light rays emerging from the surface as it approaches the Schwarzschild radius, one finds

$$\lim_{r_+\to 2M} \tau \propto \lim_{\delta\to 0} 4M\,\ln|\delta|\,, \tag{5.29}$$

so that they present a logarithmic divergence. Thus we here also find the event horizon to be identified with the spherical null surface of radius equal to the Schwarzschild radius, $r_+ = 2M$.

Causal Structure

The apparent horizon was seen to be identified with the shell's trajectory after it passes the Schwarzschild radius. With the remaining elements studied, the causal structure of the whole spacetime can now be constructed for exterior Painlevé-Gullstrand coordinates, Figure 5.9. Shown are the trajectory of the collapsing thin shell, as well as those of the outgoing light rays. The event and apparent horizons are made evident.

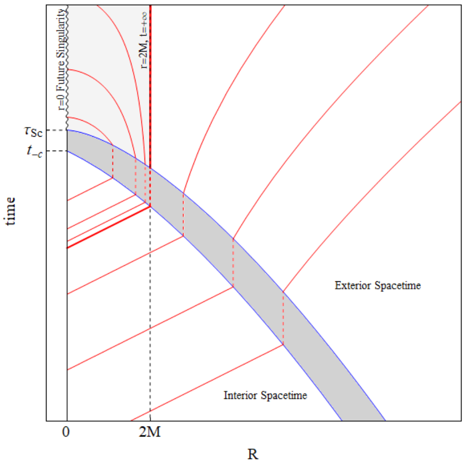

Figure 5.9: The causal structure of spacetime for $M = m$ in exterior Painlevé-Gullstrand coordinates and interior Minkowski. The trajectory of the shell is the blue line. In red are drawn the outgoing null rays, with the last one reaching infinity, shown in a thicker line, corresponding to the event horizon. The light shaded region is the region of trapped surfaces and the timelike surface delimiting it, interior to the event horizon, corresponds to the apparent horizon. The dark shaded region is non physical and is used to separate the two different spacetimes. The singularity is the endpoint of the evolution and is shown in a curvilinear line.

5.4.4 Painlevé-Gullstrand Coordinates with $E > 1$

We turn now to the description of the system in Painlevé-Gullstrand coordinates with $E > 1$. This system of coordinates is reviewed in Appendix C.4. The system is expressed in coordinates $(\tau, r_+, \theta, \phi)$ related to the old coordinates through the closed form relation

$$\begin{aligned}\tau =& E\,t_+ + r_+\left(E^2 - 1 + \frac{2M}{r_+}\right)^{1/2} - 2ME\,\ln\left|\frac{2M - r_+ + 2E^2 r_+ + 2E r_+ (E^2 - 1 + 2M/r_+)^{1/2}}{r_+ - 2M}\right| + \\ &+ M\frac{2E^2-1}{(E^2-1)^{1/2}}\,\ln\left[2r_+\left(E^2 - 1 + \frac{2M}{r_+}\right)^{1/2} + 2\frac{M + (E^2-1)r_+}{(E^2-1)^{1/2}}\right].\end{aligned} \tag{5.30}$$

The trajectory of the shell in the new coordinate system can now be obtained by application of the transformation relation, Eq. (5.30), to the description in Schwarzschild coordinates, Eq. (5.14),

$$\begin{aligned}\tau_S(R) =& \frac{4ME}{3} - \frac{1}{3}(R + 4M)E\left(1 + \frac{4R}{M}\right)^{1/2} + 2ME\ln\left|\frac{1}{2}\frac{3\,M^{1/2} + (M+4R)^{1/2}}{3\,M^{1/2} - (M+4R)^{1/2}}\right| + \\ &+ R\left(E^2 - 1 + \frac{2M}{R}\right)^{1/2} - 2ME\ln\left|\frac{2M - R + 2E^2 R + 2ER(E^2 - 1 + 2M/R)^{1/2}}{R - 2M}\right| + \\ &+ M\frac{2E^2-1}{(E^2-1)^{1/2}}\ln\left[2R\left(E^2 - 1 + \frac{2M}{R}\right)^{1/2} + 2\frac{M + (E^2-1)R}{(E^2-1)^{1/2}}\right],\end{aligned} \tag{5.31}$$

In this coordinate system the shell's trajectory does not present any divergence at the Schwarzschild radius, $R = 2M$, as can be seen in Figure 5.10.

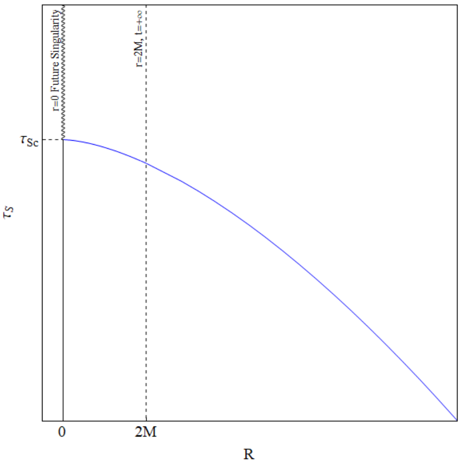

Figure 5.10: Trajectory of the thin shell described in external Painlevé-Gullstrand coordinates with $E > 1$. In this coordinate system no singularity is observed at the Schwarzschild radius, $R = 2M$.

Light Rays in the Exterior Spacetime in Painlevé-GullStrand Coordinates with $E > 1$

Applying the transformation relation, Eq. (5.30), to the description of outgoing light ray trajectories in Schwarzschild coordinates, Eq. (5.15), we find

$$\begin{aligned}\tau =&\tau_S(R) + r_+\left(E^2 - 1 + \frac{2M}{r_+}\right)^{1/2} - R\left(E^2 - 1 + \frac{2M}{R}\right)^{1/2} - \\ &- 2ME\,\ln\left|\left(\frac{R-2M}{r_+-2M}\right)^2 \frac{2M - r_+ + 2E^2 r_+ + 2Er_+(E^2-1+2M/r_+)^{1/2}}{2M - R + 2E^2 R + 2ER(E^2-1+2M/R)^{1/2}}\right| + \\ &+ M\frac{2E^2-1}{(E^2-1)^{1/2}}\,\ln\left[\frac{r_+(E^2-1)^{1/2}(E^2-1+2M/r_+)^{1/2} + M + (E^2-1)r_+}{R(E^2-1)^{1/2}(E^2-1+2M/R)^{1/2} + M + (E^2-1)R}\right].\end{aligned} \tag{5.32}$$

Event Horizon

The thin shell's trajectory, Eq. (5.31), had been seen to be regular over the Schwarzschild radius in this system of coordinates. The same does not happen for the trajectories of outgoing light rays, described by Eq. (5.32). Indeed, for light rays emerging when the thin shell is near the Schwarzschild radius we find

$$\lim_{r_+ \to 2M} \tau \propto \lim_{\delta \to 0} 4ME\,\ln|\delta| \tag{5.33}$$

so that they do diverge in its vicinity. Thus here we also find the event horizon to correspond to the spherical null surface of radius equal to the Schwarzschild radius.

Causal Structure

The apparent horizon was seen to be defined by the trajectory of the thin shell after it has passed the Schwarzschild radius. With the remaining elements added, we can now build the causal structure of the whole spacetime for exterior Painlevé-Gullstrand coordinates, Figure 5.11. The trajectories of the thin shell and outgoing light rays are shown and the event and apparent horizons are made evident.

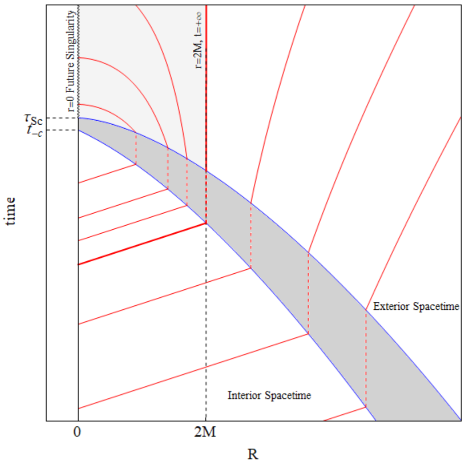

Figure 5.11: The causal structure of spacetime for $M = m$ in exterior Painlevé-Gullstrand coordinates with $E > 1$ and interior Minkowski. The trajectory of the shell is the blue line. In red are drawn the outgoing null rays, with the last one reaching infinity, shown in a thicker line, corresponding to the event horizon. The light shaded region is the region of trapped surfaces and the timelike surface delimiting it, interior to the event horizon, corresponds to the apparent horizon. The dark shaded region is non physical and is used to separate the two different spacetimes. The singularity is the endpoint of the evolution and is shown in a curvilinear line.

5.4.5 Ingoing Eddington-Finkelstein Coordinates

Trajectory of the Shell as seen by an External Observer

We now take the description to the Eddington-Finkelstein coordinate system with null coordinate v. This system of coordinates is reviewed in Appendix C.5. The system is expressed in coordinates (v, r_+, θ, ϕ) related to the old coordinates by the closed form relation

$$v = t_+ + r_+ + 2M \ln |r_+ - 2M| \,. \tag{5.34}$$

We obtain the trajectory of the shell in this system off coordinates by application of the transformation relation, Eq. (5.34), to the description in Schwarzschild coordinates, Eq. (5.14). Doing so, we find

$$V(R) = \frac{4M}{3} + R - \frac{1}{3}(R + 4M)\left(1 + \frac{4R}{M}\right)^{1/2} + 2M \ln \left[\frac{5M + 2R + 3[M(M + 4R)]^{1/2}}{8M}\right], \tag{5.35}$$

where the divergence at the Schwarzschild radius, $R = 2M$, is seen to be absent. The trajectory is drawn in Figure 5.12.

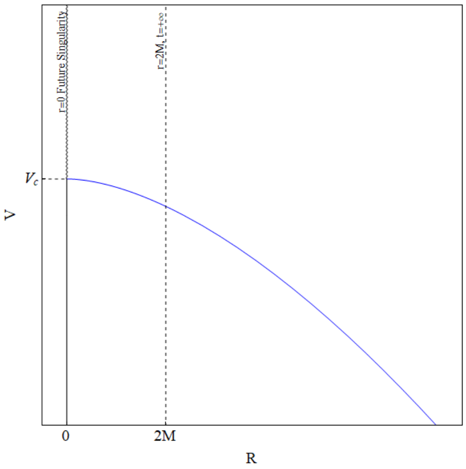

Figure 5.12: Trajectory of the thin shell described in external Eddington-Finkelstein coordinates. In this coordinate system the singularity seen in Schwarzschild coordinates at $R = 2M$ is absent.

Light Rays in the Exterior Eddington-Finkelstein Coordinates

Applying now the transformation relation, Eq. (5.34), to the light ray trajectories in Schwarzschild coordinates, Eq. (5.15), we find

$$v = V(R) + 2(r_+ - R) + 4M \, \ln \left| \frac{r_+ - 2M}{R - 2M} \right| , \tag{5.36}$$

which is a form similar to that found in Schwarzschild coordinates.

Event Horizon

The shell's trajectory, Eq. (5.35), does not display any singularity at the Schwarzcshild radius, but the same does not happen for the trajectory of the outgoing light rays, Eq. (5.36). Taking the limit of light rays emerging very close to the Schwarzschild radius, we find

$$\lim_{r_+ \to 2M} v = \lim_{\delta \to 0} 4M \, \ln |\delta| \, , \tag{5.37}$$

so the divergence is still present. As such, the light rays emitted near the Schwarzschild radius do not reach infinity and this marks the spherical null surface with $r_+ = 2M$ as the event horizon.

Causal Structure

The apparent horizon is defined by the trajectory of the shell after it passes the Schwarzschild radius. We can now build the causal structure of the spacetime in Eddington-Finkelstein coordinates, Figure 5.13. The trajectories of the shell and light rays are drawn and the event and apparent horizons are made evident.

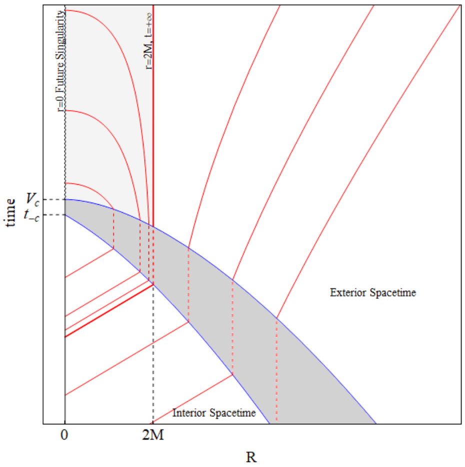

Figure 5.13: The causal structure of spacetime for $M = m$ in exterior Eddington-Finkelstein coordinates and interior Minkowski. The trajectory of the shell is the blue line. In red are drawn the outgoing null rays, with the last one reaching infinity, shown in a thicker line, corresponding to the event horizon. The light shaded region is the region of trapped surfaces and the timelike surface delimiting it, interior to the event horizon, corresponds to the apparent horizon. The dark shaded region is non physical and is used to separate the two different spacetimes. The singularity is the endpoint of the evolution and is shown in a curvilinear line.

5.4.6 Novikov Coordinates

Trajectory of the Shell as seen by an External Observer

We now continue with coordinate systems obtained through two coordinate transformations. We start with the description in Novikov coordinates, reviewed in Appendix C.6. This system is expressed in coordinates $(\tau, \rho, \theta, \phi)$ related to the old coordinates by a series of relations

$$\rho = \left(\frac{r_0}{2M} - 1\right)^{1/2}, \tag{5.38}$$

$$r_+ = \frac{r_0}{2}(1 + \cos\eta), \tag{5.39}$$

$$\tau = \left(\frac{r_0^3}{8M}\right)^{1/2} (\eta + \sin\eta), \tag{5.40}$$

$$t_+ = 2M \ln\left|\frac{(r_0/2M - 1)^{1/2} + \tan(\eta/2)}{(r_0/2M - 1)^{1/2} - \tan(\eta/2)}\right| + 2M\left(\frac{r_0}{2M} - 1\right)^{1/2}\left(\eta + \frac{r_0}{4M}(\eta + \sin\eta)\right). \tag{5.41}$$

These relations are based on the trajectory of a marginally bound particle. To obtain any trajectory, we start by taking points $(T(R), R)$ in the Schwarzschild description and obtaining the pair r_0 and η by application of Eqs. (5.39) and (5.41). Then ρ and τ can be obtained. Doing so for the trajectory of the shell, Eq. (5.14), we obtain Figure 5.14. One sees the usual singularity at the Schwarzschild radius is now absent.

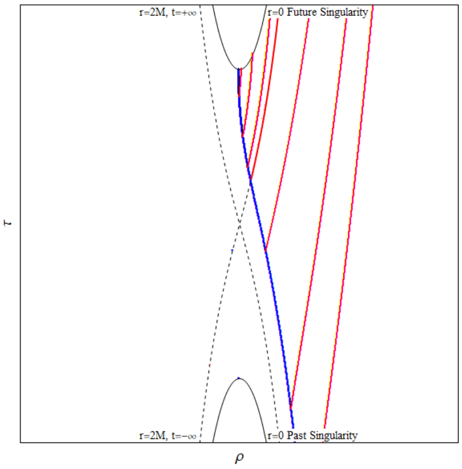

Figure 5.14: Trajectory of the thin shell described in external Novikov coordinates, in blue. In red are the outgoing null geodesics obtained in the same manner. In this coordinate system the singularity seen in Schwarzschild coordinates at $R = 2M$ is absent for the shell's trajectory.

Light Rays in the Exterior Novikov Coordinates

The trajectories of the light rays are obtained numerically, by the same process, as the trajectory of the thin shell before.

Event Horizon

The event horizon can be seen by inspection of Figure 5.14 to coincide with the line $r_+ = 2M$. The latter can be obtained in closed form by using Eqs. (5.38) through (5.40),

$$\tau = M(\rho^2 + 1)^{3/2} \left[\frac{2\rho}{1+\rho^2} + \arccos\left(\frac{1-\rho^2}{1+\rho^2} \right) \right] . \tag{5.42}$$

Causal Structure

The apparent horizon was seen to correspond to the trajectory of the shell after passing the Schwarzschild radius in its contraction. Using the elements discussed, we can build the causal structure of the whole spacetime for exterior Novikov coordinates, Figure 5.15. The trajectories of the shell and outgoing light rays are displayed and the event and apparent horizons are made evident.

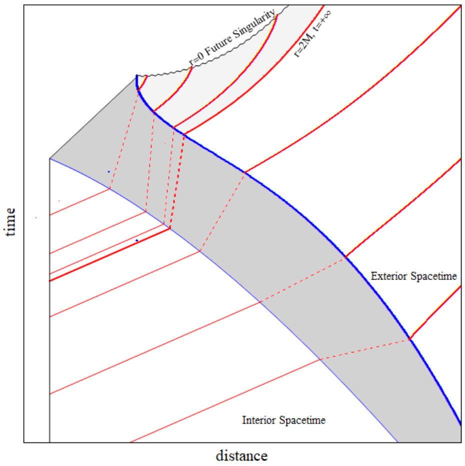

Figure 5.15: The causal structure of spacetime for $M = m$ in exterior Novikov coordinates and interior Minkowski. The trajectory of the shell is the blue line. In red are drawn the outgoing null rays, with the last one reaching infinity, shown in a thicker line, corresponding to the event horizon. The light shaded region is the region of trapped surfaces and the timelike surface delimiting it, interior to the event horizon, corresponds to the apparent horizon. The dark shaded region is non physical and is used to separate the two different spacetimes. The singularity is the endpoint of the evolution and is shown in a curvilinear line.

5.4.7 Lemaître Coordinates

Trajectory of the Shell as seen by an External Observer

We now study the system in Lemaître coordinates. These are reviewed in Appendix C.7. This system is expressed in coordinates $(\tau, \rho, \theta, \phi)$ related to the old coordinates by two closed form relations

$$\rho = t_+ + 4M\left(\frac{r_+}{2M}\right)^{1/2} - 2M\,\ln\left|\frac{r^{1/2}+(2M)^{1/2}}{r^{1/2}-(2M)^{1/2}}\right| + \frac{2}{3}\left(\frac{r^3}{2M}\right)^{1/2} \tag{5.43}$$

$$\tau = t_+ + 4M\left(\frac{r_+}{2M}\right)^{1/2} - 2M\,\ln\left|\frac{r^{1/2}+(2M)^{1/2}}{r^{1/2}-(2M)^{1/2}}\right| . \tag{5.44}$$

The form of these relations does not allow one to obtain a function $\tau(\rho)$ for the trajectory of the shell. One can however still obtain it parametrically by using Eq. (5.14) and using r_+ as a parameter. Doing so, we find the parameterized form of the solution in Lemaître coordinates

$$\begin{aligned}\rho_S = {} & \frac{4M}{3} - \frac{1}{3}(R+4M)\left(1+\frac{4R}{M}\right)^{1/2} + 4M\left(1+\frac{R}{3(2M)}\right)\left(\frac{R}{2M}\right)^{1/2} + \\ & + 2M\,\ln\left|\frac{1}{2}\left(\frac{3\,M^{1/2}+(M+4R)^{1/2}}{3\,M^{1/2}-(M+4R)^{1/2}}\right)\left(\frac{R^{1/2}-(2M)^{1/2}}{R^{1/2}+(2M)^{1/2}}\right)\right| ,\end{aligned} \tag{5.45}$$

$$\begin{aligned}\tau_S = {} & \frac{4M}{3} - \frac{1}{3}(R+4M)\left(1+\frac{4R}{M}\right)^{1/2} + 4M\left(\frac{R}{2M}\right)^{1/2} + \\ & + 2M\,\ln\left|\frac{1}{2}\left(\frac{3\,M^{1/2}+(M+4R)^{1/2}}{3\,M^{1/2}-(M+4R)^{1/2}}\right)\left(\frac{R^{1/2}-(2M)^{1/2}}{R^{1/2}+(2M)^{1/2}}\right)\right| ,\end{aligned} \tag{5.46}$$

The trajectory is drawn in Figure 5.16. One can see the singularity at the Schwarzschild radius, $R = 2M$, is absent in this system of coordinates.

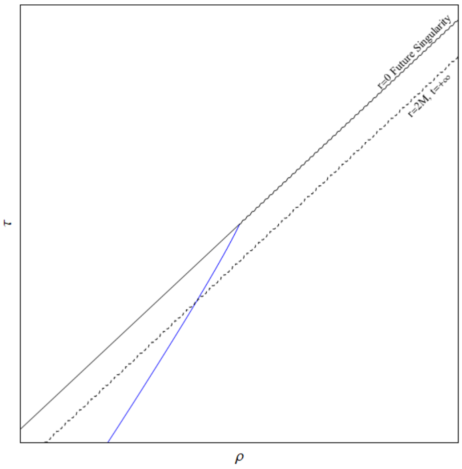

Figure 5.16: Trajectory of the thin shell described in external Lemaître coordinates. In this coordinate system the singularity seen in Schwarzschild coordinates at $R = 2M$ is absent.

Light Rays in the Exterior Lemaître Coordinates

As in the case of the shell's trajectory, we obtain a parametric form for the light's trajectory by application of the transformation relations, Eqs. (5.43) and (5.44), to the trajectory in Schwarzschild coordinates, Eq (5.15). From this results

$$\begin{aligned}\rho_L &= \rho_S + r_+ - R + 4M\left(1+\frac{r_+}{3(2M)}\right)\left(\frac{r_+}{2M}\right)^{1/2} - 4M\left(1+\frac{R}{3(2M)}\right)\left(\frac{R}{2M}\right)^{1/2} + \\ &+ 2M\,\ln\left|\frac{(r_+-2M)(R^{1/2}+(2M)^{1/2})(r_+^{1/2}-(2M)^{1/2})}{(R-2M)(R^{1/2}-(2M)^{1/2})(r_+^{1/2}+(2M)^{1/2})}\right|,\end{aligned} \tag{5.47}$$

$$\begin{aligned}\tau_L &= \tau_S + r_+ - R + 4M\left(\frac{r_+}{2M}\right)^{1/2} - 4M\left(\frac{R}{2M}\right)^{1/2} + \\ &+ 2M\,\ln\left|\frac{(r_+-2M)(R^{1/2}+(2M)^{1/2})(r_+^{1/2}-(2M)^{1/2})}{(R-2M)(R^{1/2}-(2M)^{1/2})(r_+^{1/2}+(2M)^{1/2})}\right|.\end{aligned} \tag{5.48}$$

Event Horizon

From Figure 5.16 one sees no singularity at the Schwarzschild radius, $R = 2M$. For the light rays emerging from the shell when this is in the vicinity of $R = 2M$, we find

$$\lim_{r_+\to 2M} \rho = \lim_{\delta\to 0} 4M\ln|\delta|\,, \tag{5.49}$$

$$\lim_{r_+\to 2M} \tau = \lim_{\delta\to 0} 4M\ln|\delta|\,, \tag{5.50}$$

so that there is still a divergence, and we find here as well that the spherical null surface of radius $r_+ = 2M$ corresponds to the event horizon.

Causal Structure

With the apparent horizon being defined by the trajectory of the shell after it crosses the Schwarzcshild radius, and using the remaining elements, we build the causal structure of the whole spacetime, Figure

5.17. Drawn are the trajectories of the shell and outgoing light rays, and the event and apparent horizons are made evident.

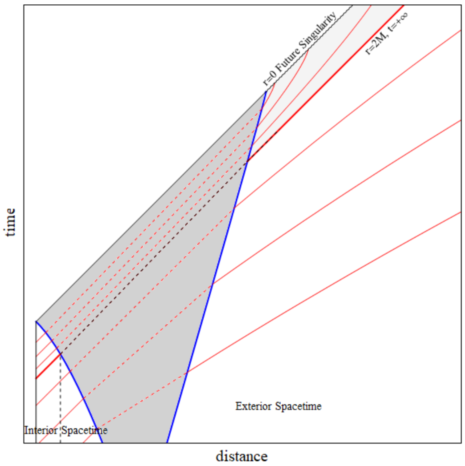

Figure 5.17: The causal structure of spacetime for $M = m$ in exterior Lemaître coordinates and interior Minkowski. The horizontal axis represents r_- for the interior region and ρ for the exterior, while the vertical axis represents t_- and τ respectively. The trajectory of the shell is the blue line. In red are drawn the outgoing null rays, with the last one reaching infinity, shown in a thicker line, corresponding to the event horizon. The light shaded region is the region of trapped surfaces and the timelike surface delimiting it, interior to the event horizon, corresponds to the apparent horizon. The dark shaded region is non physical and is used to separate the two different spacetimes. The singularity is the endpoint of the evolution and is shown in a curvilinear line.

5.4.8 Lemaître Coordinates with $E > 1$

Trajectory of the Shell as seen by an External Observer

We extend the study to the generalization of Lemaître coordinates for $E > 1$, reviewed in Appendix C.8. The system is expressed in coordinates $(\tau, \rho, \theta, \phi)$ related to the old coordinates by two closed form relations

$$\begin{aligned}\rho = E\,t_+ + \frac{E^2 r_+}{E^2-1}\left(E^2 - 1 + \frac{2M}{r_+}\right)^{1/2} - 2ME\,\ln\left|\frac{2M - r_+ + 2E^2 r_+ + 2Er_+(E^2-1+2M/r_+)^{1/2}}{r_+ - 2M}\right| + \\ + \frac{2E^2-3}{(E^2-1)^{3/2}}ME^2\,\ln\left[2r_+\left(E^2 - 1 + \frac{2M}{r_+}\right)^{1/2} + 2\frac{M + (E^2-1)r_+}{(E^2-1)^{1/2}}\right],\end{aligned} \tag{5.51}$$

$$\begin{aligned}\tau = E\,t_+ + r_+\left(E^2 - 1 + \frac{2M}{r_+}\right)^{1/2} - 2ME\,\ln\left|\frac{2M - r_+ + 2E^2 r_+ + 2Er_+(E^2-1+2M/r_+)^{1/2}}{r_+ - 2M}\right| + \\ + \frac{2E^2-1}{(E^2-1)^{1/2}}M\,\ln\left[2r_+\left(E^2 - 1 + \frac{2M}{r_+}\right)^{1/2} + 2\frac{M + (E^2-1)r_+}{(E^2-1)^{1/2}}\right].\end{aligned} \tag{5.52}$$

Using these two transformation relations on the trajectory of the shell in Schwarzschild coordinates, Eq. (5.14), we find the parameterized solution in Lemaître coordinates with $E > 1$

$$\begin{aligned}\rho_S = {}& \frac{4ME}{3} - \frac{E}{3}(R+4M)\left(1+\frac{4R}{M}\right)^{1/2} + \frac{E^2}{E^2-1}R\left(E^2-1+\frac{2M}{R}\right)^{1/2} + \\ &+ 2ME\,\ln\left|\frac{(3\,M^{1/2}+(M+4R)^{1/2})(R-2M)}{2(3\,M^{1/2}-(M+4R)^{1/2})(2M-R+2E^2R+2ER(E^2-1+2M/R)^{1/2})}\right| + \\ &+ \frac{2E^2-3}{(E^2-1)^{3/2}}ME^2\,\ln\left[2R\left(E^2-1+\frac{2M}{R}\right)^{1/2}+2\frac{M+(E^2-1)R}{(E^2-1)^{1/2}}\right],\end{aligned} \tag{5.53}$$

$$\begin{aligned}\tau_S = {}& \frac{4ME}{3} - \frac{E}{3}(R+4M)\left(1+\frac{4R}{M}\right)^{1/2} + R\left(E^2-1+\frac{2M}{R}\right)^{1/2} + \\ &+ 2ME\,\ln\left|\frac{(3\,M^{1/2}+(M+4R)^{1/2})(R-2M)}{2(3\,M^{1/2}-(M+4R)^{1/2})(2M-R+2E^2R+2ER(E^2-1+2M/R)^{1/2})}\right| + \\ &+ \frac{2E^2-1}{(E^2-1)^{1/2}}ME^2\,\ln\left[2R\left(E^2-1+\frac{2M}{R}\right)^{1/2}+2\frac{M+(E^2-1)R}{(E^2-1)^{1/2}}\right].\end{aligned} \tag{5.54}$$

The trajectory is drawn in Figure 5.18. One sees the singularity at the Schwarzschild radius, $R = 2M$, to be absent.

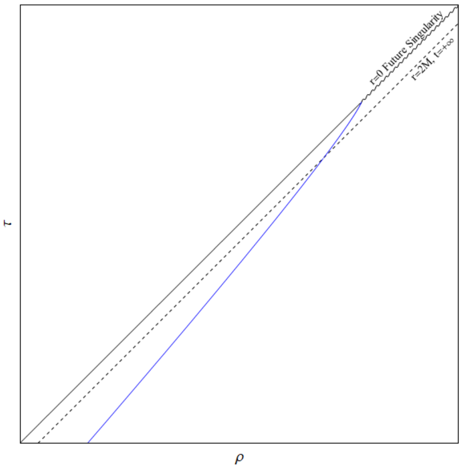

Figure 5.18: Trajectory of the thin shell described in external Lemaître coordinates with energy parameter $E > 1$. In this coordinate system the singularity seen in Schwarzschild coordinates at $R = 2M$ is absent.

Light Rays in the Exterior Lemaître Coordinates with $E > 1$

Identically to the trajectory of the shell, the trajectory of outgoing light rays can be obtained by application of the trajectory n Schwarzschild coordinates, Eq. (5.15), to the transformation relations, Eqs. (5.51) and

(5.52). Doing so yields

$$\begin{aligned}\rho_L = \rho_S + r_+ - R + \frac{E^2 r_+}{E^2-1}\left(E^2 - 1 + \frac{2M}{r_+}\right)^{1/2} - \frac{E^2 R}{E^2-1}\left(E^2 - 1 + \frac{2M}{R}\right)^{1/2} + \\ + 2ME\,\ln\left|\frac{(2M - R + 2E^2R + 2ER(E^2-1+2M/R)^{1/2})(r_+ - 2M)(r_+^{1/2} - (2M)^{1/2})}{(2M - r_+ + 2E^2r_+ + 2Er_+(E^2-1+2M/r_+)^{1/2})(R - 2M)(R^{1/2} - (2M)^{1/2})}\right| + \\ + \frac{2E^2-3}{(E^2-1)^{3/2}}ME^2\,\ln\left(\frac{r_+(E^2-1)^{1/2}(E^2-1+2M/r_+)^{1/2} + M + (E^2-1)r_+}{R(E^2-1)^{1/2}(E^2-1+2M/R)^{1/2} + M + (E^2-1)R}\right),\end{aligned} \tag{5.55}$$

$$\begin{aligned}\tau_L = \tau_S + + r_+ - R + r_+\left(E^2 - 1 + \frac{2M}{r_+}\right)^{1/2} - R\left(E^2 - 1 + \frac{2M}{R}\right)^{1/2} + \\ + 2ME\,\ln\left|\frac{(2M - R + 2E^2R + 2ER(E^2-1+2M/R)^{1/2})(r_+ - 2M)(r_+^{1/2} - (2M)^{1/2})}{(2M - r_+ + 2E^2r_+ + 2Er_+(E^2-1+2M/r_+)^{1/2})(R - 2M)(R^{1/2} - (2M)^{1/2})}\right| + \\ + \frac{2E^2-1}{(E^2-1)^{1/2}}M\,\ln\left(\frac{r_+(E^2-1)^{1/2}(E^2-1+2M/r_+)^{1/2} + M + (E^2-1)r_+}{R(E^2-1)^{1/2}(E^2-1+2M/R)^{1/2} + M + (E^2-1)R}\right).\end{aligned} \tag{5.56}$$

Event Horizon

We trajectory of the shell, given by Eqs. (5.53) and (5.54), does not display any divergence at the Schwarzschild radius, but the same does not happen to the trajectory of light rays. Taking the appropriate limit for Eqs. (5.55) and (5.56), we find

$$\lim_{r_+\to 2M} \rho_L = \lim_{\delta\to 0} 4ME\,\ln|\delta|\,, \tag{5.57}$$

$$\lim_{r_+\to 2M} \tau_L = \lim_{\delta\to 0} 4ME\,\ln|\delta|\,, \tag{5.58}$$

so that we find a divergence at $r_+ = 2M$ and the event horizon is identified with the spherical null surface of radius equal to the Schwarzschild radius.

Causal Structure

The apparent horizon was seen to be identified with the trajectory of the shell after passing the Schwarzschild radius. Taking the elements discussed, we build the causal structure of the whole spacetime, Figure 5.19. The trajectories of the thin shell and outgoing light rays are drawn and the apparent and event horizons are made evident.

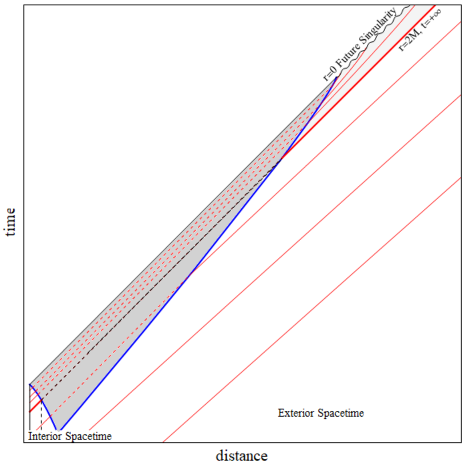

Figure 5.19: The causal structure of spacetime for $M = m$ in exterior Lemaître coordinates with energy parameter $E > 1$ and interior Minkowski. The horizontal axis represents r_- for the interior region and ρ for the exterior, while the vertical axis represents t_- and τ respectively. The trajectory of the shell is the blue line. In red are drawn the outgoing null rays, with the last one reaching infinity, shown in a thicker line, corresponding to the event horizon. The light shaded region is the region of trapped surfaces and the timelike surface delimiting it, interior to the event horizon, corresponds to the apparent horizon. The dark shaded region is non physical and is used to separate the two different spacetimes. The singularity is the endpoint of the evolution and is shown in a curvilinear line.

5.4.9 Kruskal-Szekeres Coordinates

Trajectory of the Shell as seen by an External Observer

The last coordinate system, obtained by a change of two coordinates, we will consider is the Kruskal-Szekeres system, reviewed in Appendix C.9. This system is expressed in coordinates (v, u, θ, ϕ) related to the Schwarzschild coordinates by, for $r_+ < 2M$

$$u = \left(1 - \frac{r_+}{2M}\right)^{1/2} \mathrm{e}^{r_+/4M} \sinh\left(\frac{t_+}{4M}\right), \tag{5.59}$$

$$v = \left(1 - \frac{r_+}{2M}\right)^{1/2} \mathrm{e}^{r_+/4M} \cosh\left(\frac{t_+}{4M}\right), \tag{5.60}$$

and for $r_+ > 2M$

$$u = \left(\frac{r_+}{2M} - 1\right)^{1/2} \mathrm{e}^{r_+/4M} \cosh\left(\frac{t_+}{4M}\right), \tag{5.61}$$

$$v = \left(\frac{r_+}{2M} - 1\right)^{1/2} \mathrm{e}^{r_+/4M} \sinh\left(\frac{t_+}{4M}\right). \tag{5.62}$$

The trajectory of the thin shell in Kruskal-Szekeres is obtained parametrically by direct application of its description in Schwarzschild coordinates, Eq. (5.14), to the transformation relations, Eqs. (5.59) through (5.62). Doing so, we find, for $R < 2M$

$$U = \left(1 - \frac{R}{2M}\right)^{1/2} \mathrm{e}^{R/4M} \sinh\left(\frac{1}{3} - \frac{1}{3}\frac{R + 4M}{4M} + \frac{1}{2}\ln\left|\frac{1}{2}\frac{3\,M^{1/2} + (M + 4R)^{1/2}}{3\,M^{1/2} - (M + 4R)^{1/2}}\right|\right), \tag{5.63}$$

$$V = \left(1 - \frac{R}{2M}\right)^{1/2} \mathrm{e}^{R/4M} \cosh\left(\frac{1}{3} - \frac{1}{3}\frac{R + 4M}{4M} + \frac{1}{2}\ln\left|\frac{1}{2}\frac{3\,M^{1/2} + (M + 4R)^{1/2}}{3\,M^{1/2} - (M + 4R)^{1/2}}\right|\right), \tag{5.64}$$

and for $R > 2M$

$$U = \left(\frac{R}{2M} - 1\right)^{1/2} \mathrm{e}^{R/4M} \cosh\left(\frac{1}{3} - \frac{1}{3}\frac{R+4M}{4M} + \frac{1}{2}\ln\left|\frac{1}{2}\frac{3\,M^{1/2} + (M+4R)^{1/2}}{3\,M^{1/2} - (M+4R)^{1/2}}\right|\right), \tag{5.65}$$

$$V = \left(\frac{R}{2M} - 1\right)^{1/2} \mathrm{e}^{R/4M} \sinh\left(\frac{1}{3} - \frac{1}{3}\frac{R+4M}{4M} + \frac{1}{2}\ln\left|\frac{1}{2}\frac{3\,M^{1/2} + (M+4R)^{1/2}}{3\,M^{1/2} - (M+4R)^{1/2}}\right|\right). \tag{5.66}$$

The trajectory is drawn in Figure 5.20. The singularity present in Schwarzschild coordinates at the Schwarzschild radius, $R = 2M$, is seen to be absent.

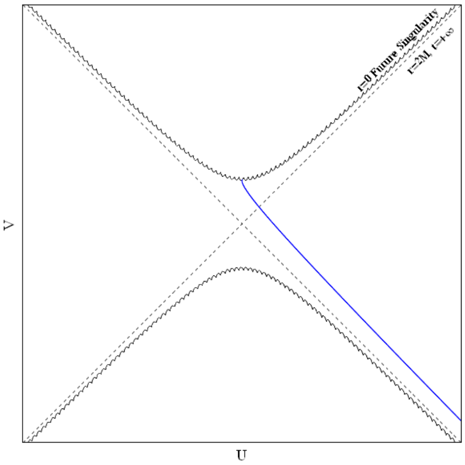

Figure 5.20: Trajectory of the thin shell described in external Kruskal-Szekeres coordinates. In this coordinate system the singularity seen in Schwarzschild coordinates at $R = 2M$ is absent.

Light Rays in Exterior Kruskal-Szekeres

Following the metric in the Kruskal-Szekeres coordinate system, the light rays follow along diagonals. We thus have

$$v_L = V + u - U\,. \tag{5.67}$$

Event Horizon

From the transformation relations, Eqs. (5.59) through (5.62), we find the following

$$t_+ = \operatorname{arctanh}\left(\frac{u}{v}\right)\ ,\ \ r_+ < 2M \quad , \qquad t_+ = \operatorname{arctanh}\left(\frac{v}{u}\right)\ ,\ \ r_+ > 2M\,, \tag{5.68}$$

so that $t_+ \to \infty$ for $u = v$. The latter defines a specific light ray by Eq. (5.67). In addition, r_+ is defined implicitly by the relation

$$\left(1 - \frac{r_+}{2M}\right)\mathrm{e}^{r_+/2M} = v^2 - u^2\,, \tag{5.69}$$

so that it follows the ray defined by $v = u$ is that for which $r_+ = 2M$. As such, also here we find the event horizon to be defined by the spherical null surface of radius equal to the Schwarzschild radius.

Causal Structure

The apparent horizon was seen to be defined by the trajectory of the shell after it has passed the Schwarzschild radius. With the remaining elements we can build the causal structure of the whole spacetime, Figure 5.21. The trajectories of the shell and outgoing light rays are drawn and the apparent and event horizons are made evident.

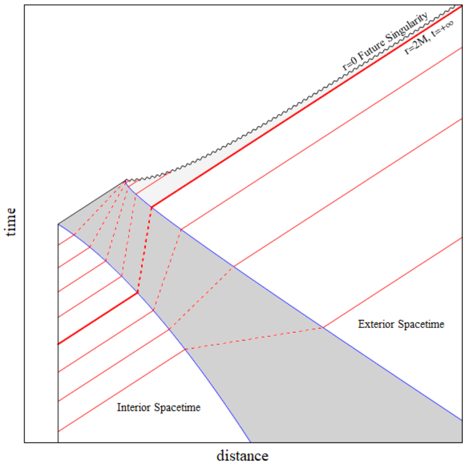

Figure 5.21: The causal structure of spacetime for $M = m$ in exterior Kruskal-Szekeres coordinates and interior Minkowski. The trajectory of the shell is the blue line. In red are drawn the outgoing null rays, with the last one reaching infinity, shown in a thicker line, corresponding to the event horizon. The light shaded region is the region of trapped surfaces and the spacelike surface delimiting it, interior to the event horizon, corresponds to the apparent horizon. The dark shaded region is non physical and is used to separate the two different spacetimes. The singularity is the endpoint of the evolution and is shown in a curvilinear line.

Chapter 6

Collapsing Thin Shell: Unbound Case

6.1 Equation of Motion

We now take the case where $M > m$. Taking the equation of motion, Eq. (5.1) with the minus sign, we have

$$\dot{R} = -\left(\frac{M^2}{m^2} - 1 + \frac{M}{R} + \frac{m^2}{4R^2}\right)^{1/2} . \tag{6.1}$$

It is seen that Eq. (6.1) does not allow for a zero value of the velocity $\dot{R}$ whatever the value of R may be. In fact we find

$$R \to \infty \implies \dot{R} = -\left(\frac{M^2}{m^2} - 1\right)^{1/2} < 0 \, , \tag{6.2}$$

which implies this as being the case of unbound collapse with initial velocity $v_0 = -(M^2/m^2 - 1)^{1/2}$. This shell is thus analogous to the case of the collapsing star with interior FLRW metric with $k = -1$, studied in Chapter 3. The extensive study of Eq. (6.1) in the two regions, interior and exterior, can be consulted in Appendix A.

6.2 Proper Time Solution

Trajectory of the Shell as seen by a Local Observer

The differential equation, Eq. (6.1), pertains to the description due to a local observer, i.e. one that falls with the shell. The equation can be rewritten in a form in which the proper time is a function of distance, that form being amenable to resolution. The solution thus obtained is

$$\tau(R) = \frac{m^3}{2(M^2 - m^2)}\left(1 - \frac{1}{m^2}\xi(R) + \frac{M}{(M^2 - m^2)^{1/2}} \ln\left[\frac{m^2 M + 2(M^2 - m^2)R + (M^2 - m^2)^{1/2}\xi(R)}{m^2[M + (M^2 - m^2)^{1/2}]}\right]\right) , \tag{6.3}$$

where $\xi(R) = [m^2(M^2 + 4MR) + 4(M^2 - m^2)R^2]^{1/2}$. The shell comes from infinity at $\tau \to \infty$ and collapses in the center of coordinates, $R = 0$, at the instant $\tau = 0$ forming a singularity. The time reported between the shell crossing the Schwarzschild radius, $R = 2M$, and collapsing is

$$\tau(2M) = -\frac{m(2M^2 - m^2)}{M^2 - m^2} + \frac{m^3 M}{2(M^2 - m^2)^{3/2}} \ln \left[\frac{2M^2 - m^2 + 2M(M^2 - m^2)^{1/2}}{m^2} \right] . \tag{6.4}$$

Various trajectories, for different values of m in relation to M, are drawn in Figure 6.1. We see that in the limit $m \to M$ these trajectories approach the one seen in the marginally bound case, as expected.

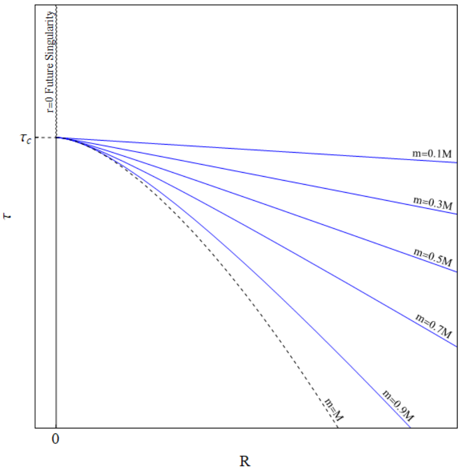

Figure 6.1: With blue lines, the unbound thin shell collapse measured in proper time for different values of the rest mass of the shell, m, in relation to its energy parameter M. The dashed black line shows the trajectory of the marginally bound collapsing shell, studied in chapter 5.

6.3 Interior Time Solution

Trajectory of the Shell as seen by an Internal Observer

The solution for the unbound shell's trajectory in the interior region is obtained by solving Eq. (A.35) for $M > m$. Doing so we obtain the closed form

$$T_-(R) = \frac{m^2 M}{2(M^2 - m^2)} \left(1 - \frac{\xi(R)}{m^2} + \frac{m^2/M}{(M^2 - m^2)^{1/2}} \ln \left[\frac{m^2 M + 2(M^2 - m^2)R + (M^2 - m^2)^{1/2} \xi(R)}{m^2[M + (M^2 - m^2)^{1/2}]} \right] \right) , \tag{6.5}$$

where once again $\xi(R) = [m^2(M^2 + 4MR) + 4(M^2 - m^2)R^2]^{1/2}$. The shell, as described by Eq. (6.5), comes from infinity at $T_- \to \infty$ and collapses at the center of coordinates, $R = 0$, at the instant $T_- = 0$ forming a singularity. Watching the collapse, the internal observer reports an interval between the shell crossing the Schwarzschild radius, $R = 2M$, and collapsing of

$$T_-(2M) = -\frac{M(2M^2 - m^2)}{M^2 - m^2} + \frac{m^4}{2(M^2 - m^2)^{3/2}} \ln \left[\frac{2M^2 - m^2 + 2M(M^2 - m^2)^{1/2}}{m^2} \right] . \tag{6.6}$$

We verify from Eqs. (6.4) and (6.6),

$$T_-(2M) - \tau(2M) = -\frac{(M - m)(2M^{-} m^2)}{M^2 - m^2} - \frac{m^3 (M - m)}{2(M^2 - m^2)^{3/2}} \ln \left[\frac{2M^2 - m^2 + 2M(M^2 - m^2)^{1/2}}{m^2} \right] < 0 , \tag{6.7}$$

so that the time reported by the internal observer is greater than that reported by the local observer[1]. Various trajectories, for different values of m in relation to M, are drawn in Figure 6.2. We see that in the limit $m \to M$ the trajectories approach that of the marginally bound case, which was expected. However there is one additional limit case in the form of $m \to 0$. In this, the trajectories approach that of ingoing light rays, described by Eq. (5.11) with the minus sign.

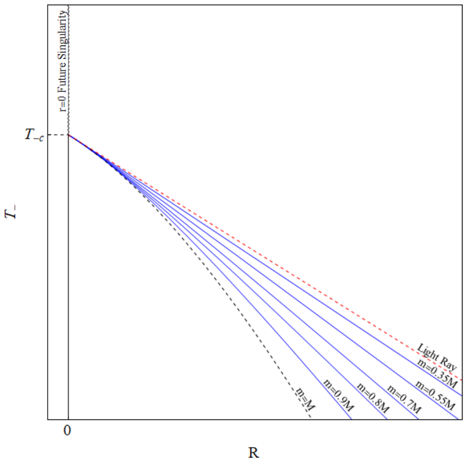

Figure 6.2: With blue lines, the unbound shell collapse measured in internal time for different values of the rest mass of the shell, m, in relation to its energy parameter M. The dashed black line represents the trajectory of the marginally bound collapsing shell, studied in chapter 5. The dashed red line represents an ingoing null geodesic.

The Limit of Zero Mass Shell with Fixed Energy

Following the previous remarks on the trajectories of the thin shell with decreasing m/M, we search for the limit $m \to 0$ of the trajectory of the shell seen by the internal observer. Using Eq. (6.5), we find

$$\lim_{m \to 0} T_-(R) = -R\,, \tag{6.8}$$

which is indeed the equation describing the trajectory of ingoing light rays converging on $r_- = 0$ at the instant $t_- = 0$ in Minkowski spacetime, Eq. (5.11). This result follows from massless particles, such as photons, travelling along null geodesics. As the rest mass of the dust shell approaches zero, with its energy being kept fixed, the matter composing it behaves more like photons of energy M. As such, at this point the shell may be seen as a converging flash of light of energy M.

6.4 Exterior Time Solution

We now analyze the system in exterior spacetime. We will restrict to Schwarzschild coordinates, the remaining following the same procedure seen in the previous section. We also note that the trajectories of the light rays and event and apparent horizons are the same as those seen in the marginally bound case since, apart from the emission point, they do not depend on the particular trajectory of the source.

---

[1] Note both $T_-(R)$ and $\tau(R)$ are defined negative

As such, for the sake of brevity, we will focus on the trajectory of the shell, as the remaining elements are as developed in chapter 5.

6.4.1 Schwarzschild Coordinates

Trajectory of the Shell as seen by an External Observer

The solution to the unbound equation of motion in exterior Schwarzschild coordinates, Eq. (A.38) with $M > m$, can be obtained in closed form

$$\begin{aligned} T_+(R) = -\frac{M}{2(M^2-m^2)}\Bigg(&\frac{m^4-6m^2M^2+4M^4}{M(M^2-m^2)^{1/2}}\ln\left[\frac{m^2M+2(M^2-m^2)R+(M^2-m^2)^{1/2}\xi(R)}{m^2(M+[M^2-m^2]^{1/2})}\right]+ \\ &+\xi(R)-m^2-4(M^2-m^2)\ln\left|\frac{m^4+4m^2M^2+(8M^2-6m^2)MR+(4M^2-m^2)\xi(R)}{4m^2M(R-2M)}\right|\Bigg), \end{aligned} \tag{6.9}$$

where $\xi(R) = [m^2(m^2+4MR)+4(M^2-m^2)R^2]^{1/2}$. The shell comes from infinity at $T_+ \to \infty$. At $R = 2M$ the trajectory diverges, denouncing the coordinate singularity at the Schwarzschild radius. Various trajectories, for different values of m relative to M, are shown in Figure 6.3. As was reported by the internal observer, we see two limit cases. In the limit $m \to M$ the trajectory approaches the one seen in the marginally bound case. The opposite case, that of $m \to 0$, has the trajectory approach that of an ingoing light ray.

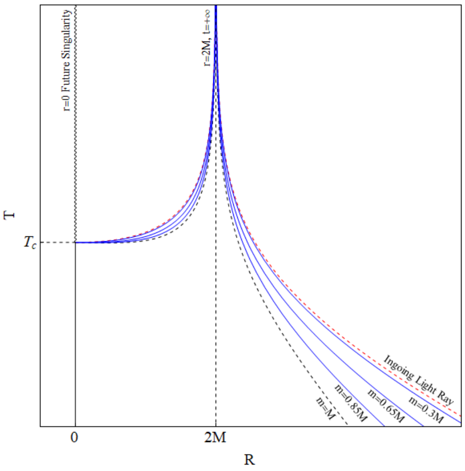

Figure 6.3: With blue lines, the unbound thin shell collapse in exterior Schwarzschild coordinates for different values of the shell's rest mass, m, relative to its energy parameter M. The dashed black line represents the trajectory of the marginally bound collapsing shell, studied in chapter 5. The dashed red line represents an ingoing null geodesic.

The Limit of Zero Mass Shell with Fixed Energy

The previous remark on the limit $m \to 0$ of the unbound shell's trajectory leads us to search for the behaviour of Eq. (6.9) with decreasing m/M. We find

$$\lim_{m \to 0} T_+(R) = -R - 2M \ln \left| \frac{R - 2M}{2M} \right| , \tag{6.10}$$

which corresponds to the trajectory of an ingoing light ray converging on $r_+ = 0$ at $t_+ = 0$ in Schwarzschild coordinates, Eq. (5.15) with the minus sign. Thus, this result also agrees with the shell made of massless particles of dust being identified with a converging flash of light of energy M.

Causal Structure

With the outgoing light rays and apparent and event horizons, already studied in chapter 5.4.1, we can build the causal structure of the whole spacetime, Figure 6.4.

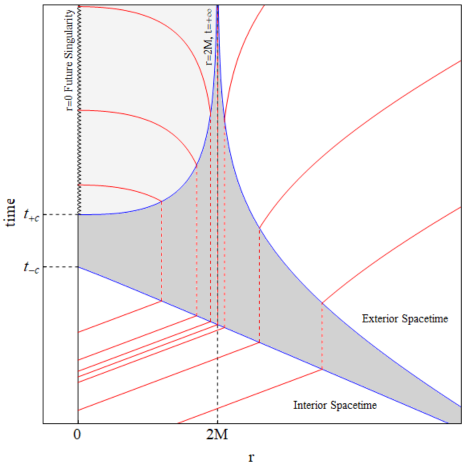

Figure 6.4: The causal structure of spacetime for $M > m$, i.e. the unbound case, in exterior Schwarzschild coordinates and interior Minkowski. The trajectory of the shell is the blue line. In red are drawn the outgoing null rays, with the last one reaching infinity, shown in a thicker line, corresponding to the event horizon. The light shaded region is the region of trapped surfaces and the spacelike surface delimiting it, interior to the event horizon, corresponds to the apparent horizon. The dark shaded region is non physical and is used to separate the two different spacetimes. The singularity is the endpoint of the evolution and is shown in a curvilinear line.

6.5 The limit of test particles, i.e., $m = 0$, and criticality

There is another limit of interest in the unbound collapse of the shell, when the masses, coupled, are taken to 0. This represents the limit of test particles and it is worthwhile to unfold the dynamics of this case. As such, we take $M = \alpha m$, with $\alpha > 1$ a constant so chosen to keep the condition of unbound collapse. The equations describing the trajectory of the shell in proper, interior and exterior times, Eqs. (6.3), (6.5) and (6.9) respectively, reduce to

$$\tau(R) = \frac{m}{2(\alpha^2-1)}\left(1 - \frac{\xi_\alpha(R)}{m} + \frac{\alpha}{(\alpha^2-1)^{1/2}}\ln\left[\frac{\alpha\, m + 2(\alpha^2-1)R + (\alpha^2-1)^{1/2}\xi_\alpha(R)}{m[\alpha + (\alpha^2-1)^{1/2}]}\right]\right)\,, \tag{6.11}$$

$$T_-(R) = \frac{\alpha\, m}{2(\alpha^2-1)}\left(1 - \frac{\xi_\alpha(R)}{m} + \frac{1}{\alpha(\alpha^2-1)^{1/2}}\ln\left[\frac{\alpha\, m + 2(\alpha^2-1)R + (\alpha^2-1)^{1/2}\xi_\alpha(R)}{m[\alpha + (\alpha^2-1)^{1/2}]}\right]\right)\,, \tag{6.12}$$

$$\begin{aligned} T_+(R) = \frac{\alpha\, m}{2(\alpha^2-1)}&\left(\frac{1-6\alpha^2+4\alpha^4}{\alpha(\alpha^2-1)^{1/2}}\ln\left[\frac{\alpha\, m + 2(\alpha^2-1)R + (\alpha^2-1)^{1/2}\xi_\alpha(R)}{m[\alpha + (\alpha^2-1)^{1/2}]}\right]-\right.\\ &\left.-1 + \frac{\xi_\alpha(R)}{m} - 4(\alpha^2-1)\ln\left|\frac{m + 4\alpha^2 m + (8\alpha^2-6)\alpha\, R + (4\alpha^2-1)m\,\xi_\alpha(R)}{4\alpha(R-2\alpha\, m)}\right|\right) \end{aligned} \tag{6.13}$$

with $\xi_\alpha(R) = [\alpha^2 m^2 + 4\alpha\, mR + 4(\alpha^2-1)R^2]^{1/2}$. Sketching the trajectory of the shell in proper time, Eq. (6.11), in the limit $m \to 0$ gives Figure 6.5. It is seen the gravitational collapse of the shell may then either end in black hole formation, Figure 6.6a, or matter dissipation, Figure 6.6b, showing criticality.

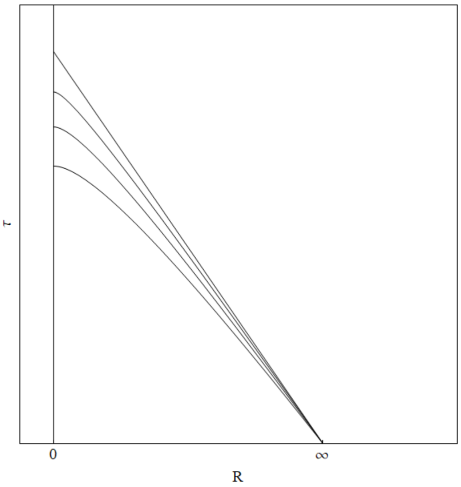

Figure 6.5: Trajectories of different shell in the limit of $m \to 0$, as seen by the local observer

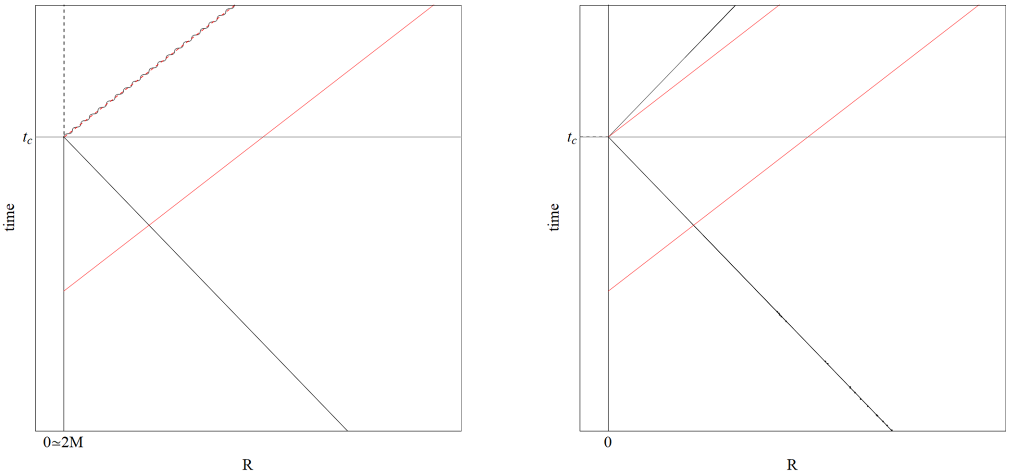

(a) Black Hole Formation.

(b) Matter Dispersion.

Figure 6.6: (6.6a) Black hole formation and (6.6b) matter dispersion in the collapse of test particles obtained in the $m \to 0$ limit of the unbound shell collapse. The diagrams correspond to causal structures of the whole spacetime, with the interior Minkowski and exterior Schwarzschild regions represented. Red lines represent outgoing light rays and the non horizontal thick black line is the trajectory of the shell. On the black hole formation, the resulting singularity is found to be null, represented by an undulating black line parallel to the red line in (6.6a).

Chapter 7

Collapsing Thin Shell: Bound Case

7.1 Equation of Motion

We proceed with the last case, that of $M < m$. We take the equation of motion, Eq. (5.1) with the minus sign,

$$\dot{R} = -\left(\frac{M^2}{m^2} - 1 + \frac{M}{R} + \frac{m^2}{4R^2}\right)^{1/2} . \tag{7.1}$$

Since $M < m$, we have $M^2/m^2 - 1 < 0$, so that there is a range of validity to Eq. (7.1), i.e. there is a finite value R_0 such that $\dot{R}(R = R_0) = 0$. This is the maximum value for the radius of the shell, given by

$$R_0 = \frac{m^2}{2(m - M)} , \tag{7.2}$$

which implies this as being a bound collapse starting at R_0 with zero velocity. This shell corresponds to the case of the collapsing star with interior FLRW metric with $k = 1$, studied in Chapter 4. This maximum value, Eq. (7.2), merits further inspection. It is seen to diverge for $m \to M$ and $m \to \infty$, the former being expected as it corresponds to the marginally bound case, and the latter a statement on the conservation of energy, Eq. (5.1). Furthermore there is a minimum value for R_0, achieved at $m = 2M$ wherein $R_0 = 2M$. As such no bound thin shell can begin fall from within $r_+ = 2M$.

7.2 Proper Time Solution

Trajectory of the Shell as seen by a Local Observer

The differential equation, Eq. (7.1), refers to the trajectory of the shell described by a local observer, i.e. one that falls with the shell. Rewriting the differential equation so that proper time is differentiated with respect to distance, we can obtain its solution,

$$\tau(R) = \frac{m}{2(m^2 - M^2)}\left(\xi(R) - m^2\right) + \frac{m^3 M}{2(m^2 - M^2)^{3/2}}\left(\arcsin\left[\frac{m^2 M - 2(m^2 - M^2)R}{m^3}\right] - \arcsin\left[\frac{M}{m}\right]\right) , \tag{7.3}$$

where $\xi(R) = [m^2(m^2+4MR)+4(M^2-m^2)R^2]^{1/2}$. The shell comes from R_0 at an instant τ_0 given by

$$\tau_0 = -\frac{m^2}{4(m^2-M^2)^{3/2}}\left(2m(m^2-M^2)^{1/2}+mM\pi+2mM\arcsin\left[\frac{M}{m}\right]\right), \tag{7.4}$$

collapsing then at the center of coordinates, $R = 0$, at the instant $\tau_C = 0$, thus forming a singularity. The time reported, by the local observer, between the shell passing the Schwarzschild radius, $R = 2M$, and collapsing at the center is

$$\tau(2M) = \frac{m(|m^2-4M^2|-m^2)}{2(m^2-M^2)} - \frac{m^3M}{2(m^2-M^2)^{3/2}}\left(\arcsin\left[\frac{M(3m^2-4M^2)}{m^3}\right]+\arcsin\left[\frac{M}{m}\right]\right). \tag{7.5}$$

Various trajectories, for different values of m relative to M, both $M < m < 2M$ and $m > 2M$, are shown in Figures 7.1a and 7.1b. We see that in the limit $m \to M$ these trajectories approach that of the marginally bound collapse as expected.

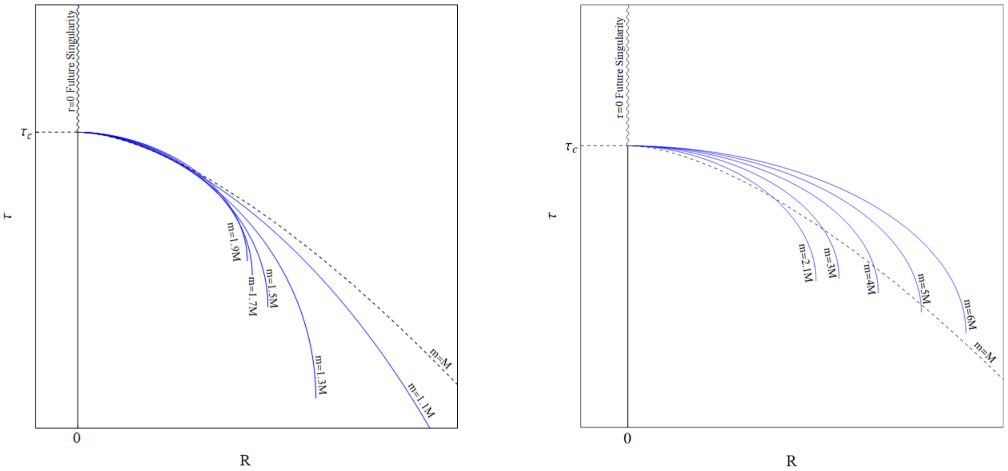

(a) Trajectories for $M < m < 2M$.

(b) Trajectories for $m > 2M$.

Figure 7.1: With blue lines, the bound shell collapse measured in proper time for different values of the rest mass of the shell, m, relative to its energy parameter M. These trajectories can be separated into two categories, those of $M < m < 2M$ in Figure 7.1a, and those of $m > 2M$ in Figure 7.1b. The dashed black line represents the trajectory of the marginally bound collapsing shell studied in chapter 5.

The extensive study of Eq. (6.1) in the two regions, which we will now regard, can be consulted in Appendix A.

7.3 Interior Time Solution

Trajectory of the Shell as seen by an Internal Observer

The solution for the bound shell's trajectory in the interior region is obtained by solving Eq. (A.35) for $m > M$. Proceeding in this fashion, we obtained the closed form

$$T_-(R) = \frac{M}{2(m^2-M^2)}\left(\xi(R)-m^2\right)+\frac{m^4}{2(m^2-M^2)^{3/2}}\left(\arcsin\left[\frac{m^2M-2(m^2-M^2)R}{m^3}\right]-\arcsin\left[\frac{M}{m}\right]\right), \tag{7.6}$$

where $\xi(R) = [m^2(m^2+4MR)+4(M^2-m^2)R^2]^{1/2}$. The shell, as described by Eq. (7.6), comes from R_0 at an instant T_{-0} given by

$$T_{-0} = -\frac{m^2}{4(m^2-M^2)^{3/2}}\left(2M(m^2-M^2)^{1/2}+m^2\pi+2m^2\arcsin\left[\frac{M}{m}\right]\right)\,, \tag{7.7}$$

collapsing then at the center of coordinates, $R = 0$, at the instant $\tau_C = 0$ forming a singularity. The time between the shell passing through the Schwarzschild radius, $R = 2M$, and collapsing at the center, reported by the internal observer, is

$$T_-(2M) = \frac{M(|m^2-4M^2|-m^2)}{2(m^2-M^2)} - \frac{m^4}{2(m^2-M^2)^{3/2}}\left(\arcsin\left[\frac{M(3m^2-4M^2)}{m^3}\right]+\arcsin\left[\frac{M}{m}\right]\right)\,. \tag{7.8}$$

Various trajectories, for different values of m relative to M, both $M < m < 2M$ and $m > 2M$, are shown in Figures 7.2a and 7.2b. We see the trajectories approach that of the marginally bound collapse as $m \to M$, as was expected. However, we find that the trajectories also approach that of ingoing light rays in the opposite limit of $m \to \infty$.

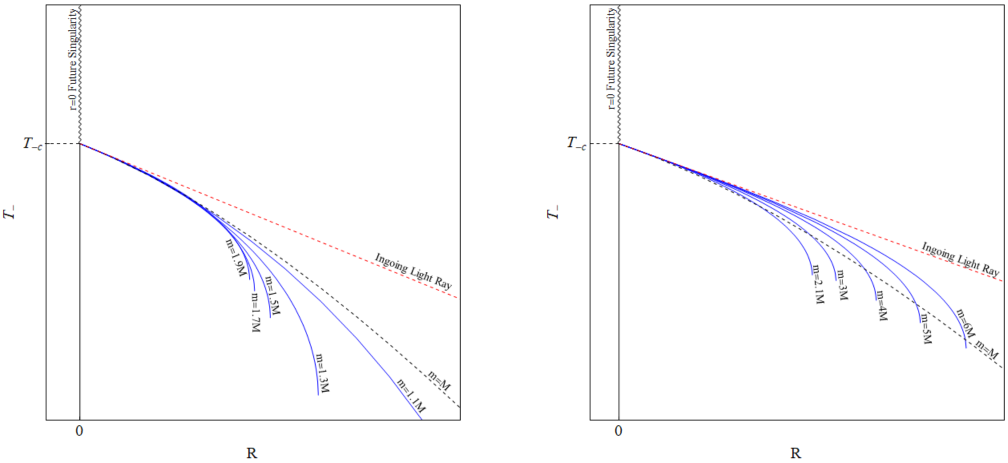

(a) Trajectories for $M < m < 2M$.

(b) Trajectories for $m > 2M$.

Figure 7.2: With blue lines, the bound shell collapse measured in internal time for different values of the rest mass of the shell, m, relative to its energy parameter M. These trajectories can be separated into two categories, those of $M < m < 2M$ in Figure 7.2a, and those of $m > 2M$ in Figure 7.2b. The dashed black line represents the trajectory of the marginally bound collapsing shell, studied in chapter 5. The dashed red line represents an ingoing null geodesic.

The Limit of Infinite Mass Shell with Fixed Energy

As per the previous remark, we search for the $m \to \infty$ limit of the bound trajectory of the shell as seen by the interior observer, Eq. (7.6). We find

$$\lim_{m\to\infty} T_-(R) = -R\,, \tag{7.9}$$

which does correspond to a flash of light converging on the center of coordinates, $r_- = 0$, at the instant $t_- = 0$ in Minkowski coordinates, Eq. (5.11) with the minus sign. To understand this, we begin by obtaining the shell's acceleration from the shell's velocity, Eq. (A.32)

$$\ddot{R} = -\frac{1}{2R}\left(\frac{M}{R} + \frac{m^2}{2R^2}\right) , \tag{7.10}$$

so that the acceleration grows with the square of the mass. Thus, unlike the case of the unbound collapsing dust shell, the high rest mass of the shell and conservation of energy, Eq. (5.1), guarantees the shell's acceleration grows rapidly with the shell's contraction. The shell then achieves the limit velocity of light, developing a trajectory indistinguishable from that of the latter.

7.4 Exterior Time Solution

We now move the analysis to the exterior spacetime. We will do so in Schwarzschild coordinate. The remaining cases follow in a similar fashion to that studied in chapter 5. We also note the trajectories of light rays and event and apparent horizons are the same as those seen in the marginally bound case since, apart from the point of emission, they do not depend on the particular trajectory of the source. As such, for the sake of brevity, we study the trajectory of the shell specifically, the remaining elements being developed as they were in chapter 5.

7.4.1 Schwarzschild Coordinates

Trajectory of the Shell as seen by an External Observer

The solution to the bound equation of motion in exterior Schwarzschild coordinates, Eq. (A.32 with $M < m$, can be obtained in closed form

$$\begin{aligned} T_+(R) = \pm\frac{1}{2(m^2-M^2)}\Bigg(&\frac{m^4-6m^2M^2+4M^4}{(m^2-M^2)^{1/2}}\left(\arccos\left[\frac{m^2M-2(m^2-M^2)R}{m^3}\right] - \arccos\left[\frac{M}{m}\right]\right) + \\ &+ M(\xi(R)-m^2) + 4M(m^2-M^2)\ln\left|\frac{m^4+4m^2M^2+(8M^2-6m^2)MR+(4M^2-m^2)\xi(R)}{4m^2M(R-2M)}\right|\Bigg) , \end{aligned} \tag{7.11}$$

with the plus sign for $M < m < 2M$ and the minus sign for $m > 2M$, and $\xi(R) = [m^2(m^2+4MR) + +4(M^2-m^2)R^2]^{1/2}$. The shell comes from R_0 at an instant T_{+0} given by

$$\begin{aligned} T_{+0} = \pm\frac{1}{2(m^2-M^2)^{3/2}}\Bigg(&(m^4-6m^2M^2+4M^4)\pi - m^2M(m^2-M^2)^{1/2} - \\ &-(m^4-6m^2M^2+4M^4)\arccos\left[\frac{M}{m}\right] - 4M(m^2-M^2)^{3/2}\ln\left[\frac{2M}{m}\right]\Bigg) , \end{aligned} \tag{7.12}$$

with the plus sign for $M < m < 2M$ and the minus sign for $m > 2M$. It then goes on to collapse at the center of coordinates, $R = 0$, at the instant $T_{+C} = 0$, thus forming a singularity. At $R = 2M$ the trajectory diverges, marking the coordinate singularity usual to the Schwarzschild coordinate system. Various trajectories, for different values of m, both $M < m < 2M$ and $m > 2M$, are shown in Figures 7.3a and 7.3b. Here we also identify the two limit cases seen in the interior solution. At the limit $m \to M$

the trajectories approach that of the marginally bound case, and at the limit $m \rightarrow \infty$ they approach the trajectories of ingoing light rays

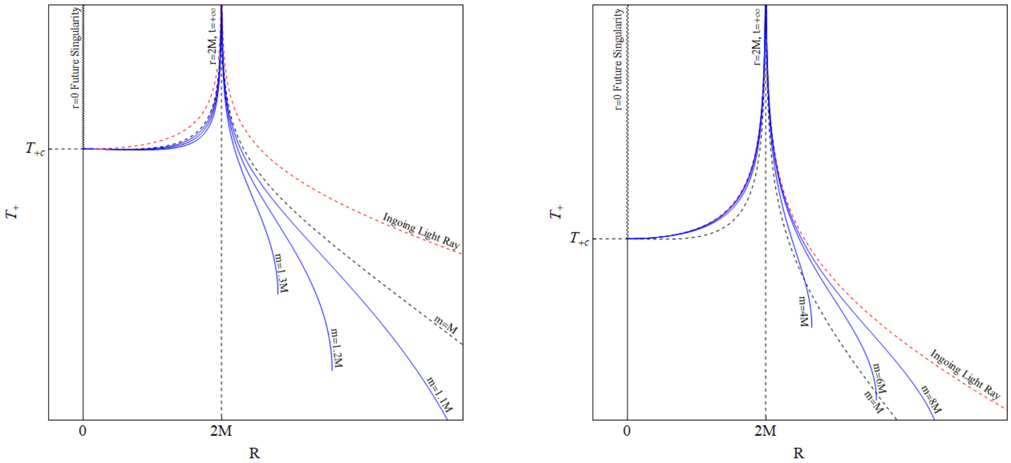

(a) Trajectories for $M < m < 2M$.

(b) Trajectories for $m > 2M$.

Figure 7.3: With blue lines, the bound shell collapse measured in external Schwarzschild time for different values of the rest mass of the shell, m, relative to its energy parameter M. These trajectories can be separated into two categories, those of $M < m < 2M$ in Figure 7.3a, and those of $m > 2M$ in Figure 7.3b. The dashed black line represents the trajectory of the marginally bound collapsing shell, studied in chapter 5. The dashed red line represents an ingoing null geodesic.

The Limit of Infinite Mass Shell with Fixed Energy

Following the previous remarks on the tendency for the bound shell's trajectory to approach that of an ingoing light ray with increasing rest mass, we search for the $m \rightarrow \infty$ limit of Eq. (7.11). Doing so, we find

$$\lim_{m\rightarrow\infty} T_+(R) = -R - 2M \ln\left|\frac{R-2M}{2M}\right| , \tag{7.13}$$

which corresponds to the trajectory of a light flash converging on the center of coordinates, $r_+ = 0$, at the instant $t_+ = 0$ by Eq. (5.15) with the minus sign. This result corroborates with the assertion on the trajectory in the interior spacetime.

Causal Structure

With the outgoing light rays and apparent and event horizons, already studied in chapter 5.4.1, we can build the causal structure of the whole spacetime, Figure 7.4.

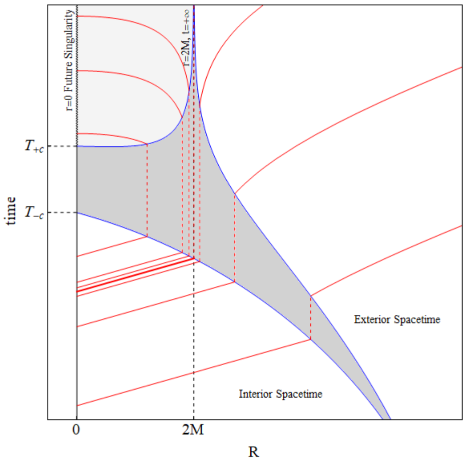
r=0 Future Singularity
r=2M, t=+∞
T_{+c}
T_{-c}
time
Exterior Spacetime
Interior Spacetime
0
2M
R

Figure 7.4: The causal structure of spacetime for $M < m$, bound case, in exterior Schwarzschild coordinates and interior Minkowski. The trajectory of the shell is the blue line. In red are drawn the outgoing null rays, with the last one reaching infinity, shown in a thicker line, corresponding to the event horizon. The light shaded region is the region of trapped surfaces and the spacelike surface delimiting it, interior to the event horizon, corresponds to the apparent horizon. The dark shaded region is non physical and is used to separate the two different spacetimes. The singularity is the endpoint of the evolution and is shown in a curvilinear line.

Chapter 8

Conclusions

While the work by Oppenheimer and Snyder presents a remarkable solution to a non trivial problem, the method they used rapidly becomes unusable as the complexity of a system increases. In this work we confirmed one can obtain a solution with much added ease by applying the junction conditions. Additionally, the solution so obtained is more complete, as we were able to obtain a complete description of the evolution of the collapsing star. With the trajectory, we found the rich causal structure of the system could be uncovered in a fully explicit form. Thus one could describe the trajectory of outgoing light rays originating from the center of spatial coordinates, as well as the event and apparent horizons, chapter 2.

With the original case studied, the extension to the cases with interior FLRW metrics of $k = -1$ and $k = 1$ was carried out with similar simplicity, chapters 3 and 4. Thus, we were able to obtain the set of possible solutions pertaining to collapsing, spherically symmetric and non rotating, stars made of dust. Similarly to the marginally bound collapsing star, the rich causal structure of the system of both the bound and unbound stars could be explicitly described in the same fashion.

The study of the analogous cases with thin shells revealed many of the general features observed by external observers to remain the same, chapters 5, 6 and 7. The calculations necessary, however, were significantly simplified as the interior Minkowski spacetime required much less attention. The results showed the causal structure of the system could identically be constructed, with the structure of interior region identical in all cases.

The unbound and bound collapsing thin shells were found to have interesting limiting cases. For the unbound shell, the trajectory in the limit $m \to 0$ was found to coincide with those of the ingoing null geodesics, chapter 6. This naturally corresponds to the case where the collapsing thin shell approximates a converging flash of light. On the other hand, the trajectory of the bound shell was found to have a similar behaviour in the opposite limit, $m \to \infty$, chapter 7. For bound shells, it is found that both the acceleration and starting distance increase with the mass m. As such, as the value of m increases, the shell achieves increasingly higher velocities, approaching the limit velocity of light. In other words its trajectory approaches that of light rays.

The study carried out pertained to simplified case of a non rotating and spherically symmetric collapsing bodies, stars and shells, made of dust. There are two natural paths that may be followed to generalize this work. One may consider distributions of non frictionless material, i.e. mass energy distributions with non zero pressures. Another case of interest is that in which the body, star or shell, is rotating, in which case the exterior spacetime may be, for example, a Kerr spacetime. The cases we considered in this work are then the limiting cases $p \to 0$ and $j \to 0$, respectively, of both generalizations proposed.

Appendix A

Junction Conditions

In solving the problem of a collapsing massive body, one eventually finds two distinct spacetimes are needed, one for the interior of said body, and another for the exterior. These solutions, however, cannot be any two respective solutions to Einstein's field equations. Instead, they must be related through the metric, which must be continuous over the surface of separation, and the extrinsic curvature, which must be continuous over the same surface unless there is a localized energy-matter distribution. While an analytic solution, continuous over the whole spacetime, like that found by J. R. Oppenheimer and H. Snyder, could be obtained directly, such proposition becomes quickly untenable as the complexity of the system under consideration increases. This difficulty is compounded as the different spacetimes may be easier to describe in different coordinate systems.

Nevertheless, each of the two independent solutions to the Einstein's field equations could still be obtained, and the relations required between both were known. The difficulties inherent to solving the field equations since their introduction, whether on the case of gravitational collapse or otherwise, motivated G. Darmois [9], C. W. Misner and D. H. Sharp [10] and W. Israel [11] to independently develop a set of junction conditions which must be verified if the solution found is to be physically sensible. As such, this allows one to find a solution, of his own choosing, for each region and then impose restrictions through those junction conditions to obtain a valid set. In the following we will use the notation and description used by E. Poisson, [25].

A.1 Theoretical development

We start by considering two different spacetimes separated by a timelike hypersurface, Figure A.1. We then take a coordinate system for each region, say x^{α}_{-} and x^{α}_{+}, and an induced coordinate system for the hypersurface, y^{a}. The hypersurface can be further described by its normal four vector, n^{α}, and its four velocity field, u^{α}, defined such that $u^{\alpha}u_{\alpha} = -1$, $n^{\alpha}n_{\alpha} = 1$ and $u^{\alpha}n_{\alpha} = 0$. We will use greek letters for indices in four dimension spacetime and latin letters for indices in three dimension spacetime. From what will be followed, the case of spacelike surfaces of separation can be obtained similarly by switching the character of the normal vector. Solving the Einstein field equations separately, we will end up with two solutions for the metric, each valid in its region. To describe the whole spacetime, we will consider a distributional formalism, writing as such

$$g_{\alpha\beta} = g_{+\alpha\beta}\,\Theta(x) + g_{-\alpha\beta}\,\Theta(-x)\,, \tag{A.1}$$

with x a measure of distance along the normal to the hypersurface and $\Theta(x)$ the Heaviside step function. The distance measure x is such that $\mathrm{d}x^\alpha = n^\alpha \mathrm{d}x$, with n_γ the spacelike four vector unit normal to the surface. The Heaviside step function takes value one with positive argument, and value zero with negative argument. If the argument is zero, the step function is indeterminate. The derivatives of the metric will give

$$\begin{aligned}\partial_\gamma g_{\alpha\beta} &= \delta(x)\,n_\gamma\,(g_{+\alpha\beta} - g_{-\alpha\beta}) + \Theta(x)\,\partial_\gamma g_{+\alpha\beta} + \Theta(-x)\,\partial_\gamma g_{-\alpha\beta} = \\ &= \delta(x)\,n_\gamma\,[g_{\alpha\beta}] + \Theta(x)\,\partial_\gamma g_{+\alpha\beta} + \Theta(-x)\,\partial_\gamma g_{-\alpha\beta}\,,\end{aligned} \tag{A.2}$$

where square brackets indicate the jump of a quantity over a boundary, i.e. $[g_{\alpha\beta}] = g_{+\alpha\beta} - g_{-\alpha\beta}$ is the jump of the metric as one crosses the boundary and $\delta(x)$ is the delta function.

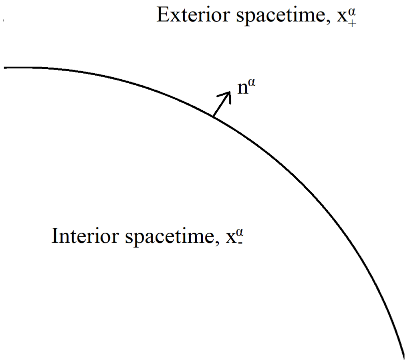
Exterior spacetime, x^α_+
n^α
Interior spacetime, x^α_-

Figure A.1: The two spacetimes separated by a timelike hypersurface. Each spacetime is described in its own coordinate system, x^α_- and x^α_+ for the interior and exterior respectively. The four vector n^α is the normal to the hypersurface.

A.1.1 First Condition

Using the metric as a distribution, Eq. (A.1), we find the Christoffel symbols to contain terms such as

$$g^{\gamma\sigma}\partial_\sigma g_{\alpha\beta} = \Big(g_+^{\alpha\beta}\,\Theta(x) + g_-^{\alpha\beta}\,\Theta(-x)\Big)\Big(\delta(x)\,n_\gamma\,[g_{\alpha\beta}] + \Theta(x)\,\partial_\gamma g_{+\alpha\beta} + \Theta(-x)\,\partial_\gamma g_{-\alpha\beta}\Big)\,. \tag{A.3}$$

We note from the previous that the Christoffel symbol will then contain products of distribution functions, such as $\Theta(\pm x)\Theta(\pm x)$, $\Theta(\pm x)\Theta(\mp x)$ and $\delta(x)\Theta(x)$. While the first two are defined as distribution functions, the third is not. Therefore, no terms proportional to them may be present, which leads us to the first junction condition, that of continuity of the metric over the hypersurface. If we were to express the whole spacetime in one coordinate system (t, r, θ, ϕ), this would be written

$$[g_{\alpha\beta}]\Big|_{r\to R} = 0\,. \tag{A.4}$$

This can be written in a coordinate invariant form, fit for the separation of the spacetime into two regions, if we take into account the coordinate system on the surface, y^a, as well as those of the surrounding regions, x^α_- and x^α_+. Using the surface coordinate basis, $e^\alpha_{\ a} = \partial x^\alpha_\pm/\partial y^a$, Eq. (A.4) can be written for the surface induced metric $h_{ab} = g_{\alpha\beta}e^\alpha_{\ a}e^\beta_{\ b}$,

$$[h_{ab}] = 0\,. \tag{A.5}$$

A.1.2 Second Condition

To solve Einstein's field equations, one has to compute the Einstein and Ricci tensors. These depend in some way of the derivatives of Christoffel symbols, so that the tensorial quantities also present delta function discontinuities. Proceeding as before, we obtain for the Riemann tensor

$$\begin{aligned} R^\alpha_{\ \beta\gamma\delta} &= \Theta(x)R_+{}^\alpha_{\ \beta\gamma\delta} + \Theta(-x)R_-{}^\alpha_{\ \beta\gamma\delta} + \delta(x)\left([\Gamma^\alpha_{\ \beta\delta}]n_\gamma - [\Gamma^\alpha_{\ \beta\gamma}]n_\delta\right) \\ &= \Theta(x)R_+{}^\alpha_{\ \beta\gamma\delta} + \Theta(-x)R_-{}^\alpha_{\ \beta\gamma\delta} + \delta(x)A^\alpha_{\ \beta\gamma\delta}\,, \end{aligned} \tag{A.6}$$

where the normal vector appears once again with the application of the differentiation operator to the Heaviside step function. From the Riemann tensor, Eq. (A.6), one finds an induced curvature discontinuity. This can be related with the extrinsic curvature. The latter is defined by

$$K_{ab} = n_{\alpha;\beta}\, e^\alpha_{\ a}\, e^\beta_{\ b} \implies [K_{ab}] = [n_{\alpha;\beta}]\, e^\alpha_{\ a}\, e^\beta_{\ b}\,, \tag{A.7}$$

with the semicolon denoting the covariant derivative. Defining now

$$\kappa_{\alpha\beta} = [g_{\alpha\beta,\gamma}]n^\gamma\,, \tag{A.8}$$

and since the induced coordinate basis vectors, $e^\alpha_{\ a}$ are tangent to the hypersurface due to the continuity of the x^α across it, one finds

$$[K_{ab}] = \frac{1}{2}\kappa_{\alpha\beta}\, e^\alpha_{\ a}\, e^\beta_{\ b}\,. \tag{A.9}$$

With these, the one can then write the curvature discontinuity found in Eq. (A.6) and its traces as

$$A^\alpha_{\ \beta\gamma\delta} = \frac{1}{2}\left(\kappa^\alpha_{\ \delta}\, n_\beta\, n_\gamma - \kappa^\alpha_{\ \gamma}\, n_\beta\, n_\delta - \kappa_{\beta\delta}\, n^\alpha\, n_\gamma + \kappa_{\beta\gamma}\, n^\alpha\, n_\delta\right)\,, \tag{A.10}$$

$$A_{\alpha\beta} = \frac{1}{2}\left(\kappa_{\mu\alpha}\, n^\mu\, n_\beta + \kappa_{\mu\beta}\, n^\mu\, n_\alpha - \kappa\, n_\alpha\, n_\beta - \kappa_{\alpha\beta}\right)\,, \tag{A.11}$$

$$A = \kappa_{\mu\nu}\, n^\mu\, n^\nu - \kappa\,. \tag{A.12}$$

The Einstein tensor's discontinuity then takes the form $A_{\alpha\beta} - \frac{1}{2} A\, g_{\alpha\beta}$. We now write the stress-energy tensor as

$$T_{\alpha\beta} = \Theta(x) T_{+\alpha\beta} + \Theta(-x) T_{-\alpha\beta} + \delta(x) S_{\alpha\beta}\,, \tag{A.13}$$

which gives the second condition

$$S_{ab} = S_{\alpha\beta}\, e^{\alpha}_{a}\, e^{\beta}_{b} = -\frac{1}{8\pi}\Big([K_{ab}] - [K]\, h_{ab}\Big)\,. \tag{A.14}$$

From Eq. (A.14) we see that unless the stress-energy tensor, Eq. (A.13), admits a surface energy distribution, then $S_{ab} = 0$ and the second junction condition reduces to

$$[K_{ab}] = 0\,, \tag{A.15}$$

i.e. the extrinsic curvature is also continuous.

The two junction conditions, Eqs. (A.5) and (A.14), must be verified by the two solutions obtained for the Einstein's field equations, if those are to make a valid solution of the system. Conversely, if one finds two such solutions, application of the two junction conditions will give the necessary properties of the system.

A.2 Thin Shells

A.2.1 Proper Time Description

The junction condition formalism developed in the previous section can be applied to any timelike surface separating any two spacetimes. As such, we now consider the particular case where all matter is confined to this surface and is non rotating, that is, the case of a non rotating thin shell of gravitating matter. Additionally we take the tangential pressure to be zero, thus imposing the shell as being composed of dust. The surface stress-energy tensor is then defined as

$$S^{ab} = \sigma\, u^a\, u^b\,, \tag{A.16}$$

with u^a the velocity field of the shell and σ its surface density. With the considerations above, Birkhoff's theorem requires the outside spacetime to be a Schwarzschild spacetime. The interior, being devoid of matter, must be a Minkowski spacetime. Thus we choose the pair of metrics

$$\mathrm{d}s_-^2 = -\mathrm{d}t_-^2 + \mathrm{d}r_-^2 + r_-^2(\mathrm{d}\theta^2 + \sin^2\theta\, \mathrm{d}\phi^2) \tag{A.17}$$

$$\mathrm{d}s_+^2 = -\left(1 - \frac{2M}{r_+}\right)\mathrm{d}t_+^2 + \left(1 - \frac{2M}{r_+}\right)^{-1}\mathrm{d}r_+^2 + r_+^2(\mathrm{d}\theta^2 + \sin^2\theta\, \mathrm{d}\phi^2)\,, \tag{A.18}$$

with (t_-, r_-, θ, ϕ) the interior spacetime coordinates and (t_+, r_+, θ, ϕ) the exterior spacetime coordinates. The appropriate junction conditions are then Eqs. (A.5) and (A.14), respectively

$$[h_{ab}]\Big|_{r\to R} = 0 \quad , \qquad S_{ab} = -\frac{1}{8\pi}\Big([K_{ab}] - [K]h_{ab}\Big) \, ,$$

From the first condition, we find

$$-\dot{T}_-^2 + \dot{R}^2 = -\left(1 - \frac{2M}{R}\right)\dot{T}_+^2 + \left(1 - \frac{2M}{R}\right)^{-1}\dot{R}^2 = -1 \tag{A.19}$$

The extrinsic curvature elements, $K_{ab} = n_{\alpha;\beta}\, e^\alpha_a\, e^\beta_b$, are then for the interior spacetime

$$K_{-\ \tau}^{\ \tau} = \frac{\ddot{R}}{(1+\dot{R})^{1/2}} \tag{A.20}$$

$$K_{-\ \theta}^{\ \theta} = \frac{(1+\dot{R}^2)^{1/2}}{R} \tag{A.21}$$

$$K_{-\ \phi}^{\ \phi} = \frac{(1+\dot{R}^2)^{1/2}}{R} \, . \tag{A.22}$$

For the exterior spacetime, the extrinsic curvature elements are

$$K_{+\ \tau}^{\ \tau} = \frac{\ddot{R} + M/R^2}{(\dot{R}^2 + 1 - 2M/R)^{1/2}} \tag{A.23}$$

$$K_{+\ \theta}^{\ \theta} = \frac{1}{R}\left(\dot{R}^2 + 1 - \frac{2M}{R}\right)^{1/2} \tag{A.24}$$

$$K_{+\ \phi}^{\ \phi} = \frac{1}{R}\left(\dot{R}^2 + 1 - \frac{2M}{R}\right)^{1/2} \, . \tag{A.25}$$

Applying Eqs. (A.20) through (A.25) to the second junction condition, Eq. (A.14), and using the stress-energy tensor, Eq. (A.16), gives two relations to be verified

$$\sigma = \frac{1}{4\pi R}\left[\left(\dot{R}^2 + 1\right)^{1/2} - \left(\dot{R}^2 + 1 - \frac{2M}{R}\right)^{1/2}\right] \tag{A.26}$$

$$0 = \frac{\ddot{R} + M/R^2}{(\dot{R}^2 + 1 - 2M/R)^{1/2}} + \frac{1}{R}\left(\dot{R}^2 + 1 - \frac{2M}{R}\right)^{1/2} - \frac{\ddot{R}}{(\dot{R}^2 + 1)^{1/2}} - \frac{1}{R}\left(\dot{R}^2 + 1\right) \, . \tag{A.27}$$

The second of these, Eq. (A.27), can be rewritten as

$$\begin{aligned} 0 &= \frac{1}{\dot{R}}\frac{\mathrm{d}}{\mathrm{d}\tau}\left[\left(\dot{R}^2 + 1 - \frac{2M}{R}\right)^{1/2} - \left(\dot{R}^2 + 1\right)^{1/2}\right] + \frac{1}{R}\left[\left(\dot{R} + 1 - \frac{2M}{R}\right)^{1/2} - \left(\dot{R}^2 + 1\right)^{1/2}\right] \iff \\ \iff 0 &= \frac{\mathrm{d}}{\mathrm{d}\tau}\left\{R\left[\left(\dot{R}^2 + 1 - \frac{2M}{R}\right)^{1/2} - \left(\dot{R}^2 + 1\right)^{1/2}\right]\right\} \end{aligned} \tag{A.28}$$

Thus, the term inside curly brackets in Eq. (A.28) is a constant. This term is also found in the other condition, Eq. (A.26), so that we get

$$m = -R\left[\left(\dot{R}^2 + 1 - \frac{2M}{R}\right)^{1/2} - \left(\dot{R}^2 + 1\right)^{1/2}\right] \tag{A.29}$$

$$m = 4\pi R^2 \sigma\,, \tag{A.30}$$

and the constant m is identified as being the mass of the shell. From Eq. (A.29) we see it must be positive, as expected. Furthermore, dividing Eq. (A.29) by R and squaring it gives

$$M = m\left(\dot{R}^2 + 1\right)^{1/2} - \frac{m^2}{2R}\,. \tag{A.31}$$

The two last equations, Eqs. (A.30) and (A.31), serve as the equations of motion describing the evolution of the self gravitating, non rotating, thin shell made of dust.

Analysing the second equation of motion, Eq. (A.31), we see it takes the form of an energy equation, the first term on the right side being the kinetic term, and the second the potential term. More insight can be obtained by inverting this equation, by which we obtain

$$\dot{R} = \pm\left(\frac{M^2}{m^2} + \frac{M}{R} + \frac{m^2}{4R^2} - 1\right)^{1/2}\,, \tag{A.32}$$

the plus sign corresponding to an expanding shell, and the minus to a contracting shell. From Eq. (A.32) we look for the condition $\dot{R} = 0$ and identify three distinct cases, $M < m$, $M = m$ and $M > m$, which correspond to the bound, marginally bound and unbound shells respectively. These mirror the cases of the collapsing star with $E < 1$, $E = 1$ and $E > 1$ studied in chapters 4, 2 and 3 respectively.

The equation of motion obtained, Eq. (A.32), describes the contraction of the shell described by a local observer, i.e. an observer falling with the shell. This follows directly from the stress-energy tensor and the induced metric, both detailed with respect to the shell. However, the use of the result of the first junction condition, Eq. (A.19), allows one to obtain the same description as seen by an internal or an external observer.

A.2.2 Interior Time Description

We now search for a description of the system as seen by an internal observer. We begin by considering the relation coming from one result of the first junction condition, Eq. (A.19),

$$-\dot{T}_-^2 + \dot{R}^2 = -1\,, \tag{A.33}$$

and rewrite it as

$$\left(\frac{\mathrm{d}T_-}{\mathrm{d}R}\frac{\mathrm{d}R}{\mathrm{d}\tau}\right)^2 + \left(\frac{\mathrm{d}R}{\mathrm{d}\tau}\right)^2 = 1 \quad \Longleftrightarrow \quad \left[\left(\frac{\mathrm{d}T_-}{\mathrm{d}R}\right)^2 - 1\right]\dot{R}^2 = 1\,. \tag{A.34}$$

We can now replace $\dot{R}$ with the equation of motion, Eq. (A.32), and simplify thus obtaining

$$\frac{\mathrm{d}T_-}{\mathrm{d}R} = -\left[\left(\frac{M^2}{m^2}-1\right)R^2 + MR + \frac{m^2}{4}\right]^{-1/2}\left(\frac{M^2}{m^2}R^2 + MR + \frac{m^2}{4}\right)^{1/2} . \tag{A.35}$$

A.2.3 Exterior Time Description

The description of the system for the external observer follows in a similar fashion to that of the interior observer. We use the relation coming from one result of the first junction condition, Eq. (A.19),

$$-\left(1-\frac{2M}{R}\right)\dot{T}_+^2 + \left(1-\frac{2M}{R}\right)^{-1}\dot{R}^2 = -1 , \tag{A.36}$$

and as before rewrite this equation as

$$\begin{aligned} -\left(1-\frac{2M}{R}\right)\left(\frac{\mathrm{d}T_+}{\mathrm{d}R}\frac{\mathrm{d}R}{\mathrm{d}\tau}\right)^2 + \left(1-\frac{2M}{R}\right)^{-1}\left(\frac{\mathrm{d}R}{\mathrm{d}\tau}\right)^2 = -1 \quad \Longleftrightarrow \\ \Longleftrightarrow \quad \left[\left(1-\frac{2M}{R}\right)\left(\frac{\mathrm{d}T_+}{\mathrm{d}R}\right)^2 - \left(1-\frac{2M}{R}\right)^{-1}\right]\dot{R}^2 = 1 . \end{aligned} \tag{A.37}$$

We now replace $\dot{R}$ with the equation of motion, Eq. (A.32), and simplify thus obtaining

$$\frac{\mathrm{d}T_+}{\mathrm{d}R} = -\left(1-\frac{2M}{R}\right)^{-1}\left[\left(\frac{M^2}{m^2}-1\right)R^2 + MR + \frac{m^2}{4}\right]^{-1/2}\left(\frac{M^2}{m^2}R^2 - MR + \frac{m^2}{4}\right)^{1/2} \tag{A.38}$$

A.2.4 Newtonian Limit

We now finish this chapter by looking at the Newtonian limit of the equation of motion governing the trajectory of the shell, Eq. (A.31), that is the limit where the velocity, $\dot{R}$, is small. Here we find Eq. (A.31) to verify

$$M \approx m + \frac{1}{2}m\,\dot{R}^2 - \frac{m^2}{2R} , \tag{A.39}$$

This form can be identified with the energy equation of a thin shell in classical Newtonian mechanics. We begin by taking the shell to be of some width. Then, the force acting on a layer of the shell is given by the average of the force acting on either side [39]. Identically, the potential at the same layer is given by the average on either side. Since the shell is empty, the potential inside is zero, while on the outside is given by $-m/R$. Thus, the identification with Eq. (A.39) is made. The first term is the rest mass term, the second is the kinetic energy and the third is the average of the potential energy. This justifies taking the equation of motion Eq. (A.31) as being the relativistic energy equation of the shell.

Appendix B

Oppenheimer-Snyder Collapse as done by Oppenheimer and Snyder

Oppenheimer and Snyder [4] solve the system by finding an analytic solution of the Einstein field equations describing the whole spacetime. To do so, we start by ignoring the influence of any escaping matter or radiation which could be ejected during the process of contraction. Furthermore, the system is taken to be non-rotating. Accordingly, the line element will be spherically symmetric, and outside of the boundary of the star, it will also be static.

B.1 General Solution

As a first approach, the interior of the star is taken to be represented by a general metric

$$\mathrm{d}s^2 = -\mathrm{e}^{\nu}\,\mathrm{d}t^2 + \mathrm{e}^{\zeta}\,\mathrm{d}r^2 + r^2(\mathrm{d}\theta^2 + \sin^2\theta\,\mathrm{d}\phi^2)\,, \tag{B.1}$$

with ν and ζ functions of the space-time coordinates, i.e. $\nu \equiv \nu(t, r)$ and $\zeta \equiv \zeta(t, r)$. The field equations give the relations

$$8\pi T^0_{\ 0} = -\mathrm{e}^{-\zeta}\left(\frac{\zeta'}{r} - \frac{1}{r^2}\right) - \frac{1}{r^2}\,, \tag{B.2}$$

$$8\pi T^1_{\ 1} = \mathrm{e}^{-\zeta}\left(\frac{\nu'}{r} + \frac{1}{r^2}\right) - \frac{1}{r^2}\,, \tag{B.3}$$

$$8\pi T^2_{\ 2} = 8\pi T^3_{\ 3} = \mathrm{e}^{-\zeta}\left(\frac{\nu''}{2} + \frac{\nu'^2}{4} - \frac{\zeta'\nu'}{2} + \frac{\nu' - \zeta'}{2r}\right) - \mathrm{e}^{-\nu}\left(\frac{\ddot{\zeta}}{2} + \frac{\dot{\zeta}^2}{4} - \frac{\dot{\zeta}\dot{\nu}}{4}\right)\,, \tag{B.4}$$

$$8\pi T^1_{\ 0} = \mathrm{e}^{-\zeta}\frac{\dot{\zeta}}{r}\,, \tag{B.5}$$

$$8\pi T^0_{\ 1} = -\mathrm{e}^{-\nu}\frac{\dot{\zeta}}{r}\,, \tag{B.6}$$

with the dot denoting differentiation with respect to t and prime the differentiation with respect to r. The energy-momentum tensor $T^{\alpha}_{\ \beta}$ contains the contribution to both energy density and pressure coming from matter and radiation. The field equations are difficult to solve analytically for all but the simplest distributions of matter. Still, they allows us to derive some qualitative behaviours of the system.

For a contracting star, no element of the stress-energy tensor should be singular if we are to have a physically sensible description. As such, we can take the first two restrictions from Eqs. (B.2) and (B.3). It is seen ζ should go to zero as fast or faster than r^2 and ν' as fast or faster than r in the limit $r \to 0$ so that $T^0_{\ 0}$ and $T^1_{\ 1}$ may remain non-singular. Furthermore, Eq. (B.2) may be integrated. First we note it can be written as

$$8\pi T^0_{\ 0} = -\mathrm{e}^{-\zeta}\left(\frac{\zeta'}{r} - \frac{1}{r^2}\right) - \frac{1}{r^2} \iff 8\pi\, r^2\, T^0_{\ 0} = -\frac{\partial}{\partial r}\left(-r\mathrm{e}^{-\zeta} + r\right) .$$

Taking now $\zeta(r=0) = \zeta_0$, this can be solved to give

$$\zeta = \zeta_0 - \ln\left(1 + \frac{8\pi}{r}\int_0^r \bar{r}^2\, T^0_{\ 0}\, \mathrm{d}\bar{r}\right) . \tag{B.7}$$

Because $T^0_{\ 0} \leq 0$ it follows the argument of the logarithm is smaller than 1 and so $\zeta \geq \zeta_0$. In particular, setting $\zeta_0 = 0$ we get that ζ is non-negative.

Similarly, we note Eq. (B.3) can be written in the form

$$\mathrm{e}^{-\zeta}\frac{\nu'}{r} = 8\pi T^1_{\ 1} + \frac{1-\mathrm{e}^{-\zeta}}{r^2} \implies \frac{\partial \nu}{\partial r} = r\mathrm{e}^{\zeta}\left(\frac{1-\mathrm{e}^{-\zeta}}{r^2} + 8\pi T^1_{\ 1}\right) \geq 0\,, \tag{B.8}$$

because $T^1_{\ 1} \geq 0$ and $\zeta \geq 0$. Thus, $\nu' \geq 0$. The condition of asymptotic flatness of the space-time imposes the conditions $\lim_{r\to\infty}\zeta = 0$ and $\lim_{r\to\infty}\nu = 0$. From the latter and the restriction on ν' we get that $\nu \leq 0$.

It is also possible to relate the behaviours of ζ and ν. Subtracting Eq. (B.2) from Eq. (B.3) we get

$$8\pi(T^1_{\ 1} - T^0_{\ 0}) = \mathrm{e}^{-\zeta}\frac{\nu' + \zeta'}{r} . \tag{B.9}$$

And since $T^0_{\ 0}$ is non-negative and $T^1_{\ 1}$ is positive, it follows directly

$$\zeta' + \nu' \geq 0 \implies \zeta + \nu \leq 0 . \tag{B.10}$$

The latter, as before, due to the asymptotic flatness. In particular, the first relation is consistent with the imposed restriction that ν' vanish faster than r and ζ' faster than r^2 in the limit $r \to 0$ and $\nu' \geq 0$ for all r.

Finally, since $T^1_{\ 0} \geq 0$, it is seen from Eq. (B.5) that $\dot{\zeta} \geq 0$, that is ζ increases with time as a function of r. On the other hand,

$$V = \int_{V_{star}} \sqrt{|g_{ab}|}\, \mathrm{d}V = 4\pi \int_0^R \mathrm{e}^{\zeta/2}\, r^2\, \mathrm{d}r\,, \tag{B.11}$$

with $|g_{ab}|$ the determinant of the induced 3-metric. The volume must be limited, so is necessary that ζ converges in the limit $t \to \infty$ to some finite value as a function of r, i.e. the system evolves towards a new stable configuration.

B.2 Collapse of a Ball of Dust

We now look at a particular and simpler case, that for which the pressure is zero. This in effect corresponds to a star composed of dust. The energy-momentum tensor has the components

$$\begin{aligned} &T^0{}_0 = -\rho\,, \\ &T^\alpha{}_\beta = 0\,, \quad \text{for the other components}\,. \end{aligned} \tag{B.12}$$

For the metric describing the interior of the star, there is a natural choice in the system of coordinates that accompanies the collapse, i.e. a comoving system of coordinates. In this case, we take the proper time and the fractional distance, from the center of the star to its boundary, as the time and radial coordinates respectively. The metric will thus be,

$$\mathrm{d}s^2 = -\mathrm{d}\tau^2 + \mathrm{e}^\lambda \mathrm{d}\xi^2 + \mathrm{e}^\omega(\mathrm{d}\theta^2 + \sin^2\theta\,\mathrm{d}\phi^2)\,, \tag{B.13}$$

with $\lambda \equiv \lambda(\tau,\xi)$ and $\omega \equiv \omega(\tau,\xi)$. The Einstein field equations give

$$-8\pi T^0{}_0 = 8\pi\rho = \mathrm{e}^{-\omega} + \left(\frac{\lambda'\,\omega'}{2} - \frac{3\,\omega'^2}{4} - \omega''\right)\mathrm{e}^{-\lambda} + \frac{\dot\lambda\,\dot\omega}{2} + \frac{\dot\omega^2}{4}\,, \tag{B.14}$$

$$8\pi T^0{}_1 = 0 = \frac{\dot\lambda\,\omega'}{2} - \frac{\dot\omega\,\omega'}{2} - \dot\omega'\,, \tag{B.15}$$

$$8\pi T^1{}_1 = 0 = \frac{\omega'^2}{4}\mathrm{e}^{-\lambda} - \mathrm{e}^{-\omega} - \frac{3\,\dot\omega^2}{4} - \ddot\omega\,, \tag{B.16}$$

$$8\pi T^2{}_2 = 0 = \left(-\frac{\lambda'\,\omega'}{4} + \frac{\omega'^2}{4} + \frac{\omega''}{2}\right)\mathrm{e}^{-\lambda} - \frac{\dot\lambda^2}{4} - \frac{\dot\lambda\,\dot\omega}{4} - \frac{\dot\omega^2}{4} - \frac{\ddot\lambda}{2} - \frac{\ddot\omega}{2}\,, \tag{B.17}$$

with a dot denoting differentiation with respect to τ and a prime differentiation with respect to ξ now and for the remainder of this section. Equation (B.15) can be rewritten in the form

$$0 = \frac{\dot\omega}{2} - \frac{\dot\lambda}{2} + \frac{\dot\omega'}{\omega'} \iff 0 = \frac{\mathrm{d}}{\mathrm{d}\tau}\left(\frac{\omega}{2} - \frac{\lambda}{2} + \ln\omega'\right)\,.$$

This can be integrated to give

$$\mathrm{e}^\lambda = \frac{\omega'^2\,\mathrm{e}^\omega}{4f^2(\xi)}\,, \tag{B.18}$$

where $f^2(\xi)$ is an arbitrary function introduced in the integration with respect to τ. Henceforth, this will be set to 1. Introducing now Eq. (B.18) into Eq. (B.16) we get

$$0 = \ddot\omega + \frac{3}{4}\dot\omega^2\,. \tag{B.19}$$

This can be solved

$$0 = \frac{\partial}{\partial\tau}\left(\frac{3}{4}\frac{\partial\omega}{\partial\tau}\right) + \left(\frac{3}{4}\frac{\partial\omega}{\partial\tau}\right)^2 \implies \frac{3}{4}\frac{\partial\omega}{\partial\tau} = \frac{1}{\tau + a(\xi)} \implies \omega = \frac{4}{3}\ln\left(\tau + a(\xi)\right) + \frac{4}{3}\ln b(\xi)\,,$$

with $a(\xi)$ and $b(\xi)$ arbitrary functions introduced on integration. We thus obtain

$$\mathrm{e}^{\omega} = (F\tau + G)^{4/3}\,, \tag{B.20}$$

where $F \equiv F(\xi)$ and $G \equiv G(\xi)$ are redefinitions of the previously introduced functions. The equations (B.18) and (B.20) can be used to get λ, ω and their derivatives described in terms of F, G and their derivatives. We have

$$\omega = \frac{4}{3}\ln(F\tau + G)\,, \quad \lambda = \ln\left(\frac{4}{9}\frac{(F'\tau + G')^2}{(F\tau + G)^{2/3}}\right)\,, \tag{B.21}$$

$$\omega' = \frac{4}{3}\frac{F'\tau + G'}{F\tau + G}\,, \quad \lambda' = 2\frac{F''\tau + G''}{F'\tau + G'} - \frac{2}{3}\frac{F'\tau + G'}{F\tau + G}\,, \tag{B.22}$$

$$\dot{\omega} = \frac{4}{3}\frac{F}{F\tau + G}\,, \quad \dot{\lambda} = \frac{4}{3}\frac{F}{F\tau + G} + 2\frac{F'G - FG'}{(F'\tau + G')(F\tau + G)}\,. \tag{B.23}$$

Inserting Eqs. (B.21), (B.22) and (B.23) into Eq. (B.14) we get

$$8\pi\rho = \frac{4}{3}\frac{FF'}{(F\tau + G)(F'\tau + G')}\,. \tag{B.24}$$

Now one may notice that if we were to carry with a change of variable $\xi \equiv \xi(\xi^*)$ then Eqs. (B.15) and (B.16) would still have given Eqs. (B.18) and (B.20) respectively, so that we can impose some restriction on the functions $F(\xi)$ and $G(\xi)$. We choose $G(\xi) = \xi^{\frac{3}{2}}$, and now apply it to Eq. (B.24) at $\tau = 0$. Doing so gives

$$8\pi\rho_0 = \frac{8}{9}\frac{FF'}{\xi^2} \iff FF' = 9\pi\xi^2\rho_0(\xi),. \tag{B.25}$$

We will now take the star to be homogeneous, i.e. ρ is independent of ξ.

While $G(\xi)$ was taken to have a specific form, $F(\xi)$ must have a form dependent on whether we are working with the metric inside or outside the star, otherwise there would be no distinction. As such we consider the particular case

$$FF' = \begin{cases} \alpha\xi^2 & ,\xi < R\,, \\ 0 & ,\xi > R\,, \end{cases} \tag{B.26}$$

with α a positive constant. This is solved with

$$F(\xi) = \left(2\int FF'\mathrm{d}\xi + \mathrm{constant}\right)^{1/2}\,.$$

On the other hand, Eq. (B.26) can be inserted into Eq. (B.25) to give

$$\alpha\xi^2 = 9\pi\xi^2\rho_0 \implies \alpha = 9\pi\rho_0\,, \quad \rho_0 = \frac{3}{8}\frac{2M}{\pi R^3} \implies \alpha = \left(\frac{3}{2R}\right)^3\,,$$

and thus, both these can be used to obtain

$$F(\xi) = \begin{cases} -\frac{3}{2}(2M)^{1/2}\left(\frac{\xi}{R}\right)^{3/2} & ,\xi < R\,, \\ -\frac{3}{2}(2M)^{1/2} & ,\xi > R\,. \end{cases} \tag{B.27}$$

With these, the metric is defined inside and outside of the star.

$$\mathrm{e}^{\lambda} = \begin{cases} \left(1 - \frac{3}{2}\frac{(2M)^{1/2}}{R^{3/2}}\tau\right)^{4/3} & ,\xi < R \\ \left(1 - \frac{3}{2}\frac{(2M)^{1/2}}{\xi^{3/2}}\tau\right)^{-2/3} & ,\xi > R \end{cases}, \quad \mathrm{e}^{\omega} = \begin{cases} \left(1 - \frac{3}{2}\frac{(2M)^{1/2}}{R^{3/2}}\tau\right)^{4/3}\xi^2 & ,\xi < R \\ \left(\xi^{3/2} - \frac{3}{2}(2M)^{1/2}\tau\right)^{4/3} & ,\xi > R \end{cases}. \tag{B.28}$$

For the interior, $\xi < R$, this gives explicitly the metric

$$\mathrm{d}s^2 = -\mathrm{d}\tau^2 + \left(1 - \frac{3}{2}\frac{(2M)^{1/2}}{R^{3/2}}\tau\right)^{4/3}\left[\mathrm{d}\xi^2 + \xi^2\left(\mathrm{d}\theta^2 + \sin^2\theta\,\mathrm{d}\phi^2\right)\right] , \tag{B.29}$$

which is identified as a Friedmann-Lemaître-Robertson-Walker (FLRW) metric, Eq. (2.4), with $k = 0$. As for the outside, i.e. for $\xi > R$, one should note the metric must reduce to the Schwarzschild form, Eq. (2.6). Thus we can immediately identify

$$r = (F\tau + G)^{2/3} = \mathrm{e}^{\omega/2} , \quad r' = \mathrm{e}^{\lambda/2} , \tag{B.30}$$

where the second can be obtained from Eq. (B.18).

Even if this identification can be made, it is useful to obtain a coordinate transformation from the set of comoving coordinates to the static one, Eq. (B.1). Such a transformation may give us further information on the dynamics of the system. To do so, we define a change of variables to the new pair (t, r) as functions of the old, (τ, ξ). We can obtain the relations connecting both sets using the inverse metric, $g^{\mu\nu}$. We find

$$-\mathrm{e}^{-\nu}\partial_t^2 + \mathrm{e}^{-\zeta}\partial_r^2 = -\partial_\tau^2 + \mathrm{e}^{-\zeta}\partial_\xi^2 = -\left(\frac{\partial t}{\partial\tau}\partial_t + \frac{\partial r}{\partial\tau}\partial_r\right)^2 + \left(\frac{\partial t}{\partial\xi}\partial_t + \frac{\partial r}{\partial\xi}\partial_r\right)^2 .$$

And grouping the terms

$$-\mathrm{e}^{-\nu}\partial_t^2 + \mathrm{e}^{-\zeta}\partial_r^2 = -\left(\dot{t}^2 - \frac{t'^2}{r'^2}\right)\partial_t^2 + \left(-\dot{r}^2 + 1\right)\partial_r^2 + 2\left(\dot{t}\,\dot{r} - \frac{t'}{t'}\right)\partial_t\partial_r ,$$

and this gives the differential equations

$$\mathrm{e}^{-\nu} = \dot{t}^2 - t'^2/r'^2 , \tag{B.31}$$

$$\mathrm{e}^{-\zeta} = 1 - \dot{r}^2 , \tag{B.32}$$

$$0 = \dot{t}\,\dot{r} - t'/r' . \tag{B.33}$$

Of these, Eq. (B.33) can be solved. Using Eqs. (B.28) and (B.30), we can write

$$\frac{t'}{\dot{t}} = \dot{r}\,r' = \begin{cases} -(2M)^{\frac{1}{2}}\,\xi\,R^{-\frac{3}{2}}\,\left(1 - \frac{3}{2}\frac{(2M)^{1/2}\,\tau}{R^{\frac{3}{2}}}\right)^{\frac{1}{3}} & ,\xi < R \\ -(2M)^{\frac{1}{2}}\,\xi^{\frac{1}{2}}\,\left(\xi^{\frac{3}{2}} - \frac{3}{2}(2M)^{\frac{1}{2}}\,\tau\right)^{-\frac{2}{3}} & ,\xi > R \end{cases}. \tag{B.34}$$

Equation (B.34) can be solved (the solution is left to the end of this Appendix, section B.4), its general solution being

$$t = M(y)\,, \quad y = \frac{1}{2}\left[\left(\frac{\xi}{R}\right)^2 - 1\right] + \frac{r\,R}{2M\,\xi} \qquad ,\xi < R\,, \tag{B.35}$$

$$t = L(x)\,, \quad x = \frac{2}{3}(2M)^{-\frac{1}{2}}\left(R^{\frac{3}{2}} - r^{\frac{3}{2}}\right) - 2(2M\,r)^{\frac{1}{2}} + 2M\ln\frac{r^{\frac{1}{2}} + (2M)^{\frac{1}{2}}}{r^{\frac{1}{2}} - (2M)^{\frac{1}{2}}} \qquad ,\xi > R\,, \tag{B.36}$$

with L and M arbitrary functions of their arguments.

For the particular case of the exterior of the star the line element should equate the Schwarzschild line element. Then

$$\mathrm{e}^{\nu} = \left(1 - \frac{2M}{r}\right)\,, \quad \mathrm{e}^{\lambda} = \left(1 - \frac{2M}{r}\right)^{-1}\,. \tag{B.37}$$

With a specific form for e^{ν} we can make use of Eq. (B.31) and determine the specific form for the function L. We get

$$\mathrm{e}^{-\nu} = \dot{t}^2 - \frac{t'^2}{r'^2}\,, \quad \dot{t} = \frac{\partial L}{\partial x}\frac{1}{r - 2M}\left(\xi^{3/2} - \frac{3}{2}(2M)^{1/2}\,\tau\right)\,, \quad t' = -\frac{\partial L}{\partial x}\frac{(2M)^{1/2}\,\xi^{1/2}}{r - 2M}\,,$$

and applying these along with Eq. (B.30) we get

$$\frac{\partial L}{\partial x} = \pm 1 \implies L(x) = \pm x + \mathrm{constant}\,. \tag{B.38}$$

Thus we set $L(x) = x$, from which follows that the Schwarzschild space-time demands

$$t = \frac{2}{3}(2M)^{-\frac{1}{2}}\left(R^{\frac{3}{2}} - r^{\frac{3}{2}}\right) - 2(2M\,r)^{\frac{1}{2}} + 2M\ln\frac{r^{\frac{1}{2}} + (2M)^{\frac{1}{2}}}{r^{\frac{1}{2}} - (2M)^{\frac{1}{2}}}\,. \tag{B.39}$$

To be physically sensible, the metric should be continuous over the surface of separation of the two regions, the interior and exterior of the star. In that regard the functions M, Eq. (B.35), and L, Eq. (B.36), should be equal over the surface, i.e. when $\xi = R$. This translates to

$$\lim_{\xi \to R^{(-)}} M(y) = \lim_{\xi \to R^{(+)}} L(x)\,, \tag{B.40}$$

with the $(-)$ and $(+)$ denoting limits where ξ approaches R from below and above, respectively. Using the identification $L(x) = t$ with Eq. (B.39) as well as the limit $\xi \to R$ on y from Eq. (B.35), we get

$$\lim_{\xi \to R^{(-)}} y = \frac{1}{2M}\lim_{\xi \to R^{(-)}} r\,, \quad \lim_{\xi \to R^{(-)}} M(y) = \lim_{\xi \to R^{(-)}}\left(\frac{2}{3}\frac{\xi^{\frac{3}{2}} - r^{\frac{3}{2}}}{(2M)^{\frac{1}{2}}} - 2(2M)^{\frac{1}{2}}\,\xi^{\frac{1}{2}} + 2M\,\ln\frac{r^{\frac{1}{2}} + (2M)^{\frac{1}{2}}}{r^{\frac{1}{2}} - (2M)^{\frac{1}{2}}}\right)\,.$$

Using both, we get

$$t(\xi = R) = \frac{2}{3}(2M)^{-\frac{1}{2}}\left(R^{\frac{3}{2}} - (2M)^{\frac{3}{2}}\,y^{\frac{3}{2}}\right) - 2(2M)\,y^{\frac{1}{2}}2M\ln\frac{y^{\frac{1}{2}} + 1}{y^{\frac{1}{2}} - 1}\,. \tag{B.41}$$

And so Eqs. (B.30) and (B.41) define the transformation between coordinate systems. If we now take a as the surface of the star in Schwarzschild coordinates, then over the surface of the star $y = a/2M$ and the previous relation, Eq. (B.41), reduces to

$$t(\tau,R)=\left(\frac{2}{3}\frac{R_0^{3/2}}{(2M)^{1/2}}\right)-\frac{2}{3(2M)^{1/2}}\left(a^{3/2}+6M\,a^{1/2}\right)+2M\ln\left|\frac{a^{1/2}+(2M)^{1/2}}{a^{1/2}-(2M)^{1/2}}\right|\,, \tag{B.42}$$

which is seen to be the same relation as those obtained using junction conditions, Eq. (2.23), with the constant identified as $T(0)=2R_0^{3/2}/3(2M)^{1/2}$. This is seen to be the same as the constant chosen for the instant of total contraction in proper time.

B.3 Asymptotic Limits

The relation Eq. (B.41) may also give us the asymptotic behaviour of the star. For large values of t we first note any external observer will see the surface of the star approach the Schwarzschild radius at an infinite time, so that

$$\lim_{t\to\infty} r=2M\,,\quad \lim_{\xi\to R} r=2M\,\lim_{\xi\to R} y\implies \lim_{t\to\infty} y=1^{(+)}\,,$$

i.e. y goes to 1 from values above. From this we get that $y^{\frac{1}{2}}\approx y$ so that we can take the approximation,

$$t(\xi=R)=\frac{2}{3}(2M)^{-\frac{1}{2}}\left(R^{\frac{3}{2}}-(2M)^{\frac{3}{2}}\,y^{\frac{3}{2}}\right)-2(2M)\,y^{\frac{1}{2}}2M\ln\frac{y^{\frac{1}{2}}+1}{y^{\frac{1}{2}}-1}\approx-2M\,\ln(y-1)\,.$$

Now, using the definition of y, Eq. (B.35), and of the function F for $\xi>R$, Eq. (B.27) we obtain

$$y=\frac{1}{2}\left[\left(\frac{\xi}{R}\right)^2-1\right]+\frac{R}{2M}\left[1-\frac{3}{2}\frac{(2M)^{\frac{1}{2}}\,\tau}{R^{\frac{3}{2}}}\right]^{\frac{2}{3}}\,.$$

Joining the last two equations, we get the asymptotic form for t

$$t\approx-2M\,\ln\left(\frac{1}{2}\left[\left(\frac{\xi}{R}\right)^2-3\right]+\frac{R}{2M}\left[1-\frac{3}{2}\frac{(2M)^{\frac{1}{2}}\tau}{\xi^{\frac{3}{2}}}\right]\right)\,. \tag{B.43}$$

It is seen that, in the limit where t goes to infinity, τ remains bound by a value proportional to ξ. Indeed, setting the argument of the logarithm to 0 in Eq. (B.43), we find

$$\tau\leq\frac{2}{3}(2M)^{-\frac{1}{2}}\,\xi^{\frac{3}{2}}\left(1-\left(\frac{2M}{2R}\right)^{\frac{3}{2}}\left[3-\left(\frac{\xi}{R}\right)^2\right]\right)\,. \tag{B.44}$$

Likewise, we can find the asymptotic forms of the metric components by applying Eqs. (B.43) and (B.30) to Eqs. (B.31) and (B.32)

$$\mathrm{e}^{-\lambda}\approx1-\left(\frac{\xi}{R}\right)^2\left(\mathrm{e}^{-\frac{t}{2M}}-\frac{1}{2}\left[\left(\frac{\xi}{R}\right)^2-3\right]\right)^{-1}\,, \tag{B.45}$$

$$\mathrm{e}^{\nu}=\mathrm{e}^{\lambda-2\frac{t}{2M}}\left(\mathrm{e}^{-\frac{t}{2M}}-\frac{1}{2}\left[\left(\frac{\xi}{R}\right)^2-3\right]\right)\,. \tag{B.46}$$

We can now verify from these the asymptotic behaviour as t goes to infinity. For the case where $\xi < R$ we find that $\mathrm{e}^{\lambda} \approx 1$ and $\mathrm{e}^{\nu} \approx \mathrm{e}^{-2\frac{t}{2M}}$. When $\xi = R$ we find that $\mathrm{e}^{\lambda} \approx \mathrm{e}^{t}2m$, while $\mathrm{e}^{\nu} \approx \mathrm{e}^{-\frac{t}{2M}}$. Thus e^{λ} may either diverge or converge but e^{ν} goes always to zero.

Having done the analysis, one should remark that, while they were done for the simpler case where the pressure is zero, we would expect the same qualitative behaviour otherwise, provided the star is massive enough. Indeed, what is relevant is whether the gravitational field is strong enough to overcome the opposition from the pressure. Thus the total gravitational collapse of a star is inevitable should the star have enough mass.

B.4 The First-Order Partial Differential Equations

When searching for the coordinate transformation that takes one from the comoving coordinate system proposed by Oppenheimer and Snyder, Eq. (B.13), to the standard static coordinate system, Eq. (B.1), one is faced with a complicated first-order partial differential equation, Eq. (B.34). To solve it we write it first explicitly

$$\frac{t'}{\dot{t}} = \dot{r}\,r' = \begin{cases} -(2M)^{\frac{1}{2}}\,\xi\,R^{-\frac{3}{2}}\,\left(1 - \frac{3}{2}\frac{(2M)^{1/2}\,\tau}{R^{\frac{3}{2}}}\right)^{\frac{1}{3}} & ,\xi < R \\ -(2M)^{\frac{1}{2}}\,\xi^{\frac{1}{2}}\,\left(\xi^{\frac{3}{2}} - \frac{3}{2}(2M)^{\frac{1}{2}}\,\tau\right)^{-\frac{2}{3}} & ,\xi > R \end{cases}. \tag{B.47}$$

where, once again a dot denotes differentiation with respect to the coordinate τ and a prime differentiation with respect with the coordinate ξ, both of the comoving metric. The coordinate function r was previously identified, Eq. (B.30), so we have

$$r = \begin{cases} \left(\xi^{\frac{3}{2}} - \frac{3}{2}(2M)^{\frac{1}{2}}\left(\frac{\xi}{R}\right)^{\frac{3}{2}}\tau\right)^{\frac{2}{3}} & ,\xi < R \\ \left(\xi^{\frac{3}{2}} - \frac{3}{2}(2M)^{\frac{1}{2}}\tau\right)^{\frac{2}{3}} & ,\xi > R \end{cases}. \tag{B.48}$$

The ratio between t' and $\dot{t}$ in Eq. (B.47) allows us to define the coordinate function t in terms of an arbitrary function of a new variable, say z. That this is so can be seen from the application of the chain rule for differentiation, which guarantees that the derivative of the arbitrary function in terms of the variable z vanishes in the ratio and thus does not contribute.

$$t = \Psi(z) \implies \frac{t'}{\dot{t}} = \frac{\frac{\partial \Psi}{\partial z} z'}{\frac{\partial \Psi}{\partial z}\dot{z}} = \frac{z'}{\dot{z}}\,, \tag{B.49}$$

with exemplary $\Psi(z)$ and z. We will proceed by solving Eq. (B.47), using Eq. (B.48), for the two regions, $\xi > R$ and $\xi < R$.

B.4.1 Solution for $\xi < R$

The equations to be solved here are

$$r = \left(\xi^{\frac{3}{2}} - \frac{3}{2}(2M)^{\frac{1}{2}}\left(\frac{\xi}{R}\right)^{\frac{3}{2}}\tau\right)^{\frac{2}{3}}\,, \quad \frac{t'}{\dot{t}} = -(2M)^{\frac{1}{2}}\xi\, R^{-\frac{3}{2}}\left(1 - \frac{3}{2}(2M)R^{-\frac{3}{2}}\tau\right)^{\frac{1}{3}}\,. \tag{B.50}$$

We will now define a function M kept arbitrary, but such that $t = M(y)$, with y to be obtained. This definition entails

$$t' = \frac{\partial M}{\partial y}y'\,, \quad \dot{t} = \frac{\partial M}{\partial y}\dot{y}\,,$$

and applying to Eq. (B.50), we get

$$(2M)^{\frac{1}{2}}\xi\, R^{-\frac{3}{2}}\left(1 - \frac{3}{2}(2M)R^{-\frac{3}{2}}\tau\right)^{\frac{1}{3}}\dot{y} + y' = 0\,. \tag{B.51}$$

This motivates us to define new variables (v, u) such that

$$u = \xi\,, \quad v = \left(1 - \frac{3}{2}(2M)^{\frac{1}{2}}R^{-\frac{3}{2}}\tau\right)^{\frac{2}{3}} \implies \xi = u\,, \quad \tau = \frac{2}{3}(2M)^{-\frac{1}{2}}R^{\frac{3}{2}}\left(1 - v^{\frac{3}{2}}\right)\,, \tag{B.52}$$

which verify

$$\begin{cases} \frac{\partial u}{\partial \xi} = 1 \\ \frac{\partial u}{\partial \tau} = 0 \end{cases}\,, \quad \begin{cases} \frac{\partial v}{\partial \xi} = 0 \\ \frac{\partial v}{\partial \tau} = -(2M)^{\frac{1}{2}}R^{-\frac{3}{2}}v^{-\frac{1}{2}} \end{cases}\,, \tag{B.53}$$

Applying Eqs. (B.52) to Eq. (B.51) using the chain rule with Eqs. (B.53), we get the simpler

$$R^2\frac{1}{u}\frac{\partial y}{\partial u} = \frac{2M}{R}\frac{\partial y}{\partial v}\,. \tag{B.54}$$

We now try the particular class of solutions $y(v, u) = y_v(v) + y_u(u)$. We note Eq. (B.54) allows for separation of variables, and as such we take

$$R^2\frac{1}{u}\frac{\partial y}{\partial u} = 1 = \frac{2M}{R}\frac{\partial y}{\partial v}\,, \tag{B.55}$$

with the constant automatically chosen to be 1. We note this constant has no physical meaning since its effect is only to scale the function $y1$ and, as such, it can be absorbed into the arbitrary function M. Both differential equations in Eq. (B.55) are easy to solve, giving

$$\begin{cases} y = \frac{1}{2}\left(\frac{u}{R}\right)^2 + y_v \\ y = \frac{R}{2M}v + y_u \end{cases} \implies y = \frac{1}{2}\left(\frac{u}{R}\right)^2 + \frac{R}{2M}v - \frac{1}{2}\,. \tag{B.56}$$

Applying again the coordinate transformations, Eqs. (B.52), we finally get

$$t = M(y)\,, \quad y = \frac{1}{2}\left[\left(\frac{\xi}{R}\right)^2 - 1\right] + \frac{R}{2M}\left[1 - \frac{3}{2}(2M)^{\frac{1}{2}}R^{-\frac{3}{2}}\tau\right]^{\frac{2}{3}}\,. \tag{B.57}$$

B.4.2 Solution for $\xi > R$

The procedure will be similar to the previous section. The equations to be solved here are

$$r = \left(\xi^{\frac{3}{2}} - \frac{3}{2}(2M)^{\frac{1}{2}}\tau\right)^{\frac{2}{3}} \,, \quad \frac{t'}{\dot{t}} = -(2M\,\xi)^{\frac{1}{2}} \left(\xi^{\frac{3}{2}} - \frac{3}{2}(2M)^{\frac{1}{2}}\tau\right)^{-\frac{2}{3}} \,. \tag{B.58}$$

And now we will define the function L which is kept arbitrary, but such that $t = L(x)$, with x to be obtained. From this definition follows,

$$t' = \frac{\partial L}{\partial x}x' \,, \quad \dot{t} = \frac{\partial L}{\partial x}\dot{x}$$

and applying these to Eq. (B.58), we obtain

$$(2M\,\xi)^{\frac{1}{2}} \left[\xi^{\frac{3}{2}} - \frac{3}{2}(2M)^{\frac{1}{2}}\tau\right]^{-\frac{2}{3}} \dot{x} + x' = 0 \,. \tag{B.59}$$

And we now define the new variables (v, u) such that

$$u = \left(\xi^{\frac{3}{2}} - \frac{3}{2}(2M)^{\frac{1}{2}}\tau\right)^{\frac{2}{3}} = r \,, \quad v = \tau \implies \xi = \left(u^{\frac{3}{2}} + \frac{3}{2}(2M)^{\frac{1}{2}}\tau\right)^{\frac{2}{3}} \,, \quad \tau = v \,, \tag{B.60}$$

which verify

$$\begin{cases} \frac{\partial u}{\partial \xi} = \left(u^{\frac{3}{2}} + \frac{3}{2}(2M)^{\frac{1}{2}}\tau\right)^{\frac{1}{3}} u^{-\frac{1}{2}} \\ \frac{\partial u}{\partial \tau} = -(2M)^{\frac{1}{2}} u^{-\frac{1}{2}} \end{cases} \,, \quad \begin{cases} \frac{\partial v}{\partial \xi} = 0 \\ \frac{\partial v}{\partial \tau} = 1 \end{cases} \,. \tag{B.61}$$

Applying now Eqs. (B.60) to Eq. (B.59) using the chain rule with Eqs. (B.61), we get the simpler

$$\frac{\partial x}{\partial v} + u^{\frac{1}{2}}(2M)^{-\frac{1}{2}} \left(1 - \frac{2M}{u}\right) \frac{\partial x}{\partial u} = 0 \,. \tag{B.62}$$

We try the class of solutions $x(v, u) = x_v(v) + x_u(u)$. We note Eq. (B.62) allows for separation of variables, so we take

$$\frac{\partial x}{\partial v} = 1 = -u^{\frac{1}{2}}(2M)^{-\frac{1}{2}} \left(1 - \frac{2M}{u}\right) \frac{\partial x}{\partial u} \,, \tag{B.63}$$

where the constant was again chosen to be 1. The constant, like in the previous section, has no physical meaning since it only serves as a scaling factor for the function x and thus can be absorbed into the arbitrary function L. The two differential equations present in Eq. (B.63) are easy to solve, giving

$$\begin{cases} x = v + x_u(u) \\ x = -2(2M\,u)^{\frac{1}{2}} + 2M \ln \frac{u^{\frac{1}{2}} + (2M)^{\frac{1}{2}}}{u^{\frac{1}{2}} - (2M)^{\frac{1}{2}}} + x_v(v) \end{cases} \implies x = -2(2M\,u)^{\frac{1}{2}} + 2M \ln \frac{u^{\frac{1}{2}} + (2M)^{\frac{1}{2}}}{u^{\frac{1}{2}} - (2M)^{\frac{1}{2}}} + v \,. \tag{B.64}$$

And applying again the coordinate transformations, Eq. (B.60), we get

$$t = L(x) \,, \quad x = \frac{2}{3}(2M)^{-\frac{1}{2}} \left(\xi^{\frac{3}{2}} - r^{\frac{3}{2}}\right) - 2(2M\,r)^{\frac{1}{2}} + 2M \ln \frac{r^{\frac{1}{2}} + (2M)^{\frac{1}{2}}}{r^{\frac{1}{2}} - (2M)^{\frac{1}{2}}} \,. \tag{B.65}$$

Appendix C

Different Coordinate Systems

The first solution to the Einstein's field equations were obtained one year after they were published. In 1916, K. Schwarzschild [2] considered a non rotating point source surrounded by vacuum, and was able to describe the resulting static spherically symmetric spacetime. The solution had a simple mathematical description, but nevertheless showed many remarkable features. Most immediate among them is the existence of two singularities, one at the origin of spatial coordinates, $r = 0$, and the other at the radius $r = 2M$. The constant of integration M would be identified with the mass of the source.

Various other solutions, for the same conditions, would be shown in the coming years either through direct evaluation of the field equations or through a coordinate transformation applied to Schwarzschild's solution. Whichever the case, a theorem discovered independently by G. D. Birkhoff [40] and J. T. Jebsen [41] stated that all such solutions represented the same spacetime: the Schwarzschild spacetime. Nevertheless, these solutions would bring to light various features of the original solution, one among them being that the singularity at $r = 2M$ was a coordinate singularity and not a true singularity.

In this section we give a brief review some of these solutions. A summary of this is shown in Figure C.1. The coordinate systems considered are all obtained applying either one or two coordinate transformations, with the first being always on the time coordinate. With this procedures, the Novikov and Kruskal-Szekeres coordinate systems reveal themselves to be maximal extensions of the Schwarzschild spacetime, while the Lemaître coordinate system does not. One also notices the limit $E \to \infty$ gives the Eddington-Finkelstein coordinate system from the Gullstrand-Painlevé generalization to $E > 1$, but the same does not happen between the Kruskal-Szekeres coordinate system and the Lematître $E > 1$ generalization. We will take the chance to explore the limiting case of the $E > 1$ generalization of the Lemaître coordinate system in section C.8.

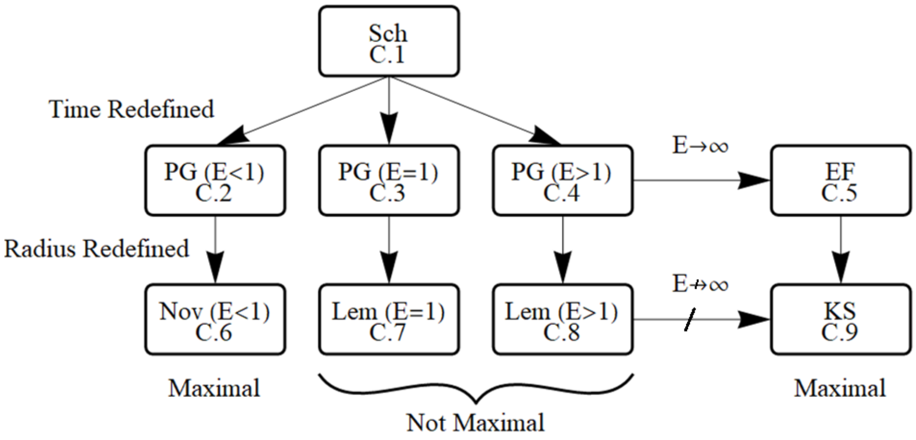

Figure C.1: The relations between the different coordinate systems, representing the Schwarzschild spacetime, reviewed for one and two coordinate transformations. The Novikov and Kruskal-Szekeres coordinate systems are maximal extensions of the Schwarzschild spacetime, while the Lemaître coordinate system and its generalization to $E > 1$ are not. The generalization of the Gullstrand-Painlevé coordinate system gives the Eddington-Finkelstein coordinate system as a limit case, of $E \to \infty$. The same does not occur between the generalization of the Lemaître coordinate system to $E > 1$ and the Kruskal-Szekeres coordinate system.

C.1 Schwarzschild Coordinates

We first consider the solution due to Schwarzschild. Taking coordinates (t, r, θ, ϕ), the line element takes the form

$$\mathrm{d}s^2 = -\left(1 - \frac{2M}{r}\right)\mathrm{d}t^2 + \left(1 - \frac{2M}{r}\right)^{-1}\mathrm{d}r^2 + r^2(\mathrm{d}\theta^2 + \sin^2\theta\,\mathrm{d}\phi^2)\,, \tag{C.1}$$

where M is a constant of integration identified with the mass of the point source. The singularity at the null surface $r = 2M$ is seen to be a coordinate singularity since a scalar invariant, the Krestchmann scalar, can be found which does not diverge at that radius

$$K_S = \frac{48M^2}{R^6}\,. \tag{C.2}$$

While the singularity $r = 2M$ is an artefact of the coordinate system, it does define the event horizon, the null surface, the interior from which no information can escape. A congruence of null geodesics in the presence of a black hole in Schwarzschild coordinates is displayed in Figure C.2.

C.2 Painlevé-Gullstrand Coordinates with $E < 1$

The extension of the usual Painlevé-Gullstrand coordinate system, to a particle falling with any energy, was given by Gautreau and Hoffmann [42]. We begin by considering the coordinate transformation

$$\mathrm{d}t = \frac{1}{E}\mathrm{d}\tau - \frac{1}{E}\left(1 - \frac{2M}{r}\right)^{-1}\left(E^2 - 1 + \frac{2M}{r}\right)^{1/2}\mathrm{d}r\,, \tag{C.3}$$

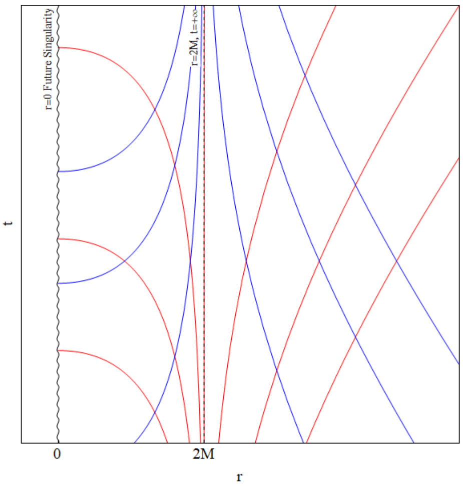

Figure C.2: The null congruence for the black hole solution in Schwarzschild coordinates is displayed. For $r > 2M$ in red are the outgoing null geodesics and in blue are the ingoing null geodesics. For $r < 2M$ they are switched, red are ingoing and blue outgoing. The undulating line represents the singularity at the center of spatial coordinates. The dashed line represents the event horizon, at $r = 2M$.

where $E > 0$ is the energy parameter of the falling particle. Appplying the transformation, Eq. (C.3), to the Schwarzschild metric, Eq. (C.1), one finds the new, generalized, metric

$$\mathrm{d}s^2 = -\frac{1}{E^2}\left(1-\frac{2M}{r}\right)\mathrm{d}\tau^2 + 2\frac{1}{E^2}\left(E^2-1+\frac{2M}{r}\right)^{1/2}\mathrm{d}\tau\,\mathrm{d}r + \frac{1}{E^2}\mathrm{d}r^2 + r^2(\mathrm{d}\theta^2+\sin^2\theta\,\mathrm{d}\phi^2)\,. \tag{C.4}$$

Both the transformation, Eq. (C.3), and the metric, Eq. (C.4), are not changed by the particular value of $E > 0$, thus general. However, the solution to the transformation relation, Eq. (C.3), does require such consideration. For $0 < E < 1$, associated with a bound falling particle, we find the closed form relation

$$\begin{aligned}\tau = Et + r\left(E^2-1+\frac{2M}{r}\right)^{1/2} - 2ME\ln\left|\frac{2E^2-1+\frac{2M}{r}+2E\left(E^2-1+\frac{2M}{r}\right)^{1/2}}{1-\frac{2M}{r}}\right| - \\ - M\frac{1-2E^2}{(1-E^2)^{1/2}}\arccos\left(\frac{M-(1-E^2)r}{M}\right).\end{aligned} \tag{C.5}$$

The congruence of null geodesics for the black hole solution in Painlevé-Gullstrand coordinates with $E < 1$ is displayed in Figure C.3. It is seen from the definition, Eq. (C.3), that this coordinate system is valid up to a maximum radius $r_0 = 2M/(1-E^2)$, the particle's starting distance. The inability to describe events occurring outside the hypersurface of radius r_0 implies this particular coordinate system is of little physical interest.

C.3 Painlevé-Gullstrand Coordinates

The usual Painlevé-Gullstrand coordinate system, found independently by Painlevé [43] and Gullstrand [44], is obtained by using the proper time coordinate of a falling marginally bound particle. Thus we start

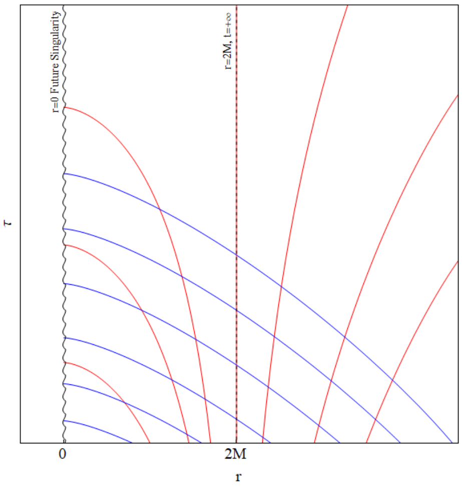

Figure C.3: The null congruence for the black hole solution in Painlevé-Gullstrand coordinates, with $E < 1$, is displayed. In red are the outgoing null geodesics and in blue are the ingoing null geodesics. The undulating line represents the singularity at the center of spatial coordinates. The dashed line represents the event horizon, $r = 2M$. Due to the coordinate transformation, Eq. (C.3), the ingoing null geodesics do not display any discontinuity at the event horizon.

by considering the coordinate transformation

$$\mathrm{d}t = \mathrm{d}\tau - \left(1 - \frac{2M}{r}\right)^{-1}\left(\frac{2M}{r}\right)^{1/2}\mathrm{d}r\,, \tag{C.6}$$

which, when applied to the Schwarzschild metric, Eq. (C.1), gives

$$\mathrm{d}s^2 = -\left(1 - \frac{2M}{r}\right)\mathrm{d}\tau^2 + 2\left(\frac{2M}{r}\right)^{1/2}\mathrm{d}\tau\,\mathrm{d}r + \mathrm{d}r^2 + r^2(\mathrm{d}\theta^2 + \sin^2\theta\,\mathrm{d}\phi^2)\,. \tag{C.7}$$

Both Eqs. (C.6) and C.7) are seen to be the $E \to 1$ limit of Eqs. (C.3) and (C.4), respectively. The closed form solution to Eq. (C.6) is

$$\tau = t + 4M\left(\frac{r}{2M}\right)^{1/2} - 2M\ln\left|\frac{r^{1/2} + (2M)^{1/2}}{r^{1/2} - (2M)^{1/2}}\right|. \tag{C.8}$$

The congruence of null geodesics for the black hole solution in Painlevé-Gullstrand coordinates is displayed in Figure C.4.

C.4 Painlevé-Gullstrand Coordinates with $E > 1$

The extension of Painlevé-Gullstrand coordinates to $E > 1$ follows similarly to the $E < 1$ case. We start with the coordinate transformation of Eq. (C.3), i.e.

$$\mathrm{d}t = \frac{1}{E}\mathrm{d}\tau - \frac{1}{E}\left(1 - \frac{2M}{r}\right)^{-1}\left(E^2 - 1 + \frac{2M}{r}\right)^{1/2}\mathrm{d}r\,, \tag{C.9}$$

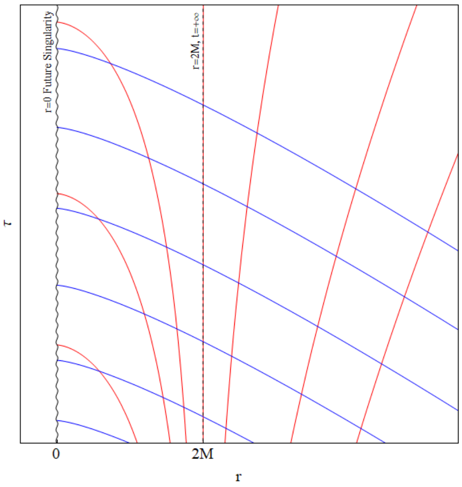

Figure C.4: The null congruence for the black hole solution in Painlevé-Gullstrand coordinates is displayed. In red are the outgoing null geodesics and in blue are the ingoing null geodesics. The undulating line represents the singularity at the center of spatial coordinates. The dashed line represents the event horizon, $r = 2M$. Due to the coordinate transformation, Eq. (C.6), the ingoing null geodesics do not display any discontinuity at the event horizon.

where $E > 0$ is the energy parameter of the falling particle. Applying the transformation, Eq. (C.9), to the Schwarzschild metric, Eq. (C.1), one finds again the generalized metric Eq. (C.4), i.e.

$$\mathrm{d}s^2 = -\frac{1}{E^2}\left(1-\frac{2M}{r}\right)\mathrm{d}\tau^2 + 2\frac{1}{E^2}\left(E^2-1+\frac{2M}{r}\right)^{1/2}\mathrm{d}\tau\,\mathrm{d}r + \frac{1}{E^2}\mathrm{d}r^2 + r^2(\mathrm{d}\theta^2+\sin^2\theta\,\mathrm{d}\phi^2)\,. \tag{C.10}$$

As before, both the transformation, Eq. (C.9), and the metric, Eq. (C.10), are not changed by the particular value of $E > 0$, thus general. However, the solution to the transformation relation, Eq. (C.9), does require such consideration. For $E > 1$, associated with an unbound falling particle with initial non zero velocity, we find the closed form relation

$$\begin{aligned}\tau = Et + r\left(E^2-1+\frac{2M}{r}\right)^{1/2} - 2ME\ln\left|\frac{2E^2-1+\frac{2M}{r}+2E\left(E^2-1+\frac{2M}{r}\right)^{1/2}}{1-\frac{2M}{r}}\right| + \\ + M\frac{2E^2-1}{(E^2-1)^{1/2}}\ln\left[\frac{r}{M}\left(E^2-1+\frac{M}{r}+(E^2-1)^{1/2}\left(E^2-1+\frac{2M}{r}\right)^{1/2}\right)\right],\end{aligned} \tag{C.11}$$

which is found to give the usual Painlevé-Gullstrand coordinates in the $E \to 1$ limit. The congruence of null geodesics for the black hole solution in Painlevé-Gullstrand coordinates with $E > 1$ is displayed in Figure C.5.

C.5 Eddington-Finkelstein Coordinates

The Eddington-Finkelstein, first discovered by Eddington [45] and later recovered by Finkelstein [46], follows by taking the null geodesics in Schwarzschild spacetime. Thus, we start with the coordinate transformation

$$\mathrm{d}t = \mathrm{d}v - \left(1-\frac{2M}{r}\right)^{-1}\mathrm{d}r\,, \tag{C.12}$$

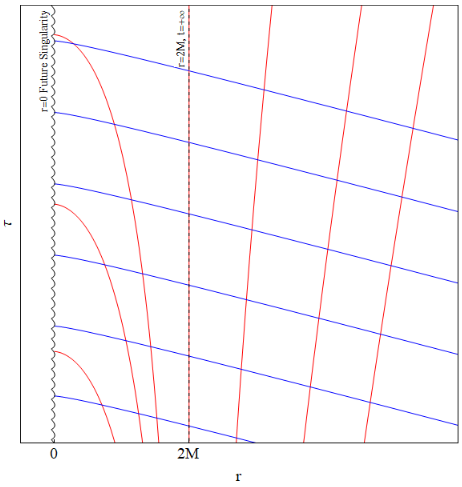

Figure C.5: The null congruence for the black hole solution in Painlevé-Gullstrand coordinates, with $E > 1$, is displayed. In red are the outgoing null geodesics and in blue are the ingoing null geodesics. The undulating line represents the singularity at the center of spatial coordinates. The dashed line represents the event horizon, $r = 2M$. Due to the coordinate transformation, Eq. (C.9), the ingoing null geodesics do not display any discontinuity at the event horizon.

and apply to the Schwarzschild metric, Eq. (C.1), finding

$$\mathrm{d}s^2 = -\left(1 - \frac{2M}{r}\right)\mathrm{d}v^2 + 2\mathrm{d}v\,\mathrm{d}r + r^2(\mathrm{d}\theta^2 + \sin^2\theta\,\mathrm{d}\phi^2)\,, \tag{C.13}$$

The transformation relation, Eq. (C.12), admits the closed form relation

$$v = t + r + 2M\ln\left|\frac{r-2M}{2M}\right|\,, \tag{C.14}$$

which is identified with the usual formula describing outgoing null geodesics. One also sees that the infinitesimal transformation relation and metric, Eqs. (C.12) and (C.13), can be obtained from the generalized Painlevé-Gullstrand transformation relation and metric, Eqs. (C.9) and (C.10), respectively, by considering the $E \to \infty$ limit of the form

$$\lim_{E\to\infty}\frac{1}{E}\mathrm{d}\tau = \mathrm{d}v \tag{C.15}$$

The congruence of null geodesics for the black hole solution in Painlevé-Gullstrand coordinates is displayed in Figure C.6.

C.6 Novikov Coordinates

The Novikov coordinate system, introduced by Novikov [47], describes the spacetime in terms of bound falling particles of energies $0 < E < 1$. Using the parametric solution, we consider the relevant set of

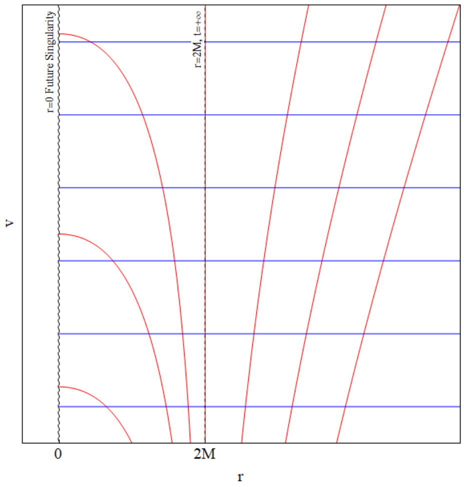

Figure C.6: The null congruence for the black hole solution in Eddington-Finkelstein coordinates is displayed. In red are the outgoing null geodesics and in blue are the ingoing null geodesics. The undulating line represents the singularity at the center of spatial coordinates. The dashed line represents the event horizon, $r = 2M$. Due to the coordinate transformation, Eq. (C.12), the ingoing null geodesics do not display any discontinuity at the event horizon.

equations

$$r = \frac{1}{2} r_m (1 + \cos\eta)\,, \tag{C.16}$$

$$t^* = \left(\frac{r_m^3}{8M}\right)^{1/2} (\eta + \sin\eta)\,, \tag{C.17}$$

$$r^* = \left(\frac{r_m}{2M} - 1\right)^{1/2}\,, \tag{C.18}$$

$$t = 2M \ln\left|\frac{r^* + \tan\frac{\eta}{2}}{r^* - \tan\frac{\eta}{2}}\right| + 2Mr^* \left[\eta + \frac{1}{2}(r^{*2} + 1)(\eta + \sin\eta)\right]\,, \tag{C.19}$$

with r_m the maximum distance of the bound trajectory. Making use of these equations is similar to using the coordinate transformation

$$\mathrm{d}r = -\left[\frac{1}{1 + r^{*2}}\left(\frac{1 - \cos\eta}{1 + \cos\eta}\right)\right]^{1/2} \mathrm{d}t^* + \frac{\partial r}{\partial r^*}\mathrm{d}r^*\,. \tag{C.20}$$

Since $E = \left(r^{*2}/(1 + r^{*2})\right)^{1/2}$, applying the transformation relation Eq. (C.20) to the generalized Painlevé-Gullstrand metric, Eq. (C.4), we get the Novikov line element

$$\mathrm{d}s^2 = -\mathrm{d}t^{*2} + \left(\frac{1 + r^{*2}}{r^{*2}}\right)\left(\frac{\partial r}{\partial r^*}\right)^2 \mathrm{d}r^{*2} + r^2(\mathrm{d}\theta^2 + \sin^2\theta\,\mathrm{d}\phi^2)\,. \tag{C.21}$$

It is seen from the coordinate relations, Eqs. (C.16) through (C.19), that there aren't closed form expressions describing $t*$ and $r*$ as functions of t and r. As such, the geodesics in Novikov coordinates are obtained through numerical resolutions. In Figure C.7 the null geodesics for the black hole and white hole solutions, i.e. the maximal analytical extension, in Novikov coordinates are displayed.

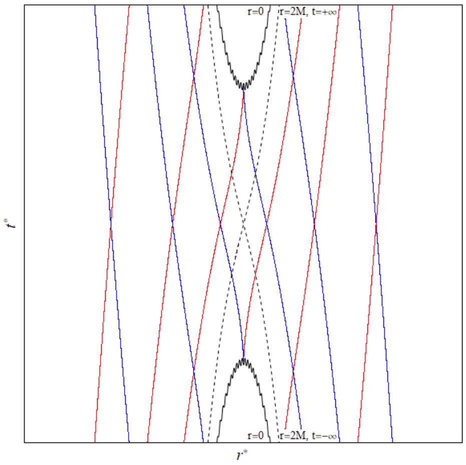

Figure C.7: The null congruence in Novikov coordinates is displayed. In red are the outgoing null geodesics and in blue are the ingoing null geodesics. The undulating line at the top represents the black hole singularity, and the one at the bottom the white hole singularity. The dashed lines represent the event horizon, $r = 2M$, of each solution. With the coordinate transformations, Eqs. (C.3) and (C.20), outgoing and ingoing null geodesics become continuous through the event horizon.

C.7 Lemaître Coordinates

The Lemaître coordinate system [48] starts with the Painlevé-Gullstrand coordinate system, and gives a partial analytical extension to the Schwarzschild extension. In this coordinate system, one takes the only free parameter of the timelike geodesic of a marginally bound falling particle, and promotes it to the new spatial coordinate. This is equivalent to taking the new coordinate transformation

$$\mathrm{d}r = -\left(\frac{2M}{r}\right)^{1/2}(\mathrm{d}\tau - \mathrm{d}\rho)\,. \tag{C.22}$$

Applying then the coordinate transformation, Eq. (C.22), to the Painlevé-Gullstrand metric, Eq. (C.7), we obtain

$$\mathrm{d}s^2 = -\mathrm{d}\tau^2 + \frac{2M}{r}\mathrm{d}\rho^2 + r^2(\mathrm{d}\theta^2 + \sin^2\phi\,\mathrm{d}\phi^2)\,. \tag{C.23}$$

The introduced transformation relation, Eq. (C.22), admits the closed form relation

$$r = (2M)^{1/3}\left[\frac{3}{2}(\rho - \tau)\right]^{2/3}\,, \tag{C.24}$$

which corresponds to the trajectory of a marginally bound falling particle when one makes the substitution $\tau_0 \to \rho$. The congruence of null geodesics for the black hole solution in Lemaître coordinates is shown in Figure C.8.

C.8 Lemaître Coordinates with $E > 1$

The generalization of the usual Lemaître coordinate system can be obtained by applying similar considerations. Now we take the trajectory of the falling particle, now unbound, i.e. with any $E > 1$, and

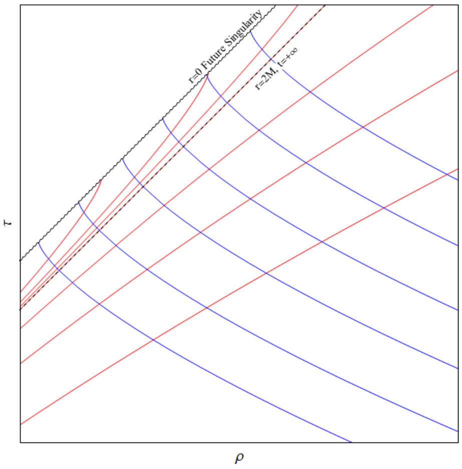

Figure C.8: The null congruence for the black hole solution in Lemaître coordinates is displayed. In red are the outgoing null geodesics and in blue are the ingoing null geodesics. The undulating line represents the singularity at the center of spatial coordinates. The dashed line represents the event horizon, $r = 2M$.

promote the free parameter to a variable, $\tau_0 \to \rho$. Doing so, we obtain the coordinate transformation

$$\mathrm{d}r = -\left(E^2 - 1 + \frac{2M}{r}\right)^{1/2} (\mathrm{d}\tau - \mathrm{d}\rho)\,, \tag{C.25}$$

which, when applied to the generalized Painlevé-Gullstrand coordinate system with the same parameter $E > 1$, gives the generalized Lemaître coordinate system with $E > 1$

$$\mathrm{d}s^2 = -\mathrm{d}\tau^2 + \frac{1}{E^2}\left(E^2 - 1 + \frac{2M}{r}\right)\mathrm{d}\rho^2 + r^2(\mathrm{d}\theta^2 + \sin^2\theta\,\mathrm{d}\phi^2)\,. \tag{C.26}$$

Additionally, the new transformation relation, Eq. (C.25), admits the closed form relation

$$\begin{aligned}\rho = Et + \frac{2E^2 - 3}{(E^2 - 1)^{3/2}} ME^2 \ln\left[\frac{r}{M}\left(E^2 - 1 + \frac{M}{r} + (E^2 - 1)^{1/2}\left(E^2 - 1 + \frac{2M}{r}\right)^{1/2}\right)\right] + \\ + \frac{E^2}{E^2 - 1} r \left(E^2 - 1 + \frac{2M}{r}\right)^{1/2} - 2ME \ln\left|\frac{2E^2 - 1 + \frac{2M}{r} + 2E\left(E^2 - 1 + \frac{2M}{r}\right)^{1/2}}{1 - \frac{2M}{r}}\right|.\end{aligned} \tag{C.27}$$

One finds, from Eqs. (C.25) through (C.27), that the equations of the usual Lemaître coordinate system, Eqs. (C.22) through (C.24), are recovered in the $E \to 1$ limit. The congruence of null geodesics for the black hole solution in generalized Lemaître coordinates, with energy $E > 1$, is shown in Figure C.9.

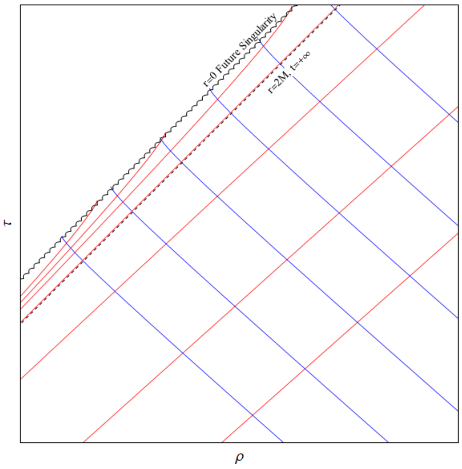

Figure C.9: The null congruence for the black hole solution in generalized Lemaître coordinates, with energy $E > 1$, is displayed. In red are the outgoing null geodesics and in blue are the ingoing null geodesics. The undulating line represents the singularity at the center of spatial coordinates. The dashed line represents the event horizon, $r = 2M$.

Let us now consider the asymptotic limit of the generalized Lemaître coordinate system. We start with its line element

$$\mathrm{d}s^2 = -\mathrm{d}\tau^2 + \frac{1}{E^2}\left(E^2 - 1 + \frac{2M}{r}\right)\mathrm{d}\rho^2 + r^2(\mathrm{d}\theta^2 + \sin^2\theta\,\mathrm{d}\phi^2)\,, \tag{C.28}$$

with

$$\left(E^2 - 1 + \frac{2M}{r}\right)^{-1/2}\mathrm{d}r = \mathrm{d}\rho - \mathrm{d}\tau\,. \tag{C.29}$$

There are two different $E^2 \to \infty$ cases. One limit is for $\frac{M}{E^2} \leq \mathrm{constant}$. The other limit is for $\frac{M}{E^2} \to \infty$. Let us do the two limits.

We start with the $\frac{M}{E^2} \leq \mathrm{constant}$ and $E^2 \to \infty$ case. There are two subcases, namely, $\frac{M}{E^2} = 0$ with $E^2 \to \infty$ and $\frac{M}{E^2} = \mathrm{constant}$ with $E^2 \to \infty$. Let us do first, $\frac{M}{E^2} = 0$ with $E^2 \to \infty$. In this case the limit of Eq. (C.28) is clearly

$$\mathrm{d}s^2 = -\mathrm{d}\tau^2 + \mathrm{d}\rho^2 + r^2(\mathrm{d}\theta^2 + \sin^2\theta\,\mathrm{d}\phi^2)\,. \tag{C.30}$$

Applying the limit, $\frac{M}{E^2} = 0$, when $E \to \infty$ to Eq. (C.29), we find $\mathrm{d}r \to E(\mathrm{d}\rho - \mathrm{d}\tau)$ and so

$$r = E(\rho - \tau)\,, \tag{C.31}$$

in the limit. Applying the limit relation, Eq. (C.31), to the line element obtained in Eq. (C.30) it follows

$$\mathrm{d}s^2 = -\mathrm{d}\tau^2 + \mathrm{d}\rho^2 + E^2(\tau - \rho)^2\,(\mathrm{d}\theta^2 + \sin^2\theta\,\mathrm{d}\phi^2)\,. \tag{C.32}$$

To absorb the remaining E parameter, we employ a new coordinate transformation. Let us define $\bar{\theta} = E\,\theta$ and so $\theta = \frac{\bar{\theta}}{E}$. Then, clearly, $\sin\theta = \sin\left(\frac{\bar{\theta}}{E}\right) = \frac{\bar{\theta}}{E}$ in the limit. Thus, the line element for the spherical 2-space becomes $\mathrm{d}\bar{\theta}^2 + \bar{\theta}^2\,\mathrm{d}\phi^2$, which is the line element for a flat two-space in polar coordinates. Define $\bar{\bar{\theta}} = \bar{\theta}\cos\phi$ and $\bar{\bar{\phi}} = \bar{\theta}\sin\phi$, so that flat two-space in Cartesian coordinates is

$\mathrm{d}\bar{\bar{\theta}}^2 + \mathrm{d}\bar{\bar{\phi}}^2$, as expected. The line element is now $\mathrm{d}s^2 = -\mathrm{d}\tau^2 + \mathrm{d}\rho^2 + (\tau - \rho)^2(\mathrm{d}\theta^2 + \mathrm{d}\phi^2)$, where the double bar over θ and ϕ was dropped. This line element can be recast in a simpler form with an appropriate choice of coordinates. Let us choose $v = \tau - \rho$ and $u = \tau + \rho$. Then, the line element is $\mathrm{d}s^2 = -\mathrm{d}u\,\mathrm{d}v + v^2(\mathrm{d}\theta^2 + \mathrm{d}\phi^2)$. To proceed, we choose the following coordinate transformations $\mathrm{d}t = \frac{1}{2}\mathrm{d}\left[u + v(1 + \theta^2 + \phi^2)\right]$, $\mathrm{d}x = \frac{1}{2}\mathrm{d}\left[u - v(1 - \theta^2 - \phi^2)\right]$, $\mathrm{d}y = \mathrm{d}(v\theta)$, $\mathrm{d}z = \mathrm{d}(v\phi)$. The inverse transformations are $\mathrm{d}u = \left(1 + \frac{y^2+z^2}{(t-x)^2}\right)\mathrm{d}t + \left(1 - \frac{y^2+z^2}{(t-x)^2}\right)\mathrm{d}x - 2\frac{y}{t-x}\mathrm{d}y - 2\frac{z}{t-x}\mathrm{d}z$, $\mathrm{d}v = \mathrm{d}t - \mathrm{d}x$, $\mathrm{d}\theta = -\frac{y}{(t-x)^2}\mathrm{d}t + \frac{y}{(t-x)^2}\mathrm{d}x + \frac{1}{t-x}\mathrm{d}y$, and $\mathrm{d}\phi = -\frac{z}{(t-x)^2}\mathrm{d}t + \frac{z}{(t-x)^2}\mathrm{d}x + \frac{1}{t-x}\mathrm{d}z$. For the sake of completeness we write the coordinate relations in nondifferential form, i.e., $t = \frac{1}{2}[u + v(1 + \theta^2 + \phi^2)]$, $x = \frac{1}{2}[u - v(1 - \theta^2 - \phi^2)]$, $y = v\theta$, $z = v\phi$, and their inverses $u = \frac{t^2-x^2-y^2-z^2}{t-x}$, $v = t - x$, $\theta = \frac{y}{t-x}$, $\phi = \frac{z}{t-x}$. Inserting the coordinate transformations just found into the line element $\mathrm{d}s^2 = -\mathrm{d}u\,\mathrm{d}v + v^2(\mathrm{d}\theta^2 + \mathrm{d}\phi^2)$, one gets

$$\mathrm{d}s^2 = -\mathrm{d}t^2 + \mathrm{d}x^2 + \mathrm{d}y^2 + \mathrm{d}z^2\,. \tag{C.33}$$

Thus, the $\frac{M}{E^2} = 0$, when $E^2 \to \infty$, limit of the Lemaître form of the Schwarzschild metric is the Minkowski metric. Indeed, we have found it is the same limit as taking the $M \to 0$ limit of the Schwarzschild metric in the usual coordinates. The second subcase is $\frac{M}{E^2} = \text{constant}$ when $E^2 \to \infty$. This case can also be worked out in detail yielding again the Minkowski metric. In brief, the $E^2 \to \infty$ with $\frac{M}{E^2} \leq \text{constant}$ limit yields the Minkowski metric.

Now we do the other limit, namely, $\frac{M}{E^2} \to \infty$ when $E^2 \to \infty$. Then write Eq. (C.28) as $ds^2 = = -d\tau^2 + \frac{1}{E^4}\left(E^2 - 1 + \frac{2M}{r}\right)d(E\rho)^2 + r^2\left(d\theta^2 + \sin^2\theta d\phi^2\right)$, i.e., we have multiplied and divided the second term of the right hand side of Eq. (C.28) by E^2. Now define $\bar{\rho} = E\rho$ or $\rho = \dfrac{\bar{\rho}}{E}$. Taking the limit $E^2 \to \infty$ and $\frac{M}{E^2} \to \infty$ we have that the term $E^2 - 1$ is negligible in relation to $\frac{2M}{r}$, so that the Lemaître line element of Eq. (C.28) is now

$$ds^2 = -d\tau^2 + \left(\frac{2M/E^4}{r}\right)d\bar{\rho}^2 + r^2\left(d\theta^2 + \sin^2\theta d\phi^2\right)\,. \tag{C.34}$$

Note that we could have defined $\bar{\rho}$, by $\bar{\rho} = E^\alpha\rho$ with α any positive expontent, $\alpha > 0$; we have chosen $\alpha = 1$ to be definitve and to not carry throughout the calculations a new cumbersome exponent. Now let us work Eq. (C.29). Taking the limit $E^2 \to \infty$ and $\frac{M}{E^2} \to \infty$ we have again that the term $E^2 - 1$ is negligible in relation to $\frac{2M}{r}$, so that the limit of Eq. (C.29) is $\frac{dr}{\sqrt{\frac{2M}{r}}} = d\tau - d\rho$, or in terms of $\bar{\rho}$ is $\frac{dr}{\sqrt{\frac{2M}{r}}} = d\tau - \frac{d\bar{\rho}}{E}$. Then since $E \to \infty$ the term $\frac{d\bar{\rho}}{E}$ goes to zero. Taking everything together, Eq. (C.29) is now $\frac{dr}{\sqrt{\frac{2M}{r}}} = d\tau$ and so

$$r = \left(\frac{3}{2}\right)^{\frac{2}{3}}(2M)^{\frac{1}{3}}\,\tau^{\frac{2}{3}}\,. \tag{C.35}$$

So, $r^2 = \left(\frac{3}{2}\right)^{\frac{4}{3}}(2M)^{\frac{2}{3}}\,\tau^{\frac{4}{3}}$. Now, we can put into the line element given in Eq. (C.34) the result given in Eq. (C.35). The term $\left(\frac{2M/E^4}{r}\right)d\bar{\rho}^2$ in Eq. (C.34) becomes $\frac{2M/E^4}{\left(\frac{3}{2}\right)^{\frac{2}{3}}(2M)^{\frac{1}{3}}\tau^{\frac{2}{3}}}\,d\bar{\rho}^2$ which can be rewritten as $\left(\frac{2}{3}\right)^{\frac{2}{3}}\left(\frac{2M}{E^6}\right)^{\frac{2}{3}}\frac{d\bar{\rho}^2}{\tau^{\frac{2}{3}}}$. Define $\bar{m}$ finite, with units of mass or length, such that $(2\bar{m})^{\frac{2}{3}} \equiv \left(\frac{2}{3}\right)^{\frac{2}{3}}\left(\frac{2M}{E^6}\right)^{\frac{2}{3}}$. This is consistent with our limiting procedure, indeed one has then $2M = \frac{3}{2}\,(2\bar{m})\,E^6$, which goes to infinity as $E^2 \to \infty$ and also $\frac{2M}{E^2}$ goes to infinity as $E^2 \to \infty$. Then the term in $d\bar{\rho}^2$ is $\frac{(2\bar{m})^{\frac{2}{3}}}{\tau^{\frac{2}{3}}}\,d\bar{\rho}^2$. Note also that the term $r^2\left(d\theta^2+\sin^2\theta d\phi^2\right)$ that appears in Eq. (C.34) is now $\left(\frac{3}{2}\right)^{\frac{4}{3}}(2M)^{\frac{2}{3}}\,\tau^{\frac{4}{3}}\left(d\theta^2+\sin^2\theta d\phi^2\right)$. But as we have just seen $2M\to\infty$ as $2M=\frac{3}{2}\,(2\bar{m})\,E^6$, i.e., $(2M)^{\frac{2}{3}}=\left(\frac{3}{2}\right)^{\frac{2}{3}}(2\bar{m})^{\frac{2}{3}}\,E^4$, so that the term $r^2\left(d\theta^2+\sin^2\theta d\phi^2\right)$ is $(2\bar{m})^{\frac{2}{3}}\,\tau^{\frac{4}{3}}\left(\frac{3}{2}\right)^2 E^4\left(d\theta^2+\sin^2\theta d\phi^2\right)$. Putting $\left(\frac{3}{2}\right)^2 E^4$ to the inside of the spherical line element $\left(d\theta^2+\sin^2\theta d\phi^2\right)$ this turns into a flat 2-space line element $\left(d\theta^2+d\phi^2\right)$, as we already found before. So the 2-space angular part is now $(2\bar{m})^{\frac{2}{3}}\,\tau^{\frac{4}{3}}\left(d\theta^2+d\phi^2\right)$. So Eq. (C.34) becomes

$$ds^2=-d\tau^2+\frac{(2\bar{m})^{\frac{2}{3}}}{\tau^{\frac{2}{3}}}\,d\bar{\rho}^2+(2\bar{m})^{\frac{2}{3}}\,\tau^{\frac{4}{3}}\left(d\theta^2+d\phi^2\right). \tag{C.36}$$

This is the Kasner metric. To put in the more familiar form we do the following transformation, $t=$ $=(2\bar{m})^{\frac{1}{3}}\,\tau^{\frac{2}{3}}$. Then $d\tau=\frac{3}{2}\frac{\sqrt{t}}{\sqrt{2\bar{m}}}dt$ and $-d\tau^2=-\frac{9}{4}\frac{t}{2\bar{m}}dt^2$. The term $\frac{(2\bar{m})^{\frac{2}{3}}}{\tau^{\frac{2}{3}}}\,d\bar{\rho}^2$ is now $\frac{2\bar{m}}{t}\,d\bar{\rho}^2$. Define m such that $2m\equiv\frac{4}{9}\,2\bar{m}$. Redefine the radial coordinate to a new r through $r\equiv\frac{3}{2}\bar{\rho}$, and define $x\equiv\theta$ and $y\equiv\phi$. Then Eq. (C.36) turns into

$$ds^2=-\frac{t}{2m}dt^2+\frac{2m}{t}\,dr^2+t^2\left(dx^2+dy^2\right). \tag{C.37}$$

Eq. (C.37) is the usual form of the Kasner metric. The parameter m serves to set some scale, but otherwise is irrelevant. The Kretschmann scalar is $K=\dfrac{48m^2}{t^6}$ and all the components of the Einstein tensor vanish, as required for a vacuum solution. Thus, the Kasner metric is one of the two $E^2\to\infty$ limits of the Lemaître form of the Schwarzschild metric, indeed it is the $\frac{M}{E^2}\to\infty$ when $E^2\to\infty$ limit. We have found it is the same limit as taking the $M\to\infty$ limit of the Schwarzschild metric in the usual coordinates.

We have proved that the Lemaître form of the Schwarzschild metric ends in two cases when $E^2\to\infty$, one is the Minkowski metric when $\frac{M}{E^2}\leq\mathrm{constant}$, the other is the Kasner metric when $\frac{M}{E^2}\to\infty$. In one limit the geodesics with energy $E\to\infty$ are in an effectively $M=0$, i.e., Minkowski spacetime. In the other limit, the geodesics. with energy $E\to\infty$ are in an effectively $M\to\infty$, i.e., Kasner spacetime.

C.9 Kruskal-Szekeres Coordinates

The Kruskal-Szekeres coordinate system, discovered independently by Kruskal [49] and Szekeres [50], serves as an extension of Eddington-Finkelstein coordinate system. Furthermore, like the Novikov coordinate system, it provides a maximal analytical extension of the Schwarzschild spacetime. The transformation relation used to obtain the Eddington-Finkelstein coordinates, Eq. (C.12), was seen to straighten out the ingoing null geodesics, Figure C.6. One now proceeds with a new coordinate transformation which straightens out the outgoing null geodesics

$$\mathrm{d}w=\mathrm{d}t-\left(1-\frac{2M}{r}\right)^{-1}\mathrm{d}r\,, \tag{C.38}$$

which, when applied to the Schwarzschild metrc, Eq. (C.1), gives

$$\mathrm{d}s^2 = -\left(1 - \frac{2M}{r}\right)\mathrm{d}v\,\mathrm{d}w + r^2(\mathrm{d}\theta + \sin^2\theta\,\mathrm{d}\phi^2)\,. \tag{C.39}$$

The transformation relation admits the closed form relation

$$w = t - r - 2M\ln\left|\frac{r-2M}{2M}\right|\,. \tag{C.40}$$

The metric obtained, Eq. (C.39), already begets the required structure, but one usual follows it with an additional conformal transformation to bring out the special features of the maximal extension. We choose, for $r > 2M$

$$t' = \left(\frac{r}{2M} - 1\right)^{1/2}\exp\left(\frac{r}{4M}\right)\sinh\left(\frac{t}{4M}\right), \tag{C.41}$$

$$x' = \left(\frac{r}{2M} - 1\right)^{1/2}\exp\left(\frac{r}{4M}\right)\cosh\left(\frac{t}{4M}\right), \tag{C.42}$$

and, for $r < 2M$

$$t' = \left(1 - \frac{r}{2M}\right)^{1/2}\exp\left(\frac{r}{4M}\right)\cosh\left(\frac{t}{4M}\right), \tag{C.43}$$

$$x' = \left(1 - \frac{r}{2M}\right)^{1/2}\exp\left(\frac{r}{4M}\right)\sinh\left(\frac{t}{4M}\right). \tag{C.44}$$

These new transformation relations, Eqs. (C.41) through (C.44), allow the relation with r

$$t'^2 - x'^2 = \left(1 - \frac{r}{2M}\right)\exp\left(\frac{r}{2M}\right). \tag{C.45}$$

Additionally, when applied to the metric of Eq. (C.39), one gets

$$\mathrm{d}s^2 = \frac{32M^3}{r}\exp\left(-\frac{r}{2M}\right)(-\mathrm{d}t'^2 + \mathrm{d}x'^2) + r^2(\mathrm{d}\theta^2 + \sin^2\theta\,\mathrm{d}\phi^2)\,. \tag{C.46}$$

From the new line element, Eq. (C.46), it comes immediately that the null geodesics follow along diagonal straight lines. The congruence of null geodesics for the black and white hole solutions, i.e. the maximal analytical extension, in Kruskal-Szekeres are displayed in Figure C.10.

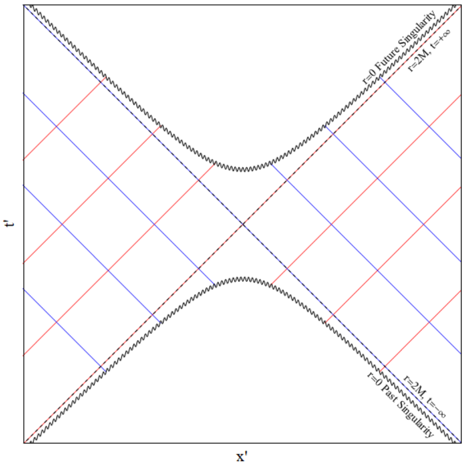
r=0 Future Singularity
r=2M, t=+∞
r=2M, t=−∞
r=0 Past Singularity
t'
x'

Figure C.10: The null congruence in Kruskal-Szekeres is displayed. In red are the outgoing geodesics and in blue are the ingoing null geodesics. The undulating line at the top represents the black hole singularity, and the one at the bottom the white hole singularity. The dashed lines represent the event horizon, $r = 2M$, of each solution.

Bibliography

[1] A. Einstein, *Sitz Preuss Akad. d. Wiss* **1915**, 844 (1915).

[2] K. Schwarzschild, *Sitz Preuss Akad. d. Wiss* **1916**, 189 (1916).

[3] J. R. Oppenheimer, G. M. Volkoff, *Physical Review* **55**, 374 (1939).

[4] J. R. Oppenheimer, H. Snyder, *Phys. Rev.* **56**, 455 (1939).

[5] R. C. Tolman, *Proc. Natl. Acad. Sci. USA* **20**, 169 (1934).

[6] C. A. R. Herdeiro, J. P. S. Lemos, *Gazeta de Física* **41**, 2 (2018). ArXiv:1811.06587v2.

[7] The Event Horizon Telescope Collaboration, *ApJ* **875** (2019). ArXiv:1906.11238.

[8] I. D. Novikov, V. Frolov, *Physics of Black Holes* (Springer Netherlands, Netherlands, 1989).

[9] G. Darmois, *Mémorial des Sciences Mathématiques Les équations de la gravitation einsteinienne*, vol. XXV (L'Académie des Sciences de Paris, 1927).

[10] C. W. Misner, D. H. Sharp, *Phys. Rev. B* **136**, 571 (1964).

[11] W. Israel, *Il Nuovo Cimento B* **44**, 1 (1966).

[12] D. L. Beckedorff, Terminal configurations of stellar evolution, Ph.D. thesis, Princeton University (1962).

[13] C. W. Misner, K. S. Thorne, J. A. Wheeler, *Gravitation* (W. H. Freeman, San Francisco, 1973).

[14] J. B. Hartle, *Relativity, Astrophysics and Cosmology*, W. Israel, ed. (Springer, 1973).

[15] B. Datt, *Zeitschrift für Physik* **108**, 314 (1938).

[16] D. Christodoulou, *Commun. Math. Phys.* **109**, 613 (1987).

[17] M. W. Choptuik, *Phys. Rev. Lett.* **70**, 9 (1993).

[18] J. V. Rocha, M. Tomašević, *Phys. Rev. D* **98**, 104063 (2018). ArXiv:1810.04907v2 [gr-qc].

[19] C. Gundlach, J. M. Martín-García, *Living Rev. Rel* **10**, 1 (2007). ArXiv:0711.4620v1 [gr-qc].

[20] P. S. Joshi, N. Dadhich, R. Maartens, *Phys. Rev. D* **65**, 101501 (2002). ArXiv:gr-qc/0109051v2.

[21] F. C. Mena, B. C. Nolan, R. Tavakol, *Phys. Rev. D* **70**, 084030 (2004). ArXiv:gr-qc/0405041v1.

[22] S. Coleman, *Phys. Rev. D* **15**, 2929 (1977).

[23] R. J. Adler, J. D. Bjorken, P. Chen, J. S. Liu, *Am. J. Phys.* **73**, 1148 (2005). ArXiv:gr-qc/0502040.

[24] C. Barrabès, W. Israel, *Physical Review D* **43**, 1129 (1991).

[25] E. Poisson, *A Relativist's Toolkit: The Mathematics of Black-Hole Mechanics* (Cambridge University Press, Cambridge, 2007), chap. 3.7.

[26] D. Lynden-Bell, J. P. S. Lemos, *Mon. Not. R. Astr. Soc.* **233**, 197 (1988).

[27] M. V. Penston, *Mon. Not. R. Astr. Soc.* **144**, 425 (1969).

[28] J. P. S. Lemos, D. Lynden-Bell, *Mon. Not. R. Astr. Soc.* **240**, 317 (1989).

[29] W. Israel, *Phys. Rev.* **153**, 1388 (1967).

[30] S. Gao, J. P. S. Lemos, *Int. J. Mod. Phys. A* **23**, 2943 (2008). ArXiv:0804.0295v1 [hep-th].

[31] G. A. S. Dias, J. P. S. Lemos, *Phys. Rev. D* **82**, 084023 (2010). ArXiv:1008.3376v1 [gr-qc].

[32] S. C. Davis, *Phys. Rev. D* **67**, 024030 (2003). ArXiv:hep-th/0208205v3.

[33] J. Crisóstomo, R. Olea, *Phys. Rev. D* **69**, 104023 (2004). ArXiv:hep-th/0311054v2.

[34] P. Hájíček, J. Kijowski, *Phys. Rev. D* **57**, 914 (1998). ArXiv:gr-qc/9707020v1.

[35] G. A. S. Dias, S. Gao, J. P. S. Lemos, *Phys. Rev. D* **75**, 024030 (2007). ArXiv:gr-qc/0612072v2.

[36] R. D'Inverno, *Introducing Einstein's Relativity* (Oxford University Press, Oxford, 1992).

[37] S. W. Hawking, G. F. R. Ellis, *The Large Scale Structure of Space-Time* (Cambridge University Press, Cambridge, 2010), chap. 9.2.

[38] D. M. Eardley, L. Smarr, *Phys. Rev. D* **19**, 2239 (1979).

[39] E. M. Purcell, *Electricity and Magnetism* (McGraw-Hill, 1965), chap. 2.7.

[40] G. D. Birkhoff, *Relativity and Modern Physics* (Harvard University Press, Cambridge Massachusetts, 1923).

[41] J. T. Jebsen, *Ark. Mat. Astr. Fys.* **15**, 1 (1921).

[42] R. Gautreau, B. Hoffmann, *Phys. Rev. D* **17**, 2552 (1978).

[43] P. Painlevé, *C.R. Acad. Sci.* **173**, 677 (1921).

[44] A. Gullstrand, *Ark. Mat. Astr. Fys.* **16**, 1 (1922).

[45] A. S. Eddington, *Nature* **113**, 192 (1924).

[46] D. Finkelstein, *Phys. Rev.* **110**, 965 (1958).

[47] I. D. Novikov, Early stages of the evolution of the universe, Ph.D. thesis, SAI Moscow (1963).

[48] G. Lemaître, *Ann. Soc. Sci. Bruxelles* **53A**, 51 (1933).

[49] M. D. Kruskal, *Phys. Rev.* **119**, 1743 (1960).

[50] G. Szekeres, *Publ. Math-Debrecen* **7**, 285 (1960).

Addendum

New Maximal Extension of Schwarzschild Coordinates

José P. S. Lemos[a] and Diogo L. F. G. Silva[b]
Centro de Astrofísica e Gravitação - CENTRA, Departamento
de Física, Instituto Superior Técnico - IST, Universidade de
Lisboa - UL, Av. Rovisco Pais 1, 1049-001 Lisboa, Portugal

---

[a] email: joselemos@ist.utl.pt
[b] email: diogo.l.silva@tecnico.ulisboa.pt

We find a specific coordinate system that goes from the Painlevé-Gullstrand partial extension to the Kruskal-Szekeres maximal extension and thus exhibit the maximal extension of the Schwarzschild metric in a unified picture. We do this by adopting two time coordinates, one being the proper time of a congruence of outgoing timelike geodesics, the other being the proper time of a congruence of ingoing timelike geodesics, both parameterized by the same energy per unit mass E. E is in the range $1 \leq E < \infty$ with the limit $E = \infty$ yielding the Kruskal-Szekeres maximal extension. So, through such an integrated description one sees that the Kruskal-Szekeres solution belongs to this family of extensions parameterized by E. Our family of extensions is different from the Novikov-Lemaître family parameterized also by the energy E of timelike geodesics, with the Novikov extension holding for $0 <$ $< E < 1$ and being maximal, and the Lemaître extension holding for $1 \leq E < \infty$ and being partial, not maximal, and moreover its $E = \infty$ limit evanescing in a Minkowski spacetime rather than ending in the Kruskal-Szekeres spacetime.

I. Introduction

The maximal analytical extension of the Schwarzschild solution was a remarkable achievement in general relativity and in the theory of black holes. For the first time the complex causal structure with a convoluted spacetime topology, stemming from the seemingly trivial generalization into general relativity of a point particle attractor in Newtonian gravitation, was unfolded.

It all started with the spherically symmetric vacuum solution of general relativity found by Schwarzschild [1], that was put in different terms and in a somewhat different coordinate system by Droste [2] and Hilbert [3], and shown to be unique by Birkhoff [4]. Leaving aside Schwarzschild's interpretation of Schwarzschild's solution, it is the solution that later gave rise to black holes. To finalize its full meaning it was necessary to understand the sphere $r = 2M$ that naturally appears in the solution and accomplish its maximal extension, i.e., finding the corresponding spacetime in which every geodesic originating from an arbitrary point in it has infinite length in both directions or ends at a singularity that cannot be removed by a coordinate transformation. These were two problems that proved difficult.

An early attempt to eliminate the $r = 2M$ sphere obstacle and its inside was provided by Einstein and Rosen [5] that tried to join smoothly at $r = 2M$ two distinct spacetime sheets in order to get some kind of fundamental particle, in what is known as an Einstein-Rosen bridge. Misner and Wheeler [6] generalized the bridge into a wormhole with a throat at its maximum opening. Wormholes became a focus of study within general relativity after Morris and Thorne [7] showed that with some suitable form of matter, albeit exotic, they could be traversable, see also, e.g., the work of Lemos, Lobo and Oliveira [8]. The Einstein-Rosen bridge in terms of the understanding of the $r = 2M$ sphere was a dead end, but as a nontraversable wormhole it reincarnated in the maximal extensions of the Schwarzschild metric, and as a traversable wormhole it can be put in firm ground once one properly defines it in order to have an admissible matter support, as disclosed by Guendelman, Nissimov, Pacheva, and Stoilov [9].

A promising way of seeing the Schwarzschild solution, whatever the motivation, came with Painlevé [10] that changed the Schwarzschild time coordinate into the proper time of a congruence of ingoing timelike geodesics, or equivalently of ingoing test particles planted over them, with energy per unit mass E equal to one, that admitted to put the line element in a new form that was not singular at $r = 2M$. This procedure was also discovered by Gullstrand [11], and the resulting line element, which works as for outgoing as for ingoing timelike geodesics, is called the Painlevé-Gullstrand line element of the Schwarzschild solution, or simply referred as Painlevé-Gullstrand solution, and in both forms it is an analytical extension, although partial, of the original Schwarzschild solution. The generalization of this line element to accommodate a congruence of timelike geodesics with any E, less or greater than one, was given by Gautreau and Hoffmann [12]. The Painlevé-Gullstrand line element, not being singular at $r = 2M$, is useful in many understandings of black hole physics. For instance, it has been used by Parikh and Wilczek to understand how Hawking radiation proceeds [13], or as a guide for a better understanding of the $r = 2M$ sphere by Martel and Poisson [14], or to understand in new ways the Kerr metric by Natário [15], or as a generalized slicing of the Schwarzschild spacetime by Finch [16] and MacLaurin [17].

An extension of the Painlevé-Gullstrand line element was given by Lemaître [18] that transformed the time and radial coordinates of the Schwarzschild solution to the proper time of ingoing timelike geodesics with $E = 1$ and to a suitable new comoving radial coordinate, and showed in a stroke that $r = 2M$ was a fine sphere, with nothing singular about it, performing thus an analytical extension, although partial, of the Schwarzschild solution. Novikov [19] understood that for timelike geodesics with $0 < E < 1$ it was possible to perform a maximal analytical extension and display the Schwarzschild solution in its fullness. The Lemaître extension, as an exterior spacetime, was implicitly used in the gravitational contraction of a cloud of dust by Oppenheimer and Snyder to discover black holes and their formation for the first time with the natural appearance of an exterior event horizon at $r = 2M$ [20]. Presentations of the Novikov-Lemaitre extensions can be seen in several places. The Novikov maximal extension is worked through in Zel'dovich and Novikov's book [21] and in Gautreau [22], and the Lemaître extension is featured, e.g., in the detailed book by Krasiński [23] and in the very useful book of Blau [24].

Remarkably, there is a parallel development that uses lightlike, or null, geodesics rather than timelike ones. Indeed, Eddington [25] used ingoing null geodesics to transform the Schwarzschild time into a new time that straightened out those very ingoing null geodesics and to put the line element in a new form that was not singular at $r = 2M$. This was recovered by Finkelstein [26], and then Penrose [27] understood that it was more natural to use the corresponding advanced null coordinate to represent the metric and the line element. This form works as for outgoing as for ingoing null geodesics, and the solution is correspondingly called the Schwarzschild solution in retarded or in advanced null Eddington-Finkelstein coordinates, respectively. Both forms are analytical extensions, although partial, of the original Schwarzschild solution. The Eddington-Finkelstein line element, not being singular at $r = 2M$ is also useful in many understandings of black hole physics. For instance, it has been used by Alcubierre and Bruegmann in black hole excision in 3+1 numerical relativity [28], or as a guide for a better understanding of the $r = 2M$ sphere by Adler, Bjorken, Chen, and Liu [29], or to understand perturbatively the accretion of matter onto a black hole [30], or to understand the stress-energy tensor of quantum fields involved in the evaporation of a black hole [31], or even to treat quantum gravitational problems related to coordinate transformations [32].

An extension to the Eddington-Finkelstein line element was given by Kruskal [33] and Szekeres [34]. By using both outgoing and ingoing null geodesics to transform the Schwarzschild time and the Schwarzschild radius coordinates into new analytical extended time and spatial coordinates, both the outgoing and the ingoing null geodesics were straightened out and in addition one could pass with ease the sphere $r = 2M$ in all directions. In this way the maximal analytical extension of the Schwarzschild solution was unfolded, in a single coordinate system, into its full form. Fuller and Wheeler [35] revealed its dynamic structure with a nontraversable Einstein-Rosen bridge, i.e., a nontraversable wormhole, lurking in-between two distinct asymptotically flat spacetime regions and driving, out of spacetime spacelike singularities at $r = 0$, the creation of a white hole into the formation of a black hole. Prior maximal extensions had also been given in Synge [36] and Fronsdal [37] using several coordinate systems or embeddings, rather than the unique coordinate system of the Kruskal-Szekeres extension. Modern presentations of the Kruskal-Szekeres solution can be seen in the books on general relativity and gravitation by Hawking and Ellis [38], Misner, Thorne, and Wheeler [39], Wald [40], d'Inverno [41], Bronnikov and Rubin [42], and Chruściel [43], and in many other places, where double null coordinates are usually employed. The Kruskal-Szekeres line element, with its maximal properties, is certainly useful in a great very many understandings of black hole physics, notably, it surely is a prototype of gravitational collapse. To name two further examples of its applicability, Zaslavskii [44] has used its properties to suitably define high energy collisions in the vicinity of the event horizon, and Hodgkinson, Louko, and Ottewill [45] have examined the response of particle detectors to fields in diverse quantum vacuum states working with Kruskal-Szekeres spacetime and coordinates.

Now, the Painlevé-Gullstrand line element uses as coordinate the proper time of a congruence of outgoing or ingoing timelike geodesics and the Eddington-Finkelstein line element uses as coordinate the retarded or advanced null parameter of a congruence of outgoing or ingoing null geodesics, respectively. There is a connection between the two coordinate systems as worked out by Lemos [46], who showed that by taking the $E = \infty$ limit of the Painlevé-Gullstrand line element, and more generally its Lemaître-Tolman-Bondi generalization to include dust matter, one obtains the Eddington-Finkelstein line element, and more generally its Vaidya generalization to include incoherent radiation. Indeed, since E is the energy per unit mass of the timelike geodesic, or of the particle placed over it, when the mass goes to zero, E goes to infinity, and the proper time along the timelike geodesic turns into a well defined affine parameter along the null geodesic, or along the lightlike particle trajectory placed over it.

But now we have a conundrum. The Novikov-Lemaitre family of solutions parameterized by E comes out of the corresponding Painlevé-Gullstrand family with the addition of an appropriate radial coordinate. On the one hand, the Novikov solution is maximal, on the other hand, the Lemaître solution is not. Moreover, although Painlevé-Gullstrand goes into Eddington-Finkelstein in the $E = \infty$ limit, Lemaître does not go into Kruskal-Szekeres in the $E = \infty$ limit, instead it dies in a Minkowski spacetime. But Eddington-Finkelstein goes into Kruskal-Szekeres. In brief, Painlevé-Gullstrand goes into Novikov-Lemaître that does not go into Kruskal-Szekeres, and Painlevé-Gullstrand goes into Eddington-Finkelstein that goes into Kruskal-Szekeres. So, there is a missing link. What is the maximal extension that starts from Painlevé-Gullstrand and in the $E = \infty$ limit goes into the Kruskal-Szekeres maximal extension?

Here, we find the maximal analytic extension of the Schwarzschild spacetime that goes from Painlevé-Gullstrand to Kruskal-Szekeres yielding a unified picture of extensions. By using two analytically extended Painlevé-Gullstrand time coordinates, we find another way of obtaining the maximal analytic extension of the Schwarzschild spacetime. It is parameterized by the energy E of the outgoing and ingoing timelike geodesics. The extension is valid for $1 \leq E < \infty$, with the case $E = \infty$ giving the Kruskal-Szekeres extension. So the Kruskal-Szekeres extension is a member of this family. It is a different family from the Novikov-Lemaître family, which does not have as its member the Kruskal-Szekeres extension, and moreover the $E \geq 1$ Lemaître extension is not maximal. It is certainly opportune to incorporate into a family of maximal E extensions of the Schwarzschild metric, the maximal extension of Kruskal and Szekeres in the year we celebrate its 60 years.

The paper is organized as follows. In Sec. II, we give the Schwarzschild metric in double Painlevé-Gullstrand coordinates for $E > 1$. In Sec. III, we extend the Schwarzschild metric for $E > 1$ past the

$r=2M$ coordinate singularity using analytical extended coordinates, and produce its maximal analytical extension. In Sec. IV, we give the $E=1$ maximal analytical extension as the limit from $E>1$. In Sec. V, we give the $E=\infty$ maximal analytical extension as the limit from $E>1$ and show that it is the Kruskal-Szekeres maximal extension. In Sec. VI, we present the causal structure of the maximal extended spacetime for several E, from $E=1$ to $E=\infty$. In Sec. VII, we conclude. In the Appendix, we show in detail the limits $E=1$ and $E=\infty$ directly from the $E>1$ generic case.

II. The Schwarzschild solution in double Painlevé-Gullstrand form

The vacuum Einstein equation $G_{ab}=0$, where G_{ab} is the Einstein tensor and a,b are spacetime indices, give for a line element $ds^2=g_{ab}(x^a)dx^a dx^b$, where $g_{ab}(x^a)$ is the metric and x^a are the coordinates, in the classical standard spherical symmetric coordinates (t,r,θ,ϕ) the Schwarzschild solution, namely,

$$\mathrm{d}s^2=-\left(1-\frac{2M}{r}\right)\mathrm{d}t^2+\frac{dr^2}{1-\frac{2M}{r}}+r^2(\mathrm{d}\theta^2+\sin^2\theta\,\mathrm{d}\phi^2)\,, \tag{1}$$

where M is the spacetime mass. We assume $M\geq 0$ and $r\geq 0$. In this form the line element, and so the metric, is singular at the, Schwarzschild, gravitational, or event horizon radius $r=2M$, and at $r=0$. For $r>2M$, the Schwarzschild coordinate t is timelike and the coordinate r is spacelike, a radial coordinate. For $r<2M$, these coordinates swap roles, the Schwarzschild coordinate t is spacelike and the coordinate r is timelike.

We now apply a first coordinate transformation such that the Schwarzschild time t in Eq. (1) goes into a new time $\mathscr{t}=\mathscr{t}(t,r)$ given in differential form by

$$\mathrm{d}\mathscr{t}=E\mathrm{d}t-\frac{\left(E^2-1+\frac{2M}{r}\right)^{1/2}}{1-\frac{2M}{r}}\mathrm{d}r\,, \tag{2}$$

with $E\geq 1$, E being a parameter. This is a Painlevé-Gullstrand coordinate transformation for the congruence of outgoing radial timelike geodesics with energy E. We can also perform a different coordinate transformation, such that the Schwarzschild time t in Eq. (1) goes into a new time $\tau=\tau(t,r)$ given in differential form by

$$\mathrm{d}\tau=E\mathrm{d}t+\frac{\left(E^2-1+\frac{2M}{r}\right)^{1/2}}{1-\frac{2M}{r}}\mathrm{d}r\,. \tag{3}$$

with $E\geq 1$, E being the same parameter as above. This is a Painlevé-Gullstrand coordinate transformation for the congruence of ingoing radial timelike geodesics with energy E. The two transformations together, $\mathscr{t}=\mathscr{t}(t,r)$ and $\tau=\tau(t,r)$, Eqs. (2) and (3), respectively, can then be seen as a transformation from the Schwarzschild time and radius (t,r) to the two new coordinates $(\mathscr{t},\tau)$. The inverse transformations, from $(\mathscr{t},\tau)$ to (t,r), in differential form are

$$E\mathrm{d}t=\frac{1}{2}\left(\,\mathrm{d}\mathscr{t}+\mathrm{d}\tau\right)\,, \tag{4}$$

$$\frac{\left(E^2-1+\frac{2M}{r}\right)^{1/2}}{\left(1-\frac{2M}{r}\right)}\mathrm{d}r=\frac{1}{2}\left(-\mathrm{d}t+\mathrm{d}\tau\right)\,. \tag{5}$$

Applying the coordinate transformation given in Eq. (2) to the Schwarzschild line element, Eq. (1), gives the line element in Painlevé-Gullstrand outgoing coordinates with energy parameter $E \geq 1$, namely, $\mathrm{d}s^2 = -\frac{1}{E^2}\left(1-\frac{2M}{r}\right)\mathrm{d}t^2 - -2\frac{1}{E^2}\sqrt{E^2-1+\frac{2M}{r}}\mathrm{d}t\,\mathrm{d}r + \frac{1}{E^2}\mathrm{d}r^2 + r^2(\mathrm{d}\theta^2+\sin^2\theta\,\mathrm{d}\phi^2)$. This form of the metric is not singular anymore at $r = 2M$, but there is still the singularity at $r = 0$ which cannot be removed. Note that inside $r = 2M$ this Painlevé-Gullstrand form has the feature of having two time coordinates, t and r. Applying the coordinate transformation given in Eq. (3) to the Schwarzschild metric, Eq. (1), gives the metric in Painlevé-Gullstrand ingoing coordinates with energy parameter $E \geq 1$, namely, $\mathrm{d}s^2 = -\frac{1}{E^2}\left(1-\frac{2M}{r}\right)\mathrm{d}\tau^2 + 2\frac{1}{E^2}\sqrt{E^2-1+\frac{2M}{r}}\mathrm{d}\tau\,\mathrm{d}r + \frac{1}{E^2}\mathrm{d}r^2 + r^2(\mathrm{d}\theta^2+\sin^2\theta\,\mathrm{d}\phi^2)$. This form of the metric is also not singular anymore at $r = 2M$, but there is still the singularity at $r = 0$ which cannot be removed. Note that inside $r = 2M$ this Painlevé-Gullstrand form has the feature of having two time coordinates, τ and r. All of this is well known.

We now apply a simultaneous coordinate transformation, given through Eqs. (2)-(3), or if one prefers Eqs. (4)-(5), to the Schwarzschild metric, Eq. (1), to get

$$\begin{aligned}\mathrm{d}s^2 = -\frac{1}{4E^2}\frac{1-\frac{2M}{r}}{E^2-1+\frac{2M}{r}}\left[-\left(1-\frac{2M}{r}\right)(\mathrm{d}t^2+\mathrm{d}\tau^2)+2\left(2E^2-1+\frac{2M}{r}\right)\mathrm{d}t\,\mathrm{d}\tau\right]+\\ +r^2(t,\tau)(\mathrm{d}\theta^2+\sin^2\theta\,\mathrm{d}\phi^2)\,,\end{aligned} \tag{6}$$

with $r(t,\tau)$ obtained via Eq. (5) and depends on whether $E = 1$ or $E > 1$. This is the Schwarzschild metric in double Painlevé-Gullstrand coordinates.

The line element of Eq. (6) is still degenerate for $r = 2M$. So, if we want to extend it past this sphere we have to perform another set of coordinate transformations. This set is given by $\frac{t'}{M} = = -\exp\left(-\frac{t}{4ME}\right)$ and $\frac{\tau'}{M} = \exp\left(\frac{\tau}{4ME}\right)$. When applied to Eq. (9), it gives, $\mathrm{d}s^2 = 4M^2\frac{1-\frac{2M}{r}}{E^2-1+\frac{2M}{r}} \times \times\left[\left(1-\frac{2M}{r}\right)\left(\frac{\mathrm{d}t'^2}{t'^2}+\frac{\mathrm{d}\tau'^2}{\tau'^2}\right)+2\left(2E^2-1+\frac{2M}{r}\right)\frac{\mathrm{d}t'}{t'}\frac{\mathrm{d}\tau'}{\tau'}\right]+r^2(t',\tau')(\mathrm{d}\theta^2+\sin^2\theta\,\mathrm{d}\phi^2)$, with $r(t',\tau')$ a function that is given implicitly. The form of this metric will depend on the value of E through the solution to the differential coordinate relations, Eqs. (2) and (3), or equivalently, Eqs. (4)-(5). Clearly, the case $E < 1$ cannot be treated from the formulas above and we have dismissed it from the start. Therefore we restrict the analysis to $1 \leq E < \infty$. The $E = 1$ and $E = \infty$ can be seen as limiting cases of the generic $E > 1$ case. Let us do the $E > 1$ case in detail and then treat $E = 1$ and $E = \infty$ as the inferior and superior limiting cases, respectively, of $E > 1$.

III. Maximal analytic extension for $E > 1$ as generic case

To start building the maximal analytic extension for $E > 1$, we find the solutions to the new coordinates $\not{t}$ and τ from Eqs. (2) and (3). When $E > 1$ they are

$$\begin{aligned} \not{t} = {} & Et - r\sqrt{E^2 - 1 + \frac{2M}{r}} - 2ME\ln\left|\frac{2M}{r}\left(\frac{\frac{r}{2M} - 1}{2E^2 - 1 + \frac{2M}{r} + 2E\sqrt{E^2 - 1 + \frac{2M}{r}}}\right)\right| - \\ & - M\frac{2E^2 - 1}{\sqrt{E^2 - 1}}\ln\left[\frac{r}{M}\left(\sqrt{E^2 - 1}\sqrt{E^2 - 1 + \frac{2M}{r}} + E^2 - 1 + \frac{M}{r}\right)\right], \end{aligned} \tag{7}$$

$$\begin{aligned} \tau = {} & Et + r\sqrt{E^2 - 1 + \frac{2M}{r}} + 2ME\ln\left|\frac{2M}{r}\left(\frac{\frac{r}{2M} - 1}{2E^2 - 1 + \frac{2M}{r} + 2E\sqrt{E^2 - 1 + \frac{2M}{r}}}\right)\right| + \\ & + M\frac{2E^2 - 1}{\sqrt{E^2 - 1}}\ln\left[\frac{r}{M}\left(\sqrt{E^2 - 1}\sqrt{E^2 - 1 + \frac{2M}{r}} + E^2 - 1 + \frac{M}{r}\right)\right]. \end{aligned} \tag{8}$$

The line element to start with is

$$\begin{aligned} \mathrm{d}s^2 = {} & -\frac{1}{4E^2}\frac{1 - \frac{2M}{r}}{E^2 - 1 + \frac{2M}{r}}\left[-\left(1 - \frac{2M}{r}\right)(\mathrm{d}\not{t}^2 + \mathrm{d}\tau^2) + 2\left(2E^2 - 1 + \frac{2M}{r}\right)\mathrm{d}\not{t}\,\mathrm{d}\tau\right] + \\ & + r^2(\mathrm{d}\theta^2 + \sin^2\theta\,\mathrm{d}\phi^2), \end{aligned} \tag{9}$$

which is taken from Eq. (6), now bearing in mind that $E > 1$ implicitly here, and with $r = r(\not{t}, \tau)$ being obtained via Eqs. (7) and (8), i.e.,

$$\begin{aligned} & r\sqrt{E^2 - 1 + \frac{2M}{r}} + 2ME\ln\left|\frac{2M}{r}\left(\frac{\frac{r}{2M} - 1}{2E^2 - 1 + \frac{2M}{r} + 2E\sqrt{E^2 - 1 + \frac{2M}{r}}}\right)\right| + \\ & \qquad M\frac{2E^2 - 1}{\sqrt{E^2 - 1}}\ln\left[\frac{r}{M}\left(\sqrt{E^2 - 1}\sqrt{E^2 - 1 + \frac{2M}{r}} + E^2 - 1 + \frac{M}{r}\right)\right] = \tfrac{1}{2}\left(-\not{t} + \tau\right). \end{aligned} \tag{10}$$

The line element Eq. (9) is still degenerate at $r = 2M$. So, if we want to extend past it we have to do something. To remove this behavior, we proceed with two new coordinate transformations given by $\frac{\not{t}'}{M} = -\exp\left(-\frac{\not{t}}{4ME}\right)$ and $\frac{\tau'}{M} = \exp\left(\frac{\tau}{4ME}\right)$, for $r > 2M$. Then, using Eqs. (7) and (8) the maximal extended coordinates t' and τ' are

$$\begin{aligned}
\frac{t'}{M} &= -\exp\left(-\frac{t}{4ME}\right), \quad \text{i.e.,} \\
\frac{t'}{M} &= -\sqrt{\frac{2M}{r}}\frac{\sqrt{\frac{r}{2M}-1}}{\sqrt{2E^2-1+\frac{2M}{r}+2E\sqrt{E^2-1+\frac{2M}{r}}}}\exp\left(-\frac{t}{4M}+\frac{r}{4ME}\sqrt{E^2-1+\frac{2M}{r}}\right)\times \\
&\quad\times\left[\frac{r}{M}\left(\sqrt{E^2-1}\sqrt{E^2-1+\frac{2M}{r}}+E^2-1+\frac{M}{r}\right)\right]^{\frac{2E^2-1}{4E\sqrt{E^2-1}}},
\end{aligned} \tag{11}$$

$$\begin{aligned}
\frac{\tau'}{M} &= \exp\left(\frac{\tau}{4ME}\right), \quad \text{i.e.,} \\
\frac{\tau'}{M} &= \sqrt{\frac{2M}{r}}\frac{\sqrt{\frac{r}{2M}-1}}{\sqrt{2E^2-1+\frac{2M}{r}+2E\sqrt{E^2-1+\frac{2M}{r}}}}\exp\left(\frac{t}{4M}+\frac{r}{4ME}\sqrt{E^2-1+\frac{2M}{r}}\right)\times \\
&\quad\times\left[\frac{r}{M}\left(\sqrt{E^2-1}\sqrt{E^2-1+\frac{2M}{r}}+E^2-1+\frac{M}{r}\right)\right]^{\frac{2E^2-1}{4E\sqrt{E^2-1}}},
\end{aligned} \tag{12}$$

respectively. Putting t' and τ' given in Eqs. (11) and (12), respectively, into the line element Eq. (9), one finds the new line element in coordinates $(t', \tau', \theta, \phi)$ given by

$$\begin{aligned}
\mathrm{d}s^2 = &-4\left(\frac{2E^2-1+\frac{2M}{r}+2E\sqrt{E^2-1+\frac{2M}{r}}}{E^2-1+\frac{2M}{r}}\right)\exp\left(-\frac{r}{2ME}\sqrt{E^2-1+\frac{2M}{r}}\right)\times \\
&\times\left(\frac{M}{r}\frac{1}{E^2-1+\frac{M}{r}+\sqrt{E^2-1}\sqrt{E^2-1+\frac{2M}{r}}}\right)^{\frac{2E^2-1}{2E\sqrt{E^2-1}}}\times \\
&\times\left[-\frac{1}{M^2}\left(2E^2-1+\frac{2M}{r}+2E\sqrt{E^2-1+\frac{2M}{r}}\right)\exp\left(-\frac{r}{2ME}\sqrt{E^2-1+\frac{2M}{r}}\right)\times\right. \\
&\times\left(\frac{M}{r}\frac{1}{E^2-1+\frac{M}{r}+\sqrt{E^2-1}\sqrt{E^2-1+\frac{2M}{r}}}\right)^{\frac{2E^2-1}{2E\sqrt{E^2-1}}}(\tau'^2\mathrm{d}t'^2+t'^2\mathrm{d}\tau'^2)+ \\
&\left.+2\left(2E^2-1+\frac{2M}{r}\right)\mathrm{d}t'\mathrm{d}\tau'\right]+r^2(\mathrm{d}\theta^2+\sin^2\theta\,\mathrm{d}\phi^2),
\end{aligned} \tag{13}$$

where $r = r(t', \tau')$ is defined implicitly as a function of t' and τ' through

$$\begin{aligned}
&\left(\frac{\frac{r}{2M}-1}{2E^2-1+\frac{2M}{r}+2E\sqrt{E^2-1+\frac{2M}{r}}}\right)\frac{2M}{r}\exp\left(\frac{r}{2ME}\sqrt{E^2-1+\frac{2M}{r}}\right)\times \\
&\times\left[\frac{r}{M}\left(E^2-1+\frac{M}{r}+\sqrt{E^2-1}\sqrt{E^2-1+\frac{2M}{r}}\right)\right]^{\frac{2E^2-1}{2E\sqrt{E^2-1}}} = -\frac{t'}{M}\frac{\tau'}{M}.
\end{aligned} \tag{14}$$

All of this is done so that t' and τ' have ranges $-\infty < t' < \infty$ and $-\infty < \tau' < \infty$, which Eqs. (13) and (14) permit. Several properties are now worth mentioning.

In terms of the coordinates (t, τ), or (t, r), the coordinate transformations that yield the maximal extended coordinates (t',τ') with infinite ranges have to be broadened, resulting in the existence of four regions, regions I, II, III, and IV. Region I is the region where the transformations Eqs. (11) and (12) hold, i.e., it is a region with $t' \leq 0$ and $\tau' \geq 0$. It is a region with $r \geq 2M$ and $-\infty < t < \infty$. Of course, in this region Eqs. (13) and (14) hold. Region II, a region for which $r \leq 2M$, gets a different set of coordinate transformations. In this $r \leq 2M$ region, due to the moduli appearing in Eqs. (7) and (8) and the change of sign in Eq. (9), one defines instead t' as $\frac{t'}{M} = +\exp\left(-\frac{t}{4ME}\right) =$ $= \sqrt{\frac{2M}{r}}\frac{\sqrt{1-\frac{r}{2M}}}{\sqrt{2E^2-1+\frac{2M}{r}+2E\sqrt{E^2-1+\frac{2M}{r}}}}\exp\left(-\frac{t}{4M}+\frac{r}{4ME}\sqrt{E^2-1+\frac{2M}{r}}\right)\left[\frac{r}{M}\left(\sqrt{E^2-1}\sqrt{E^2-1+\frac{2M}{r}}+\right.\right.$ $\left.\left.+E^2-1+\frac{M}{r}\right)\right]^{\frac{2E^2-1}{4E\sqrt{E^2-1}}}$ and τ' as $\frac{\tau'}{M} = \exp\left(\frac{\tau}{4ME}\right) = \sqrt{\frac{2M}{r}}\frac{\sqrt{1-\frac{r}{2M}}}{\sqrt{2E^2-1+\frac{2M}{r}+2E\sqrt{E^2-1+\frac{2M}{r}}}}\exp\left(\frac{t}{4M}+\right.$ $\left.+\frac{r}{4ME}\sqrt{E^2-1+\frac{2M}{r}}\right)\left[\frac{r}{M}\left(\sqrt{E^2-1}\sqrt{E^2-1+\frac{2M}{r}}+E^2-1+\frac{M}{r}\right)\right]^{\frac{2E^2-1}{4E\sqrt{E^2-1}}}$. These transformations are valid for $t' \geq 0$ and $\tau' \geq 0$. It is a region with $r \leq 2M$ and $-\infty < t < \infty$. Note that the coordinate transformations in this region give $\left(\frac{1-\frac{r}{2M}}{2E^2-1+\frac{2M}{r}+2E\sqrt{E^2-1+\frac{2M}{r}}}\right)\frac{2M}{r}\exp\left(\frac{r}{2ME}\sqrt{E^2-1+\frac{2M}{r}}\right)\left[\frac{r}{M}\left(E^2-\right.\right.$ $\left.\left.-1+\frac{M}{r}+\sqrt{E^2-1}\sqrt{E^2-1+\frac{2M}{r}}\right)\right]^{\frac{2E^2-1}{2E\sqrt{E^2-1}}} = \frac{t'}{M}\frac{\tau'}{M}$. But all this has been automatically incorporated into Eqs. (13) and (14) so there is no further concern on that. Region III is another $r \geq 2M$ region. Now one defines t' as $\frac{t'}{M} = \exp\left(-\frac{t}{4ME}\right) = \sqrt{\frac{2M}{r}}\frac{\sqrt{\frac{r}{2M}-1}}{\sqrt{2E^2-1+\frac{2M}{r}+2E\sqrt{E^2-1+\frac{2M}{r}}}}\exp\left(-\frac{t}{4M}+\frac{r}{4ME}\times\right.$ $\left.\times\sqrt{E^2-1+\frac{2M}{r}}\right)\left[\frac{r}{M}\left(\sqrt{E^2-1}\sqrt{E^2-1+\frac{2M}{r}}+E^2-1+\frac{M}{r}\right)\right]^{\frac{2E^2-1}{4E\sqrt{E^2-1}}}$ and τ' as $\frac{\tau'}{M} = -\exp\left(\frac{\tau}{4ME}\right) =$

$= -\sqrt{\frac{2M}{r}}\frac{\sqrt{\frac{r}{2M}-1}}{\sqrt{2E^2-1+\frac{2M}{r}+2E\sqrt{E^2-1+\frac{2M}{r}}}}\exp\left(\frac{t}{4M}+\frac{r}{4ME}\sqrt{E^2-1+\frac{2M}{r}}\right)\left[\frac{r}{M}\left(\sqrt{E^2-1}\sqrt{E^2-1+\frac{2M}{r}}+E^2-\right.\right.$ $\left.\left.-1+\frac{M}{r}\right)\right]^{\frac{2E^2-1}{4E\sqrt{E^2-1}}}$. These transformations are valid for the region with $t' \geq 0$ and $\tau' \leq 0$. It is a region with $r \geq 2M$ and $-\infty < t < \infty$. Note that the coordinate transformations in this region give $\left(\frac{\frac{r}{2M}-1}{2E^2-1+\frac{2M}{r}+2E\sqrt{E^2-1+\frac{2M}{r}}}\right)\frac{2M}{r}\exp\left(\frac{r}{2ME}\sqrt{E^2-1+\frac{2M}{r}}\right)\left[\frac{r}{M}\left(\sqrt{E^2-1}\sqrt{E^2-1+\frac{2M}{r}}+E^2-1+\right.\right.$ $\left.\left.+\frac{M}{r}\right)\right]^{\frac{2E^2-1}{2E\sqrt{E^2-1}}} = -\frac{t'}{M}\frac{\tau'}{M}$. But all this has been automatically incorporated into Eqs. (13) and (14) so again there is no further concern on that. Region IV is another region with $r \leq 2M$. Now, one defines t' as $\frac{t'}{M} = -\exp\left(-\frac{t}{4ME}\right) = -\sqrt{\frac{2M}{r}}\frac{\sqrt{1-\frac{r}{2M}}}{\sqrt{2E^2-1+\frac{2M}{r}+2E\sqrt{E^2-1+\frac{2M}{r}}}}\exp\left(-\frac{t}{4M}+\frac{r}{4ME}\sqrt{E^2-1+\frac{2M}{r}}\right)\left[\frac{r}{M}\times\right.$ $\left.\times\left(\sqrt{E^2-1}\sqrt{E^2-1+\frac{2M}{r}}+E^2-1+\frac{M}{r}\right)\right]^{\frac{2E^2-1}{4E\sqrt{E^2-1}}}$ and τ' as $\frac{\tau'}{M} = -\exp\left(\frac{\tau}{4ME}\right) = -\sqrt{\frac{2M}{r}}\times$ $\times\frac{\sqrt{1-\frac{r}{2M}}}{\sqrt{2E^2-1+\frac{2M}{r}+2E\sqrt{E^2-1+\frac{2M}{r}}}}\exp\left(\frac{t}{4M}+\frac{r}{4ME}\sqrt{E^2-1+\frac{2M}{r}}\right)\left[\frac{r}{M}\left(\sqrt{E^2-1}\sqrt{E^2-1+\frac{2M}{r}}+E^2-1+\right.\right.$ $\left.\left.+\frac{M}{r}\right)\right]^{\frac{2E^2-1}{4E\sqrt{E^2-1}}}$. These transformations are valid for the region with $t' \leq 0$ and $\tau' \leq 0$. It is a region with $r \leq 2M$ and $-\infty < t < \infty$. Note that the coordinate transformations in this region give $\left(\frac{1-\frac{r}{2M}}{2E^2-1+\frac{2M}{r}+2E\sqrt{E^2-1+\frac{2M}{r}}}\right)\frac{2M}{r}\exp\left(\frac{r}{2ME}\sqrt{E^2-1+\frac{2M}{r}}\right)\left[\frac{r}{M}\left(\sqrt{E^2-1}\sqrt{E^2-1+\frac{2M}{r}}+E^2-1+\right.\right.$ $\left.\left.+\frac{M}{r}\right)\right]^{\frac{2E^2-1}{2E\sqrt{E^2-1}}} = \frac{t'}{M}\frac{\tau'}{M}$. But all this has been automatically incorporated into Eqs. (13) and (14) so once again there is no further concern on that.

Furthermore, from Eq. (14) we see that the event horizon at $r = 2M$ has two solutions, $t' = 0$ and $\tau' = 0$ which are null surfaces represented by straight lines. The true curvature singularity at $r = 0$ has two solutions $\frac{t'}{M}\frac{\tau'}{M} = 1$, i.e., two spacelike hyperbolae. Implicit in the construction, there is a wormhole, or Einstein-Rosen bridge, topology, with its throat expanding and contracting. The dynamic wormhole is non traversable, but it spatially connects region I to region III through regions II and IV. Regions I and III are two asympotically flat regions causally separated, region II is the black hole region, and region IV is the white hole region of the spacetime.

Eqs. (13) and (14) together with the corresponding interpretation give the maximal extension of the Schwarzschild metric for $E > 1$, in the coordinates $(t', \tau', \theta, \phi)$. Since $1 < E < \infty$ this is a family of extensions, characterized by one parameter, the parameter E. It is a one-parameter family of extensions. The two-dimensional part (t', τ') of the coordinate system $(t', \tau', \theta, \phi)$ is shown in Figure 1, both for lines of constant t' and constant τ' in part (a) of the figure, and for lines of constant t and constant r in part (b) of the figure, conjointly with the labeling of regions I, II, III, IV, needed to cover it.

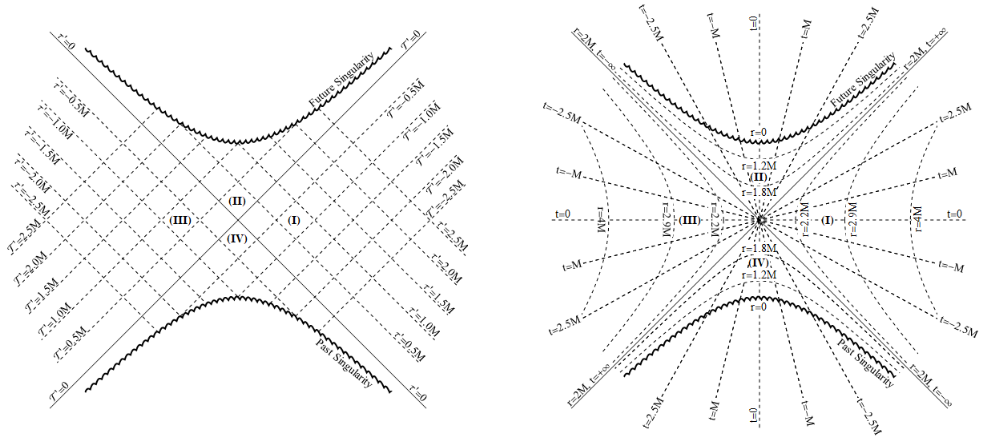

(a) (b)

Figure 1: The maximal analytical extension of the Schwarzschild metric for the parameter E generic obeying $E > 1$ in the plane (t', τ') is shown in a diagram with two different descriptions, (a) and (b). In (a) typical values for lines of constant t' and constant τ' are displayed. In (b) typical values for lines of constant t and constant r are displayed. The diagram, both in (a) and in (b), represents a a spacetime with a wormhole, not shown, that forms out of a singularity in the white hole region, i.e., region IV, and finishes at the black hole region and its singularity, i.e., region II, connecting the two separated asymptotically flat spacetimes, regions I and III.

It is also worth discussing the normals to the $t' = \text{constant}$ and $\tau' = \text{constant}$ hypersurfaces. From Eq. (13) one finds that the covariant metric has components $g_{t't'} = \frac{4}{M^2}\left(\frac{\left(2E^2-1+\frac{2M}{r}+2E\sqrt{E^2-1+\frac{2M}{r}}\right)^2}{E^2-1+\frac{2M}{r}}\right)\times$ $\times \exp\left(-\frac{r}{ME}\sqrt{E^2-1+\frac{2M}{r}}\right)\left(\frac{\frac{M}{r}}{E^2-1+\frac{M}{r}+\sqrt{E^2-1}\sqrt{E^2-1+\frac{2M}{r}}}\right)^{\frac{2E^2-1}{E\sqrt{E^2-1}}}\tau'^2$, $g_{\tau'\tau'} = \frac{4}{M^2}\times$ $\times\left(\frac{\left(2E^2-1+\frac{2M}{r}+2E\sqrt{E^2-1+\frac{2M}{r}}\right)^2}{E^2-1+\frac{2M}{r}}\right)\exp\left(-\frac{r}{ME}\sqrt{E^2-1+\frac{2M}{r}}\right)\left(\frac{\frac{M}{r}}{E^2-1+\frac{M}{r}+\sqrt{E^2-1}\sqrt{E^2-1+\frac{2M}{r}}}\right)^{\frac{2E^2-1}{E\sqrt{E^2-1}}} t'^2$, $g_{t'\tau'} = g_{\tau't'} = -4\left(\frac{2E^2-1+\frac{2M}{r}+2E\sqrt{E^2-1+\frac{2M}{r}}}{E^2-1+\frac{2M}{r}}\right)\left(2E^2-1+\frac{2M}{r}\right)\exp\left(-\frac{r}{2ME}\sqrt{E^2-1+\frac{2M}{r}}\right)\times$ $\times\left(\frac{\frac{M}{r}}{E^2-1+\frac{M}{r}+\sqrt{E^2-1}\sqrt{E^2-1+\frac{2M}{r}}}\right)^{\frac{2E^2-1}{2E\sqrt{E^2-1}}}$, $g_{\theta\theta} = r^2$, $g_{\phi\phi} = r^2\sin^2\theta$. The contravariant components of the metric can be calculated to be $g^{t't'} = -\frac{t'^2}{16M^2E^2}$, $g^{\tau'\tau'} = -\frac{\tau'^2}{16M^2E^2}$, $g^{t'\tau'} = g^{\tau't'} = -\frac{1}{16E^2}\times$ $\times\frac{1}{2E^2-1+\frac{2M}{r}+2E\sqrt{E^2-1+\frac{2M}{r}}}\left(2E^2-1+\frac{2M}{r}\right)\left[\frac{r}{M}\left(E^2-1+\frac{M}{r}+\sqrt{E^2-1}\sqrt{E^2-1+\frac{2M}{r}}\right)\right]^{\frac{2E^2-1}{2E\sqrt{E^2-1}}}\times$ $\times\exp\left(\frac{r}{2ME}\sqrt{E^2-1+\frac{2M}{r}}\right)$, $g^{\theta\theta} = \frac{1}{r^2}$, $g^{\phi\phi} = \frac{1}{r^2\sin^2\theta}$. The normals n_a to the $t' = \text{constant}$ and

$\tau' = \text{constant}$ hypersurfaces are $n^{\mathscr{t}'}{}_a = (1,0,0,0)$ and $n^{\tau'}{}_a = (0,1,0,0)$, respectively, where the superscripts $\mathscr{t}'$ and τ' in this context are not indices, they simply label the respective normal. Their contravariant components are, respectively, $n^{\mathscr{t}'a} = (g^{\mathscr{t}'\mathscr{t}'}, g^{\mathscr{t}'\tau'}, 0, 0)$ and $n^{\tau'a} = (g^{\tau'\mathscr{t}'}, g^{\tau'\tau'}, 0, 0)$, awkward writing them explicitly due to the long expression for $g^{\mathscr{t}'\tau'}$. The norms are then $n^{\mathscr{t}'}{}_a n^{\mathscr{t}'a} = -\frac{\mathscr{t}'^2}{16M^2E^2}$ and $n^{\tau'}{}_a n^{\tau'a} = -\frac{\tau'^2}{16M^2E^2}$, respectively. Thus, clearly, the normals to the $\mathscr{t}' = \text{constant}$ and $\tau' = \text{constant}$ hypersurfaces are timelike, and so $\mathscr{t}'$ and τ' are timelike coordinates, and the corresponding hypersurfaces are spacelike, only in a measure zero are they null, when $\mathscr{t}' = 0$ and $\tau' = 0$, respectively.

IV. Maximal analytic extension for $E = 1$, the lower limit of $E > 1$

To build the maximal analytic extension for $E = 1$, we take the $E \to 1$ limit from the $E > 1$ case. Using $\ln\left[\left(2\sqrt{E^2-1}\sqrt{\frac{r}{2M}}\right)+1\right] = 2\sqrt{E^2-1}\sqrt{\frac{r}{2M}}$ in this limit, we find that the coordinates $\mathscr{t}$ and τ of Eqs. (7) and (8) become

$$\mathscr{t} = t - 4M\sqrt{\frac{r}{2M}} + 2M\ln\left|\frac{\sqrt{\frac{r}{2M}}+1}{\sqrt{\frac{r}{2M}}-1}\right|, \tag{15}$$

$$\tau = t + 4M\sqrt{\frac{r}{2M}} - 2M\ln\left|\frac{\sqrt{\frac{r}{2M}}+1}{\sqrt{\frac{r}{2M}}-1}\right|. \tag{16}$$

The line element given in Eq. (9) is then in this $E = 1$ limit given by

$$\mathrm{d}s^2 = -\frac{1}{4}\frac{\left(1-\frac{2M}{r}\right)}{\frac{2M}{r}}\left[-\left(1-\frac{2M}{r}\right)(\mathrm{d}\mathscr{t}^2+\mathrm{d}\tau^2) + 2\left(1+\frac{2M}{r}\right)\mathrm{d}\mathscr{t}\,\mathrm{d}\tau\right] + r^2(\mathrm{d}\theta^2+\sin^2\theta\,\mathrm{d}\phi^2)\,, \tag{17}$$

with $r = r(\mathscr{t},\tau)$ being obtained via Eq. (10) in the $E = 1$ limit, or through Eqs. (15) and (16), i.e.,

$$4M\sqrt{\frac{r}{2M}} - 2M\ln\left|\frac{\sqrt{\frac{r}{2M}}+1}{\sqrt{\frac{r}{2M}}-1}\right| = \frac{1}{2}\left(-\mathscr{t}+\tau\right)\,. \tag{18}$$

Again, as in Eq. (9), the line element given in Eq. (17) is still degenerate at $r = 2M$. So, to extend it past $r = 2M$ we again make use of maximal extended coordinates, $\mathscr{t}'$ and τ', defined as $\frac{\mathscr{t}'}{M} = -\exp\left(-\frac{\mathscr{t}}{4M}\right)$ and $\frac{\tau'}{M} = \exp\left(\frac{\tau}{4M}\right)$, which by either taking directly the limit $E = 1$ in Eqs. (11) and (12), respectively, or using Eqs. (15) and (16), yields for $r > 2M$,

$$\frac{\mathscr{t}'}{M} = -\exp\left(-\frac{\mathscr{t}}{4M}\right), \quad \text{i.e.,} \quad \frac{\mathscr{t}'}{M} = -\sqrt{\frac{\sqrt{\frac{r}{2M}}-1}{\sqrt{\frac{r}{2M}}+1}}\exp\left(-\frac{t}{4M}+\sqrt{\frac{r}{2M}}\right), \tag{19}$$

$$\frac{\tau'}{M} = \exp\left(\frac{\tau}{4M}\right), \quad \text{i.e.,} \quad \frac{\tau'}{M} = \sqrt{\frac{\sqrt{\frac{r}{2M}}-1}{\sqrt{\frac{r}{2M}}+1}}\exp\left(\frac{t}{4M}+\sqrt{\frac{r}{2M}}\right), \tag{20}$$

respectively. Through the $E = 1$ limit of Eq. (13), or putting $\mathscr{t}'$ and τ' given in Eqs. (19) and (20), respectively, into the line element Eq. (17), one finds that the new $E = 1$ line element in coordinates

$(\mathscr{t}', \tau', \theta, \phi)$ is given by

$$\mathrm{d}s^2 = -\,4\frac{\left(1+\sqrt{\frac{2M}{r}}\right)^2}{\frac{2M}{r}} \exp\left(-2\sqrt{\frac{r}{2M}}\right)\left[-\frac{1}{M^2}\left(1+\sqrt{\frac{2M}{r}}\right)^2 \exp\left(-2\sqrt{\frac{r}{2M}}\right)(\tau'^2\,\mathrm{d}\mathscr{t}'^2 + \mathscr{t}'^2\,\mathrm{d}\tau'^2) + \right.$$
$$\left. +2\left(1+\frac{2M}{r}\right)\mathrm{d}\mathscr{t}'\,\mathrm{d}\tau'\right] + r^2(\mathrm{d}\theta^2 + \sin^2\theta\,\mathrm{d}\phi^2)\,, \tag{21}$$

with $r = r(\mathscr{t}', \tau')$ given implicitly, see Eq. (14) in the $E = 1$ limit, or directly through Eqs. (19) and (20), by

$$\frac{\sqrt{\frac{r}{2M}}-1}{\sqrt{\frac{r}{2M}}+1}\exp\left(2\sqrt{\frac{r}{2M}}\right) = -\frac{\mathscr{t}'}{M}\frac{\tau'}{M}\,. \tag{22}$$

All of this is done so that $\mathscr{t}'$ and τ' have ranges $-\infty < \mathscr{t}' < \infty$ and $-\infty < \tau' < \infty$, which Eqs. (21) and (22) permit. To obtain Eqs. (21) and (22) directly from the $E \to 1$ limit of Eqs. (13) and (14), respectively, see the Appendix. Several properties are again worth mentioning.

In terms of the coordinates $(\mathscr{t}, \tau)$, or (t, r), the coordinate transformations that yield the maximal extended coordinates $(\mathscr{t}', \tau')$ with infinite ranges have to be broadened, resulting in the existence of four regions, regions I, II, III, and IV. Region I is the region where the transformations Eqs. (19) and (20) hold, i.e., it is a region with $\mathscr{t}' \leq 0$ and $\tau' \geq 0$. It is a region with $r \geq 2M$ and $-\infty < t < \infty$. Of course, in this region Eqs. (21) and (22) hold. Region II, a region for which $r \leq 2M$, gets a different set of coordinate transformations. In this $r \leq 2M$ region, due to the moduli appearing in Eqs. (19) and (20) and the change of sign in Eq. (17), one defines instead $\mathscr{t}'$ as $\frac{\mathscr{t}'}{M} = +\exp\left(-\frac{\mathscr{t}}{4M}\right) =$ $= +\sqrt{\frac{1-\sqrt{\frac{r}{2M}}}{1+\sqrt{\frac{r}{2M}}}}\exp\left(-\frac{t}{4M}+\sqrt{\frac{r}{2M}}\right)$ and τ' as $\frac{\tau'}{M} = \exp\left(\frac{\tau}{4M}\right) = \sqrt{\frac{1-\sqrt{\frac{r}{2M}}}{1+\sqrt{\frac{r}{2M}}}}\exp\left(\frac{t}{4M}+\sqrt{\frac{r}{2M}}\right)$. These transformations are valid for $\mathscr{t}' \geq 0$ and $\tau' \geq 0$. It is a region with $r \leq 2M$ and $-\infty < t < \infty$. Note that the coordinate transformations in this region give $\frac{1-\sqrt{\frac{r}{2M}}}{1+\sqrt{\frac{r}{2M}}}\exp\left(2\sqrt{\frac{r}{2M}}\right) = \frac{\mathscr{t}'}{M}\frac{\tau'}{M}$ But all this has been automatically incorporated into Eqs. (21) and (22) so there is no further concern on that. Region III is another $r \geq 2M$ region. Now one defines $\mathscr{t}'$ as $\frac{\mathscr{t}'}{M} = \exp\left(-\frac{\mathscr{t}}{4M}\right) = \sqrt{\frac{\sqrt{\frac{r}{2M}}-1}{\sqrt{\frac{r}{2M}}+1}}\exp\left(-\frac{t}{4M}+\sqrt{\frac{r}{2M}}\right)$ and τ' as $\frac{\tau'}{M} = -\exp\left(\frac{\tau}{4M}\right) = -\sqrt{\frac{\sqrt{\frac{r}{2M}}-1}{\sqrt{\frac{r}{2M}}-1}}\exp\left(\frac{t}{4M}+\sqrt{\frac{r}{2M}}\right)$. These transformations are valid for the region with $\mathscr{t}' \geq 0$ and $\tau' \leq 0$. It is a region with $r \geq 2M$ and $-\infty < t < \infty$. Note that the coordinate transformations in this region give $\frac{\sqrt{\frac{r}{2M}}-1}{\sqrt{\frac{r}{2M}}+1}\exp\left(2\sqrt{\frac{r}{2M}}\right) = -\frac{\mathscr{t}'}{M}\frac{\tau'}{M}$ But all this has been automatically incorporated into Eqs. (21) and (22) so again there is no further concern on that. Region IV is another region with $r \leq 2M$. Now, one defines $\mathscr{t}'$ as $\frac{\mathscr{t}'}{M} = -\exp\left(-\frac{\mathscr{t}}{4M}\right) = -\sqrt{\frac{1-\sqrt{\frac{r}{2M}}}{1+\sqrt{\frac{r}{2M}}}}\exp\left(-\frac{t}{4M}+\sqrt{\frac{r}{2M}}\right)$ and τ' as $\frac{\tau'}{M} = -\exp\left(\frac{\tau}{4M}\right) = -\sqrt{\frac{1-\sqrt{\frac{r}{2M}}}{1+\sqrt{\frac{r}{2M}}}}\exp\left(\frac{t}{4M}+\sqrt{\frac{r}{2M}}\right)$. These transformations are valid for the region with $\mathscr{t}' \leq 0$ and $\tau' \leq 0$. It is a region with $r \leq 2M$ and $-\infty < t < \infty$. Note that the coordinate transformations in this region give $\frac{1-\sqrt{\frac{r}{2M}}}{1+\sqrt{\frac{r}{2M}}}\exp\left(2\sqrt{\frac{r}{2M}}\right) = \frac{\mathscr{t}'}{M}\frac{\tau'}{M}$. But all this has been automatically incorporated into Eqs. (21) and (22) so once again there is no further concern on that.

Furthermore, from Eq. (22) we see that the event horizon at $r = 2M$ has two solutions, $\mathscr{t}' = 0$ and $\tau' = 0$ which are null surfaces represented by straight lines. The true curvature singularity at $r = 0$ has two solutions $\frac{\mathscr{t}'}{M}\frac{\tau'}{M} = 1$, i.e., two spacelike hyperbolae. Implicit in the construction, there is a wormhole, or Einstein-Rosen bridge, topology, with its throat expanding and contracting. The dynamic wormhole is non traversable, but it spatially connects region I to region III through regions II and IV. Regions I and III are two asympotically flat regions causally separated, region II is the black hole region, and region IV is the white hole region of the spacetime.

Eqs. (21) and (22) together with the corresponding interpretation give the maximal extension of the Schwarzschild metric for $E = 1$, in the coordinates $(t', \tau', \theta, \phi)$. The two-dimensional part (t', τ') of the coordinate system $(t', \tau', \theta, \phi)$ is shown in Figure 2, both for lines of constant t' and constant τ' in part (a) of the figure, and for lines of constant t and constant r in part (b) of the figure, conjointly with the labeling of regions I, II, III, IV, needed to cover it.

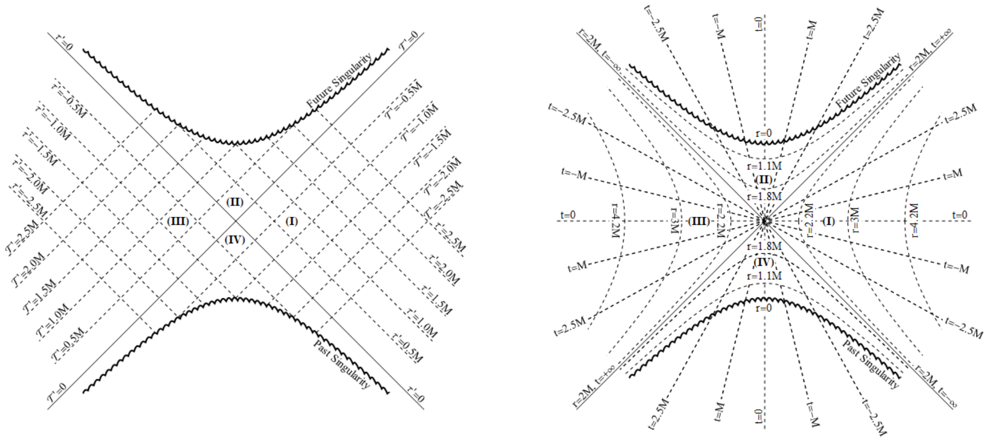

(a) (b)

Figure 2: The maximal analytical extension of the Schwarzschild metric for the parameter $E = 1$ in the plane (t', τ') is shown in a diagram with two different descriptions, (a) and (b). In (a) typical values for lines of constant t' and constant τ' are displayed. In (b) typical values for lines of constant t and constant r are displayed. The diagram, both in (a) and in (b), represents a a spacetime with a wormhole, not shown, that forms out of a singularity in the white hole region, i.e., region IV, and finishes at the black hole region and its singularity, i.e., region II, connecting the two separated asymptotically flat spacetimes, regions I and III. The $E = 1$ diagram is very similar to the $E > 1$ generic case diagram, see Figure 1, as it is expected for a maximal extension of the Schwarzschild spacetime, in particular for those extensions within the same family.

It is also worth discussing the normals to the $t' = \mathrm{constant}$ and $\tau' = \mathrm{constant}$ hypersurfaces. From Eq. (21) one finds that the metric has covariant components $g_{t't'} = \frac{4}{M^2}\frac{\left(1+\sqrt{\frac{2M}{r}}\right)^4}{\frac{2M}{r}}\exp\left(-4\sqrt{\frac{r}{2M}}\right)\tau'^2$, $g_{\tau'\tau'} = \frac{4}{M^2}\frac{\left(1+\sqrt{\frac{2M}{r}}\right)^4}{\frac{2M}{r}}\exp\left(-4\sqrt{\frac{r}{2M}}\right)t'^2$, $g_{t'\tau'} = g_{\tau't'} = -4\frac{\left(1+\sqrt{\frac{2M}{r}}\right)^2}{\frac{2M}{r}}\left(1+\frac{2M}{r}\right)\exp\left(-2\sqrt{\frac{r}{2M}}\right)$, $g_{\theta\theta} = r^2$, $g_{\phi\phi} = r^2\sin^2\theta$. The contravariant components of the metric can be calculated to be $g^{t't'} = -\frac{t'^2}{16M^2}$, $g^{\tau'\tau'} = -\frac{\tau'^2}{16M^2}$, $g^{t'\tau'} = g^{\tau't'} = -\frac{1}{16}\frac{1+\frac{2M}{r}}{\left(1+\sqrt{\frac{2M}{r}}\right)^2}\exp\left(2\sqrt{\frac{r}{2M}}\right)$, $g^{\theta\theta} = \frac{1}{r^2}$, $g^{\phi\phi} = \frac{1}{r^2\sin^2\theta}$. The normals n_a to the $t' = \mathrm{constant}$ and $\tau' = \mathrm{constant}$ hypersurfaces are ${n^{t'}}_a = (1,0,0,0)$ and ${n^{\tau'}}_a = (0,1,0,0)$, respectively, where the superscripts t' and τ' in this context are not indices, they simply label the respective normal. Their contravariant components are $n^{t'a} = (g^{t't'}, g^{t'\tau'}, 0, 0) = (-\frac{t'^2}{16M^2}, -\frac{1}{16}\frac{1+\frac{2M}{r}}{\left(1+\sqrt{\frac{2M}{r}}\right)^2}\exp\left(2\sqrt{\frac{r}{2M}}\right), 0, 0)$ and $n^{\tau'a} = (g^{\tau't'}, g^{\tau'\tau'}, 0, 0) = (-\frac{1}{16}\frac{1+\frac{2M}{r}}{\left(1+\sqrt{\frac{2M}{r}}\right)^2}\exp\left(2\sqrt{\frac{r}{2M}}\right), -\frac{\tau'^2}{16M^2}, 0, 0)$, respectively. The norms are then ${n^{t'}}_a n^{t'a} = -\frac{t'^2}{16M^2}$ and ${n^{\tau'}}_a n^{\tau'a} = -\frac{\tau'^2}{16M^2}$, respectively. Thus, clearly, the normals to the

$t' = \text{constant}$ and $\tau' = \text{constant}$ hypersurfaces are timelike, and so t' and τ' are timelike coordinates, and the corresponding hypersurfaces are spacelike, only in a measure zero are they null, when $t' = 0$ and $\tau' = 0$, respectively. The metric components and the normals can also be found from the $E > 1$ case in the $E = 1$ limit.

V. Maximal analytic extension for $E = \infty$, the upper limit of $E > 1$: The Kruskal-Szekeres maximal extension

To build the maximal analytic extension for $E = \infty$, we take the $E \to \infty$ limit from the $E > 1$ generic case. We will see that this limit is the Kruskal-Szekeres maximal analytic extension. Taking a redefinition of the coordinates τ and t of Eqs. (7) and (8) to coordinates u and v, respectively, we find that these become

$$u \equiv \lim_{E\to\infty} \frac{t}{E}\,, \quad \text{i.e.,} \qquad u = t - r - 2M \ln\left|\frac{r}{2M} - 1\right|\,, \tag{23}$$

$$v \equiv \lim_{E\to\infty} \frac{\tau}{E}\,, \quad \text{i.e.,} \qquad v = t + r + 2M \ln\left|\frac{r}{2M} - 1\right|\,. \tag{24}$$

The line element given in Eq. (9) is then in this limit

$$\mathrm{d}s^2 = -\left(1 - \frac{2M}{r}\right) dudv + r^2(\mathrm{d}\theta^2 + \sin^2\theta\,\mathrm{d}\phi^2)\,. \tag{25}$$

with $r = r(u, v)$ being obtained directly via Eq. (10) in the $E \to \infty$ limit, or through Eqs. (23) and (24), i.e.,

$$r + 2M \ln\left|\frac{r}{2M} - 1\right| = \frac{1}{2}\left(-u + v\right)\,. \tag{26}$$

Again, the line element given in Eq. (25) is still degenerate at $r = 2M$. So, to extend it past $r = 2M$, we make use of the maximal extended timelike coordinates t' and τ' defined through $\frac{t'}{M} == -\exp\left(-\frac{t}{4ME}\right)$ and $\frac{\tau'}{M} = \exp\left(\frac{\tau}{4ME}\right)$, which in this limit $E \to \infty$ are redefined to maximal extended coordinates, u' and v', respectively, obtained directly via Eqs. (11) and (12) in the $E \to \infty$ limit, or using Eqs. (23) and (24), to find

$$u' = \lim_{E\to\infty} t'\,, \ \text{i.e.,} \quad \frac{u'}{M} = -\exp\left(-\frac{u}{4M}\right), \quad \text{i.e.,} \quad \frac{u'}{M} = -\sqrt{\frac{r}{2M} - 1}\,\exp\left(-\frac{t}{4M} + \frac{r}{4M}\right), \tag{27}$$

$$v' = \lim_{E\to\infty} \tau'\,, \ \text{i.e.,} \quad \frac{v'}{M} = \exp\left(\frac{v}{4M}\right), \quad \text{i.e.,} \quad \frac{v'}{M} = \sqrt{\frac{r}{2M} - 1}\,\exp\left(\frac{t}{4M} + \frac{r}{4M}\right). \tag{28}$$

Then, the line element of (13) in the $E \to \infty$ limit, or through Eq. (25) together with Eqs. (27) and (28), yields the new line element

$$\mathrm{d}s^2 = -\frac{32M}{r} \exp\Big(-\frac{r}{2M}\Big) \mathrm{d}u' \, \mathrm{d}v' + r^2(\mathrm{d}\theta^2 + \sin^2\theta \, \mathrm{d}\phi^2)\,, \tag{29}$$

with $r = r(u', v')$ given implicitly, see Eq. (14) in the $E \to \infty$ limit, or directly through Eqs. (27) and (28), by

$$\Big(\frac{r}{2M} - 1\Big) \exp\Big(\frac{r}{2M}\Big) = -\frac{u'}{M}\frac{v'}{M}\,. \tag{30}$$

All of this is done so that u' and v' have ranges $-\infty < u' < \infty$ and $-\infty < v' < \infty$, which Eqs. (29) and (30) permit. To obtain Eqs. (29) and (30) directly from the $E \to \infty$ limit of Eqs. (13) and (14), respectively, see the Appendix. Several properties are worth mentioning.

In terms of the coordinates (u, v), or (t, r), the coordinate transformations that yield the maximal extended null coordinates (u', v') with infinite ranges have to be broadened, resulting in the existence of four regions, regions I, II, III, and IV. Region I is the region where the transformations Eqs. (27) and (28) hold, i.e., it is a region with $u' \leq 0$ and $v' \geq 0$, or a region with $r \geq 2M$ and $-\infty < t < \infty$. Region II, a region for which $r \leq 2M$, gets a different set of coordinate transformations. In this region $r \leq 2M$, due to the moduli appearing in Eqs. (23) and (24) and the change of sign in Eq. (25), one defines instead u' as $\frac{u'}{M} = +\exp\left(-\frac{u}{4M}\right) = \sqrt{1 - \frac{r}{2M}} \exp\left(-\frac{t}{4M} + \frac{r}{4M}\right)$ and v' as $\frac{v'}{M} = \exp\left(\frac{v}{4M}\right) = \sqrt{1 - \frac{r}{2M}} \exp\left(\frac{t}{4M} + \frac{r}{4M}\right)$. These transformations are valid for the region with $u' \geq 0$ and $v' \geq 0$, or the region with $r \leq 2M$ and $-\infty < t < \infty$. Note that the coordinate transformations in this region give $\left(1 - \frac{r}{2M}\right) \exp\left(\frac{r}{2M}\right) = \frac{u'}{M}\frac{v'}{M}$. But this is automatically incorporated into Eq. (30), so there is no further concern on that. Region III is another $r \geq 2M$ region. Now one defines $\frac{u'}{M} = \exp\left(-\frac{u}{4M}\right) == \sqrt{\frac{r}{2M} - 1} \exp\left(-\frac{t}{4M} + \frac{r}{4M}\right)$ and v' as $\frac{v'}{M} = -\exp\left(\frac{v}{4M}\right) = -\sqrt{\frac{r}{2M} - 1} \exp\left(\frac{t}{4M} + \frac{r}{4M}\right)$. These transformations are valid for the region with $u' \geq 0$ and $v' \leq 0$, or the region with $r \geq 2M$ and $-\infty < t < \infty$. Note that the coordinate transformations in this region give $\left(\frac{r}{2M} - 1\right) \exp\left(\frac{r}{2M}\right) = -\frac{u'}{M}\frac{v'}{M}$. But this is automatically incorporated into Eq. (30), so again there is no further concern on that. Region IV is another region with $r \leq 2M$. Now, one defines u' as $\frac{u'}{M} = -\exp\left(-\frac{u}{4M}\right) == -\sqrt{1 - \frac{r}{2M}} \exp\left(-\frac{t}{4M} + \frac{r}{4M}\right)$ and v' as $\frac{v'}{M} = -\exp\left(\frac{v}{4M}\right) = -\sqrt{1 - \frac{r}{2M}} \exp\left(\frac{t}{4M} + \frac{r}{4M}\right)$. These transformations are valid for the region with $u' \leq 0$ and $v' \leq 0$, or the region with $r \leq 2M$ and $-\infty < t < \infty$. The coordinate transformations in this region give as well $\left(1 - \frac{r}{2M}\right) \exp\left(\frac{r}{2M}\right) = \frac{u'}{M}\frac{v'}{M}$. But this is automatically incorporated into Eq. (30), so once again there is no further concern on that.

Furthermore, from Eq. (30) we see that the event horizon at $r = 2M$ has two solutions, $u' = 0$ and $v' = 0$ which are null surfaces represented by straight lines. The true curvature singularity at $r = 0$ has two solutions $\frac{u'}{M}\frac{v'}{M} = 1$, i.e., two spacelike hyperbolae. Implicit in the construction, there is a wormhole, or Einstein-Rosen bridge, topology, with its throat expanding and contracting. The dynamic wormhole is non traversable, but it spatially connects region I to region III through regions II and IV. Regions I and III are two asympotically flat regions causally separated, region II is the black hole region, and region IV is the white hole region of the spacetime.

Eqs. (29) and (30) together with the corresponding interpretation give the maximal extension of the

Schwarzschild metric for $E = \infty$, taken as the limit of $E > 1$, in the coordinates (u', v', θ, ϕ). Of course, this the Kruskal-Szekeres maximal analytical extension, now seen as the $E = \infty$ member of the family of extensions of $E > 1$. Recalling that $u' = t'|_{E=\infty}$ and $v' = \tau'|_{E=\infty}$, we see that the two timelike congruences that specify the two analytically extended time coordinates t' and τ' that yield the maximal extension for $E > 1$ turned into the two analytically extended null retarded and advanced congruences u' and v' of the Kruskal-Szekeres maximal extension. The two-dimensional part (u', v') of the coordinate system (u', v', θ, ϕ) is shown in Figure 3 , both for lines of constant u' and constant v' in part (a) of the figure, and for lines of constant t and constant r in part (b) of the figure, conjointly with the labeling of regions I, II, III, IV, needed to cover it.

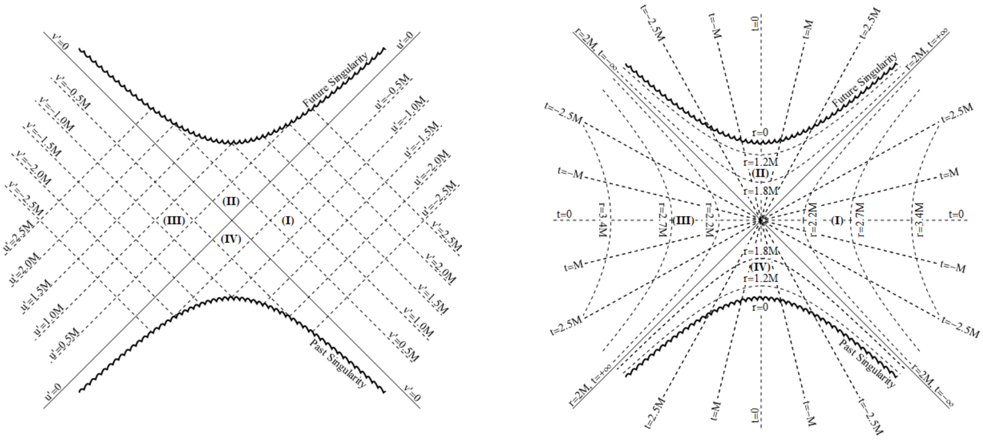

(a)

(b)

Figure 3: The maximal analytical extension of the Schwarzschild metric for the parameter $E = \infty$, i.e., the Kruskal-Szekeres maximal extension, in the plane (u', v') is shown in a diagram with two different descriptions, (a) and (b). In (a) typical values for lines of constant u' and constant v' are displayed. In (b) typical values for lines of constant t and constant r are displayed. The diagram, both in (a) and in (b), represents a spacetime with a wormhole, not shown, that forms out of a singularity in the white hole region, i.e., region IV, and finishes at the black hole region and its singularity, i.e., region II, connecting the two separated asymptotically flat spacetimes, regions I and III. The $E = \infty$ diagram, i.e., the Kruskal-Szekeres diagram, is very similar to the $E > 1$ generic case diagram, see Figure 1, as it is expected for a maximal extension of the Schwarzschild spacetime, in particular for those extensions within the same family.

It is also worth discussing the normals to the $u' = \mathrm{constant}$ and $v' = \mathrm{constant}$ hypersurfaces. For that, we see that from Eq. (13) in the limit $E \to \infty$, or directly from Eq. (29), one finds that the metric has covariant components $g_{u'u'} = 0$, $g_{v'v'} = 0$, $g_{u'v'} = g_{v'u'} = -\frac{16M}{r} \exp\left(-\frac{r}{2M}\right)$, $g_{\theta\theta} = r^2$, $g_{\phi\phi} = r^2 \sin^2\theta$. The contravariant components of the metric can be calculated to be $g^{u'u'} = 0$, $g^{v'v'} = 0$, $g^{u'v'} = g^{v'u'} = -\frac{r}{16M} \exp\left(\frac{r}{2M}\right)$, $g^{\theta\theta} = \frac{1}{r^2}$, $g^{\phi\phi} = \frac{1}{r^2 \sin^2\theta}$. The normals n_a to the $u' = \mathrm{constant}$ and $v' =$ $= \mathrm{constant}$ hypersurfaces are ${n^{u'}}_a = (1, 0, 0, 0)$ and ${n^{v'}}_a = (0, 1, 0, 0)$, respectively, where the superscripts u' and v' in this context are not indices, they simply label the respective normal. Their contravariant components are $n^{u'a} = (g^{u'u'}, g^{u'v'}, 0, 0) = (0, -\frac{r}{16M} \exp\left(\frac{r}{2M}\right), 0, 0)$ and $n^{v'a} = (g^{v'u'}, g^{v'v'}, 0, 0) =$ $= (-\frac{r}{16M} \exp\left(\frac{r}{2M}\right), 0, 0, 0)$. The norms are then ${n^{u'}}_a n^{u'a} = 0$ and ${n^{v'}}_a n^{v'a} = 0$, respectively. Thus, clearly, the normals to the $u' = \mathrm{constant}$ and $v' = \mathrm{constant}$ hypersurfaces are null, and so u' and v' are null coordinates, and the corresponding hypersurfaces are null as well.

VI. Causal diagrams from $E = 1$ to $E = \infty$

In this unified account that carries maximal extensions of the Schwarzschild metric along the parameter E, it is of interest to trace the radial null geodesics for several values of the parameter E itself, $1 \leq E \leq$ $\leq \infty$, in the plane characterized by the (t', τ') coordinates. Null geodesics have $ds^2 = 0$ along them, and if they are radial then also $d\theta = 0$ and $d\phi = 0$. Using the line element given in Eq. (13) together with Eq. (14), we can then trace the radial null geodesics, and with it the causal structure for each E, in the corresponding maximally analytic extended diagram. Figures 4, 5, 6, and 7 are the maximal extended causal diagrams for $E = 1.0$, $E = 1.1$, $E = 1.5$, and $E = \infty$, respectively. In the $E = 1$ case one can take the null geodesics directly from Eqs. (21)-(22), and in the $E = \infty$ case, i.e., the Kruskal-Szekeres extension, directly from Eqs. (29)-(30).

The features shown in the four figures are: (i) The past and future spacelike singularities at $r = 0$. (ii) The regions I, II, III, and IV, described earlier. (iii) The lines of $t' = \mathrm{constant}$ and $\tau' = \mathrm{constant}$, in the $E = \infty$ case these are the lines of $u' = \mathrm{constant}$ and $v' = \mathrm{constant}$. (iv) The outgoing null geodesics represented by red lines and the ingoing null geodesics represented by blue lines. (v) The contravariant normals to the $t' = \mathrm{constant}$ and $\tau' = \mathrm{constant}$, i.e., $n^{t'a}$ and $n^{\tau'a}$, respectively, as given in detail previously.

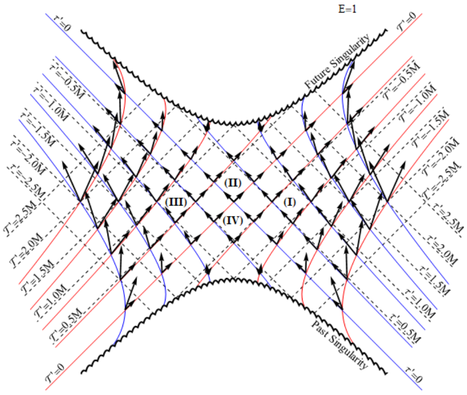

Figure 4: Causal diagram for the maximal analytical extension in the $E = 1$ case. The two singularities and the two event horizons are shown together with lines of outgoing and ingoing null geodesics, drawn in red and blue, respectively, and with lines of constant t' and τ'. The contravariant normals to the $t' = \mathrm{constant}$ and $\tau' = \mathrm{constant}$ hypersurfaces, i.e., $n^{t'a}$ and $n^{\tau'a}$, respectively, are also shown, with their timelike character clearly exhibited. See text for more details.

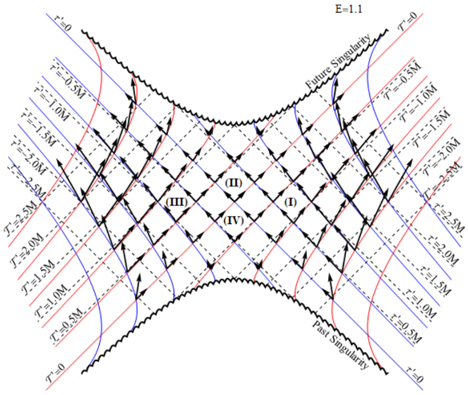
E=1.1
τ'=0
τ'=−0.5M
τ'=−1.0M
τ'=−1.5M
τ'=−2.0M
τ'=−2.5M
T'=2.5M
T'=2.0M
T'=1.5M
T'=1.0M
T'=0.5M
T'=0
T'=0
Future Singularity
T'=−0.5M
T'=−1.0M
T'=−1.5M
T'=−2.0M
T'=−2.5M
τ'=2.5M
τ'=2.0M
τ'=1.5M
τ'=1.0M
τ'=0.5M
τ'=0
Past Singularity
(II)
(III)
(I)
(IV)

Figure 5: Causal diagram for the maximal analytical extension in the $E = 1.1$ case. The two singularities and the two event horizons are shown together with lines of outgoing and ingoing null geodesics, drawn in red and blue, respectively, and with lines of constant t' and τ'. The contravariant normals to the $t' = \mathrm{constant}$ and $\tau' = \mathrm{constant}$ hypersurfaces, i.e., $n^{t'a}$ and $n^{\tau'a}$, respectively, are also shown, with their timelike character clearly exhibited. See text for more details.

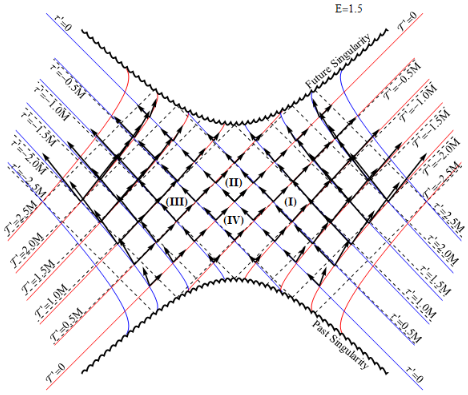
E=1.5
τ'=0
τ'=−0.5M
τ'=−1.0M
τ'=−1.5M
τ'=−2.0M
τ'=−2.5M
T'=2.5M
T'=2.0M
T'=1.5M
T'=1.0M
T'=0.5M
T'=0
T'=0
Future Singularity
T'=−0.5M
T'=−1.0M
T'=−1.5M
T'=−2.0M
T'=−2.5M
τ'=2.5M
τ'=2.0M
τ'=1.5M
τ'=1.0M
τ'=0.5M
τ'=0
Past Singularity
(II)
(III)
(I)
(IV)

Figure 6: Causal diagram for the maximal analytical extension in the $E = 1.5$ case. The two singularities and the two event horizons are shown together with lines of outgoing and ingoing null geodesics, drawn in red and blue, respectively, and with lines of constant t' and τ'. The contravariant normals to the $t' = \mathrm{constant}$ and $\tau' = \mathrm{constant}$ hypersurfaces, i.e., $n^{t'a}$ and $n^{\tau'a}$, respectively, are also shown, with their timelike character clearly exhibited. See text for more details.

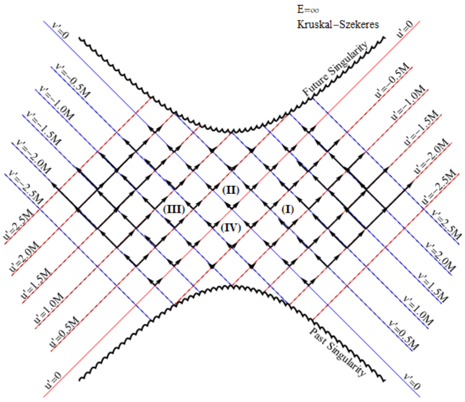

Figure 7: Causal diagram for the maximal analytical extension in the $E = \infty$ case, i.e., the Kruskal-Szekeres maximal extension. The two singularities and the two event horizons are shown together with lines of outgoing and ingoing null geodesics, drawn in red and blue, respectively, and with lines of constant $u' \equiv \lim_{E\to\infty} t'$ and $v' \equiv \lim_{E\to\infty} \tau'$. In this $E = \infty$ case these two sets of lines coincide. The contravariant normals to the $u' = \text{constant}$ and $v' = \text{constant}$ hypersurfaces, i.e., $n^{u'a}$ and $n^{v'a}$, respectively, are also shown, with their null character clearly exhibited. See text for more details.

As it had to be, the lines of $t' = \text{constant}$ and $\tau' = \text{constant}$ are tachyonic, i.e., spacelike hypersurfaces, a feature clearly seen by comparison of these lines with the ingoing and outgoing null geodesic lines, except for $t' = 0$ and $\tau' = 0$ which are null lines representing the $r = 2M$ event horizons of the solution that separate regions I, II, III, and IV. In the $E = \infty$ case, i.e., Kruskal-Szekeres, the spacelike lines turn into the null lines $u' = \text{constant}$ and $v' = \text{constant}$, with $u' = 0$ and $v' = 0$ being the event horizons separating regions I, II, III, and IV. One also sees that the contravariant normals $n^{t'a}$ and $n^{\tau'a}$, are always inside the local light cone, and so the coordinates t' and τ' are timelike, except at the horizons where they are null. In the $E = \infty$ case, i.e., Kruskal-Szekeres, the contravariant normals $n^{u'a}$ and $n^{v'a}$ are null vectors always, and so the coordinates u' and v' are null, i.e., the t' and τ' timelike coordinates turned into the u' and v' null coordinates.

VII. Conclusions

The scenario for maximally extend the Schwarzschild metric is now complete. Schwarzschild is the starting point. In the usual standard coordinates, also called Schwarzschild coordinates, its extension past the sphere $r = 2M$ is cryptic, in any case is not maximal, and to exhibit it fully one needs two coordinate patches, altogether making it very difficult to obtain a complete interpretation. Departing from it, there is one branch alone, namely, the Painlevé-Gullstrand branch that works either with outgoing or with ingoing timelike congruences, or equivalently with outgoing or ingoing test particles placed over them, parameterized by their energy per unit mass E, and that in the $E \to \infty$ limit ends in the Eddington-Finkelstein retarded or advanced null coordinates, respectively. The Painlevé-Gullstrand branch, including its Eddington-Finkelstein $E = \infty$ endpoint, partially extends the Schwarzschild metric past $r = 2M$, but it is not maximal, to have the full solution one needs two coordinate patches, which again inhibits the full interpretation of the solution. Then, from Painlevé-Gullstrand there are two bifurcartion branches. One branch is the Novikov-Lemaître that uses the Painlevé-Gullstrand time coordinate and an appropriate radial comoving coordinate. This branch extends the Schwarzschild metric past $r = 2M$, is maximal in the Novikov range $0 < E < 1$ and partial only in the Lemaître range $1 \leq E < \infty$, ending, in the $E \to \infty$ limit, in Minkowski. The other branch is the one we found here, with the two analytically extended Painlevé-Gullstrand time coordinates, one related to outgoing, the other to ingoing timelike congruences. This branch extends the Schwarzschild metric past $r = 2M$, is maximal and valid for $1 \leq E < \infty$, and ends, for $E = \infty$, directly, or if wished, via the two analytically extended Eddington-Finkelstein retarded and advanced null coordinates, in the Kruskal-Szekeres maximal extension. The maximally extended solutions of the Schwarzschild metric allow for an easy and full interpretation of its complex spacetime structure.

Indeed, whereas the partial extensions of the Schwarzschild metric are of great interest to analyze gravitational collapse of matter and physical phenomena involving black holes where a future event horizon makes its appearance, and in certain instances to analyze time reversal white hole phenomena, the maximal extensions deliver the full solution, showing a model dynamic universe with two separate spacetime sheets, containing a past spacelike singularity, with a white hole region delimited by a past event horizon, that join at a dynamic nontraversable Einstein-Rosen bridge, or wormhole whose throat expands up to $r = 2M$, to collapse into the inside of a future event horizon containing a black hole region with a future spacelike singularity separating again the two separate spacetime sheets of this model universe. Here, a family of maximal extensions of the Schwarzschild spacetime parameterized by the energy per unit mass E of congruences of outgoing and ingoing timelike geodesics has been obtained. In this unified description, the Kruskal-Szekeres maximal extension of sixty years ago is seen here as the important, but now particular, instance of this E family, namely, the one with $E = \infty$. This maximal description provides the link between Gullstrand-Painlevé and Kruskal-Szekeres.

Acknowledgments

We acknowledge FCT - Fundação para a Ciência e Tecnologia of Portugal for financial support through Project No. UIDB/00099/2020.

Appendix: Details for the $E \to 1$ limit and the $E \to \infty$ Kruskal-Szekeres limit from the $E > 1$ generic case

In order to see the continuity of the maximal extension parameterized by E, we take the generic $E > 1$ case, and from it obtain directly the limit to the case $E = 1$, and the limit to the case $E = \infty$, i.e., the Kruskal-Szekeres extension.

$E = 1$ *limit from* $E > 1$*:*

Here we take the $E \to 1$ limit of Eqs. (13) and (14). We will do it term by term in each equation. For Eq. (13) we have: $\lim_{E\to 1} -4\left(\frac{2E^2-1+\frac{2M}{r}+2E\sqrt{E^2-1+\frac{2M}{r}}}{E^2-1+\frac{2M}{r}}\right) = -4\frac{(1+\sqrt{\frac{2M}{r}})^2}{\frac{2M}{r}}$; $\lim_{E\to 1} \exp\left(-\frac{r}{2ME}\sqrt{E^2-1+\frac{2M}{r}}\right) =$

$= \exp\left(-\sqrt{\frac{r}{2M}}\right)$; $\lim_{E\to 1}\left(\frac{\frac{M}{r}}{E^2-1+\frac{M}{r}+\sqrt{E^2-1}\sqrt{E^2-1+\frac{2M}{r}}}\right)^{\frac{2E^2-1}{2E\sqrt{E^2-1}}} = \left(1+2\sqrt{E^2-1}\sqrt{\frac{r}{2M}}\right)^{-\frac{1}{2\sqrt{E^2-1}}} =$ $= \exp\left[-\frac{1}{2\sqrt{E^2-1}}\ln\left(1+2\sqrt{E^2-1}\sqrt{\frac{r}{2M}}\right)\right] = \exp\left(-\sqrt{\frac{r}{2M}}\right)$; $\lim_{E\to 1} -\frac{1}{M^2}\left(2E\sqrt{E^2-1+\frac{2M}{r}}+2E^2-1+ +\frac{2M}{r}\right) = -\frac{1}{M^2}\left(1+\sqrt{\frac{2M}{r}}\right)^2$; $\lim_{E\to 1}\exp\left(-\frac{r}{2ME}\sqrt{E^2-1+\frac{2M}{r}}\right) = \exp\left(-\sqrt{\frac{r}{2M}}\right)$; $\lim_{E\to 1}\left(\frac{\frac{M}{r}}{E^2-1+\frac{M}{r}+\sqrt{E^2-1}\sqrt{E^2-1+\frac{2M}{r}}}\right)^{\frac{2E^2-1}{2E\sqrt{E^2-1}}} = \exp\left(-\sqrt{\frac{r}{2M}}\right)$; $\lim_{E\to 1} 2\left(2E^2-1+\frac{2M}{r}\right) = 2\left(1+\frac{2M}{r}\right)$. Thus, Eq. (13) is now $\mathrm{d}s^2 = -4\frac{(1+\sqrt{\frac{2M}{r}})^2}{\frac{2M}{r}}\exp\left(-2\sqrt{\frac{r}{2M}}\right)\left[-\frac{1}{M^2}\left(1+\sqrt{\frac{2M}{r}}\right)^2\exp\left(-2\sqrt{\frac{r}{2M}}\right)\times\right.$ $\left.\times(\tau'^2\mathrm{d}t'^2+t'^2\mathrm{d}\tau'^2)+2\left(1+\frac{2M}{r}\right)\mathrm{d}t'\,\mathrm{d}\tau'^2\right]+r^2(\mathrm{d}\theta^2+\sin^2\theta\,\mathrm{d}\phi^2)$. This is the line element found for the $E=1$ case, see Eq. (21). For Eq. (14) we have: $\lim_{E\to 1}\left(\frac{\frac{r}{2M}-1}{2E^2-1+\frac{2M}{r}+2E\sqrt{E^2-1+\frac{2M}{r}}}\right)\frac{2M}{r} = \frac{\sqrt{\frac{r}{2M}}-1}{\sqrt{\frac{r}{2M}}+1}$; $\lim_{E\to 1}\exp\left(\frac{r}{2ME}\sqrt{E^2-1+\frac{2M}{r}}\right) = \exp\left(\sqrt{\frac{r}{2M}}\right)$; $\lim_{E\to 1}\left[\frac{r}{M}\left(\sqrt{E^2-1}\sqrt{E^2-1+\frac{2M}{r}}+E^2-1+ +\frac{M}{r}\right)\right]^{\frac{2E^2-1}{2E\sqrt{E^2-1}}} = \left(1+2\sqrt{E^2-1}\sqrt{\frac{r}{2M}}\right)^{\frac{1}{2\sqrt{E^2-1}}} = \exp\left[\frac{1}{2\sqrt{E^2-1}}\ln\left(1+2\sqrt{E^2-1}\sqrt{\frac{r}{2M}}\right)\right] = \exp\left(\sqrt{\frac{r}{2M}}\right)$. Thus, Eq (14) in the $E\to 1$ limit turns into $\frac{\sqrt{\frac{r}{2M}}-1}{\sqrt{\frac{r}{2M}}+1}\exp\left(2\sqrt{\frac{r}{2M}}\right) = -\frac{t'}{M}\frac{\tau'}{M}$. This is indeed Eq. (22).

$E\to\infty$ limit from $E>1$, the Kruskal-Szekeres line element:

Here we take the $E\to\infty$ limit of Eqs. (13) and (14). We will do it term by term in each equation. For Eq. (13) we have: $\lim_{E\to\infty} -4\left(\frac{2E^2-1+\frac{2M}{r}+2E\sqrt{E^2-1+\frac{2M}{r}}}{E^2-1+\frac{2M}{r}}\right) = -16$; $\lim_{E\to\infty}\exp\left(-\frac{r}{2ME}\sqrt{E^2-1+\frac{2M}{r}}\right) =$ $= \exp\left(-\frac{r}{2M}\right)$; $\lim_{E\to\infty}\left(\frac{M}{r}\frac{1}{E^2-1+\frac{M}{r}+\sqrt{E^2-1}\sqrt{E^2-1+\frac{2M}{r}}}\right)^{\frac{2E^2-1}{2E\sqrt{E^2-1}}} = \frac{M}{r}\frac{1}{2E^2}$; $\lim_{E\to\infty} -\frac{1}{M^2}\left(2E^2-1+ +\frac{2M}{r}+2E\sqrt{E^2-1+\frac{2M}{r}}\right) = -\frac{4E^2}{M^2}$; $\lim_{E\to\infty}\exp\left(-\frac{r}{2ME}\sqrt{E^2-1+\frac{2M}{r}}\right) = \exp\left(-\frac{r}{2M}\right)$; $\lim_{E\to\infty}\left(\frac{\frac{M}{r}}{E^2-1+\frac{M}{r}+\sqrt{E^2-1}\sqrt{E^2-1+\frac{2M}{r}}}\right)^{\frac{2E^2-1}{2E\sqrt{E^2-1}}} = \frac{M}{r}\frac{1}{2E^2}$; $\lim_{E\to\infty} 2\left(2E^2-1+\frac{2M}{r}\right) = 4E^2$. Thus, Eq (13) is now $\mathrm{d}s^2 = -16\exp\left(-\frac{r}{2M}\right)\frac{M}{r}\frac{1}{2E^2}\left[-\frac{4E^2}{M^2}\exp\left(-\frac{r}{2M}\right)\frac{M}{r}\frac{1}{2E^2}(v'^2\mathrm{d}u'^2+u'^2\mathrm{d}v'^2)+4E^2\mathrm{d}u'\mathrm{d}v'\right]+ +r^2(\mathrm{d}\theta^2+\sin^2\theta\,\mathrm{d}\phi^2)$, where for convenience of notation we have redefined the coordinates, $u'\equiv t'$ and $v'\equiv\tau'$. Implementing definitely the $E\to\infty$ limit, the term in $(v'^2\mathrm{d}u'^2+u'^2\mathrm{d}v'^2)$ vanishes and one gets, $\mathrm{d}s^2 = -\frac{32M}{r}\exp\left(-\frac{r}{2M}\right)\mathrm{d}u'\mathrm{d}v'+r^2(\mathrm{d}\theta^2+\sin^2\theta\,\mathrm{d}\phi^2)$. This is Eq.(29), i.e., the Kruskal-Szekeres line element. For Eq. (14) we have: $\lim_{E\to\infty}\left(\frac{\frac{r}{2M}-1}{2E^2-1+\frac{2M}{r}+2E\sqrt{E^2-1+\frac{2M}{r}}}\right)\frac{2M}{r} = \frac{\frac{r}{2M}-1}{4E^2}\frac{2M}{r}$; $\lim_{E\to\infty}\exp\left(\frac{r}{2ME}\sqrt{E^2-1+\frac{2M}{r}}\right) = \exp\left(\frac{r}{2M}\right)$; $\lim_{E\to\infty}\left[\frac{r}{M}\left(\sqrt{E^2-1}\sqrt{E^2-1+\frac{2M}{r}}+E^2-1+ +\frac{M}{r}\right)\right]^{\frac{2E^2-1}{2E\sqrt{E^2-1}}} = \frac{r}{M}2E^2$. Thus, redefining for convenience of notation the coordinates t' and τ' as $u'\equiv t'$ and $v'\equiv\tau'$, Eq (14) in the $E\to\infty$ limit turns into $\left(\frac{r}{2M}-1\right)\exp\left(\frac{r}{2M}\right) = -\frac{u'}{M}\frac{v'}{M}$. This is Eq. (30), i.e., the Kruskal-Szekeres implicit definition of r in terms of u' and v'. Seen through this direct limiting procedure, the Kruskal-Szekeres solution is indeed a particular case of the E family of maximal extensions. In no place there was explicit need to resort to Eddington-Finkelstein null coordinates and their analytical extended versions.

Bibliography

[1] K. Schwarzschild, *Sitz Preuss Akad. d. Wiss* **1916**, 189 (1916).

[2] J. Droste, *Proc K Ned Akad Wet* **19**, 197 (1917).

[3] D. Hilbert, *Nachr. Ges. Wiss. Göttingen, Math.-Phys. Klasse* **1917**, 53 (1917).

[4] G. D. Birkhoff, *Relativity and Modern Physics* (Harvard University Press, Cambridge Massachusetts, 1923).

[5] A. Einstein, N. Rosen, *Phys. Rev.* **48**, 73 (1935).

[6] C. W. Misner, J. A. Wheeler, *Ann. Phys.* **2**, 525 (1957).

[7] M. S. Morris, K. S. Thorne, *Am. J. Phys.* **56**, 395 (1988).

[8] J. P. S. Lemos, F. S. N. Lobo, S. Q. de Oliveira, *Phys. Rev. D* **68**, 064004 (2003). ArXiv:gr-qc/0302049.

[9] E. Guendelman, E. Nissimov, S. Pacheva, M. Stoilov, *Bulg. J. Phys.* **44**, 85 (2017). ArXiv:1611.04336 [gr-qc].

[10] P. Painlevé, *C.R. Acad. Sci.* **173**, 677 (1921).

[11] A. Gullstrand, *Ark. Mat. Astr. Fys.* **16**, 1 (1922).

[12] R. Gautreau, B. Hoffmann, *Phys. Rev. D* **17**, 2552 (1978).

[13] M. K. Parikh, F. Wilczek, *Phys. Rev. Lett.* **85**, 5042 (2000). ArXiv:hep-th/9907001.

[14] K. Martel, E. Poisson, *Am. J. Phys.* **69**, 476 (2001). ArXiv:gr-qc/0001069.

[15] J. Natário, *Gen. Relativ. Gravit.* **41**, 2579 (2009). ArXiv:0805.0206 [gr-qc].

[16] T. K. Finch, *Gen. Relativ. Gravit.* **47**, 56 (2015). ArXiv:1211.4337 [gr-qc].

[17] C. MacLaurin, *Einstein equations: Physical and Mathematical Aspects of General Relativity*, S. Cacciatori, B. Güneysu, S. Pigola, eds. (Birkhäuser, Cham, Switzerland, 2019), p. 267. ArXiv:1911.05988 [gr-qc].

[18] G. Lemaître, *Ann. Soc. Sci. Bruxelles* **53A**, 51 (1933).

[19] I. D. Novikov, Early stages of the evolution of the universe, Ph.D. thesis, SAI Moscow (1963).

[20] J. R. Oppenheimer, H. Snyder, *Phys. Rev.* **56**, 455 (1939).

[21] Y. B. Zel'dovich, I. D. Novikov, *Relativity and Astrophysics Volume 1: Stars and Relativity* (University of Chicago Press, Chicago, 1971).

[22] R. Gautreau, *Il Nuovo Cimento B* **56**, 49 (1980).

[23] A. Krasiński, *Inhomogeneous Cosmological Models* (Cambridge University Press, 1997).

[24] M. Blau, *Lecture Notes on General Relativity* (Author edition, Geneva, 2014).

[25] A. S. Eddington, *Nature* **113**, 192 (1924).

[26] D. Finkelstein, *Phys. Rev.* **110**, 965 (1958).

[27] R. Penrose, *Battelle Rencontres 1967*, C. M. DeWitt, J. A. Wheeler, eds. (Benjamin, New York, 1968), p. 121.

[28] M. Alcubierre, B. Brügmann, *Phys. Rev. D* **63**, 104006 (2001). ArXiv:gr-qc/0008067.

[29] R. J. Adler, J. D. Bjorken, P. Chen, J. S. Liu, *Am. J. Phys.* **73**, 1148 (2005). ArXiv:gr-qc/0502040.

[30] E. Babichev, V. Dokuchaev, Y. Eroshenko, *Class. Quantum Grav.* **29**, 115002 (2012). ArXiv:1202.2836 [gr-qc].

[31] S. Abdolrahimi, D. N. Page, C. Tzounis, *Phys. Rev. D* **100**, 124038 (2019). ArXiv:1607.05280 [hep-th].

[32] C. Gooding, W. G. Unruh, *Phys. Rev. D* **100**, 026010 (2019). ArXiv:1902.04211 [gr-qc].

[33] M. D. Kruskal, *Phys. Rev.* **119**, 1743 (1960).

[34] G. Szekeres, *Publ. Math-Debrecen* **7**, 285 (1960).

[35] R. W. Fuller, J. A. Wheeler, *Phys. Rev.* **128**, 919 (1962).

[36] J. Synge, *Proc. R. Ir. Acad. A* **53**, 83 (1950).

[37] C. Fronsdal, *Phys. Rev.* **116**, 778 (1959).

[38] S. W. Hawking, G. F. R. Ellis, *The Large Scale Structure of Space-Time* (Cambridge University Press, Cambridge, 1973).

[39] C. W. Misner, K. S. Thorne, J. A. Wheeler, *Gravitation* (W. H. Freeman, San Francisco, 1973).

[40] R. M. Wald, *General Relativity* (Chicago University Press, Chicago, 1984).

[41] R. D'Inverno, *Introducing Einstein's Relativity* (Oxford University Press, Oxford, 1992).

[42] K. A. Bronnikov, S. G. Rubin, *Black Holes, Cosmology and Extra Dimensions* (World Scientific, Singapore, 2013).

[43] P. T. Chruściel, *Elements of General Relativity* (Birkäuser Cham, Switzerland, 2020).

[44] O. B. Zaslavskii, *Phys. Rev. D* **88**, 104016 (2013). ArXiv:1301.2801 [gr-qc].

[45] L. Hodgkinson, J. Louko, A. C. Ottewill, *Phys. Rev. D* **89**, 104002 (2014). ArXiv:1401.2667 [gr-qc].

[46] J. P. S. Lemos, *Phys. Rev. Lett.* **68**, 1447 (1992).